

## **INFORMATION TO USERS**

**This manuscript has been reproduced from the microfilm master. UMI films the text directly from the original or copy submitted. Thus, some thesis and dissertation copies are in typewriter face, while others may be from any type of computer printer.**

**The quality of this reproduction is dependent upon the quality of the copy submitted. Broken or indistinct print, colored or poor quality illustrations and photographs, print bleedthrough, substandard margins, and improper alignment can adversely affect reproduction.**

**In the unlikely event that the author did not send UMI a complete manuscript and there are missing pages, these will be noted. Also, if unauthorized copyright material had to be removed, a note will indicate the deletion.**

**Oversize materials (e.g., maps, drawings, charts) are reproduced by sectioning the original, beginning at the upper left-hand corner and continuing from left to right in equal sections with small overlaps.**

**Photographs included in the original manuscript have been reproduced xerographically in this copy. Higher quality 6" x 9" black and white photographic prints are available for any photographs or illustrations appearing in this copy for an additional charge. Contact UMI directly to order.**

**ProQuest Information and Learning  
300 North Zeeb Road, Ann Arbor, MI 48106-1346 USA  
800-521-0600**

**UMI<sup>®</sup>**



**STRUCTURE AND FUNCTION OF THE DROSOPHILA PROTEIN BIG BRAIN**

by

**Gina Marie Yanocho**

---

**A Dissertation Submitted to the Faculty of the  
COMMITTEE ON PHARMACOLOGY AND TOXICOLOGY (GRADUATE)**

**In Partial Fulfillment of the Requirements  
For the Degree of**

**DOCTOR OF PHILOSOPHY**

**In the Graduate College**

**THE UNIVERSITY OF ARIZONA**

**2001**

UMI Number: 3023511

UMI<sup>®</sup>

---

UMI Microform 3023511

Copyright 2001 by Bell & Howell Information and Learning Company.

All rights reserved. This microform edition is protected against  
unauthorized copying under Title 17, United States Code.


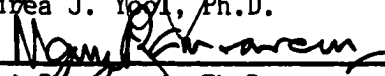
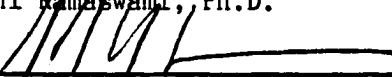


---

Bell & Howell Information and Learning Company  
300 North Zeeb Road  
P.O. Box 1346  
Ann Arbor, MI 48106-1346

THE UNIVERSITY OF ARIZONA ©  
GRADUATE COLLEGE

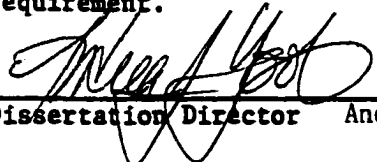
As members of the Final Examination Committee, we certify that we have read the dissertation prepared by Gina Marie Yanochko entitled Structure and Function of the Drosophila Protein Big Brain

and recommend that it be accepted as fulfilling the dissertation requirement for the Degree of Doctor of Philosophy

 Andrea J. Yool, Ph.D.	<u>May 18, 2001</u> Date
 Mani Ramaswami, Ph.D.	<u>May 18, 01</u> Date
 John W. Regan, Ph.D.	<u>5/18/2001</u> Date
 Leslie P. Tolbert, Ph.D.	<u>5/18/01</u> Date
 Richard R. Vaillancourt, Ph.D.	<u>5/18/01</u> Date

Final approval and acceptance of this dissertation is contingent upon the candidate's submission of the final copy of the dissertation to the Graduate College.

I hereby certify that I have read this dissertation prepared under my direction and recommend that it be accepted as fulfilling the dissertation requirement.

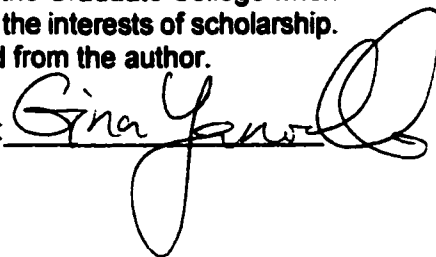
 Dissertation Director	<u>Andrea J. Yool, Ph.D.</u>	<u>May 18, 2001</u> Date
--	------------------------------	-----------------------------

### STATEMENT BY AUTHOR

This dissertation has been submitted in partial fulfillment of requirements for an advanced degree at The University of Arizona and is deposited in the University Library to be made available to borrowers under rules of the Library.

Brief quotations from this dissertation are allowable without special permission, provided that accurate acknowledgement of source is made. Requests for permission for extended quotation from or reproduction of this manuscript in whole or in part may be granted by the head of the major department or the Dean of the Graduate College when in his or her judgment the proposed use of the materials is in the interests of scholarship. In all other instances, however, permission must be obtained from the author.

SIGNED: \_\_\_\_\_

A handwritten signature in black ink, appearing to read "Gina Yaw", written over a horizontal line. The signature is cursive and includes a large loop at the end.

## **ACKNOWLEDGEMENTS**

**Andrea Yool leads by her strong, patient and knowledgeable example. Her attitude fosters a laboratory environment filled with enthusiasm, learning, and independence. I cannot imagine my graduate experience without her support and encouragement. I was fortunate to have Drs. Mani Ramaswami, John Regan, Leslie Tolbert and Richard Vaillancourt on the committee overseeing my progress. They gave generously of their time with ideas, explanations, and even allowing me into their own laboratories to conduct experiments. They challenged me at every meeting and I will be forever grateful for their efforts, energy and patience.**

**A number of fabulous educators and researchers provided me with the background and inspired the enthusiasm necessary to achieve this degree, in particular: Mr. Edwin Fankhauser; Mr. Mike Hepper; Dr. Karen Brewer at Virginia Tech whose encouragement and friendship were invaluable in this pursuit; Dr. Joseph Merola (Narf!) at Virginia Tech; and Dr. Charles Jagoe at the Savannah River Ecology Laboratory who gave me the freedom and independence to explore mercury levels in ALLIGATORS!**

**In the laboratory I have had the distinct pleasure of working with friends, who have taught me about both science and myself. I would especially like to thank Jill Steidl, Daniela Boassa and Dawn Nice for hours of conversations while injecting oocytes and at the rigs, Torsten Falk, Kate Bolles, Amy Marble (GO CAPS!), and Susan Sotardi (our RASMOL whiz) – you made the bad days bearable and the good days a blast.**

**The aspect of graduate school that I didn't anticipate was the fantastic friendships I have developed and which gave me the opportunity to explore the depths of life experiences. Jodi (The bus is HERE!) Carter, Daniela (Ampera) Boassa & Davide Dulcis, Jennifer Hensel & Jeremy Richman (who both helped with critical reading of this dissertation), L.Clark Brown, Tara McIsaac (Coffee?), Dan Stamer, Jill Steidl, Anna, Chad & Rhiannon Mitchell, Judd, Catherine & Caia Rice – thank you for the laughter, compassion and friendship you have given so freely. I could not have done this without you. In addition, Margaret Richards, Sumner Jones and Jill Hostetter helped me bridge the gap from Virginia Tech to the University of Arizona; their continued presence in my life has added a needed perspective to these five years.**

**Thanks to my parents, Ron and Marie Yanochko and sisters, Patti and Suzy for their friendship. Your love and acceptance of who I was, who I am and who I am becoming makes everyday easier.**

**And finally, a lifetime of thanks to Todd (my best everything) - his patience, laughter, and love are part of every word on these pages.**

## **DEDICATION**

**This dissertation is dedicated to my grandmothers, Anna May Yanocho and Emma DeBellis.**

## TABLE OF CONTENTS

<b>LIST OF FIGURES</b> .....	<b>8</b>
<b>LIST OF TABLES</b> .....	<b>10</b>
<b>ABSTRACT</b> .....	<b>11</b>
<b>CHAPTER 1. Background and Literature Review</b> .....	<b>13</b>
<b>1.1 DEVELOPMENT OF THE NERVOUS SYSTEM</b>	
(1) <i>The use of model systems to study development</i> .....	14
(2) <i>Drosophila nervous system development</i> .....	14
(3) <i>Neuroblast segregation and differentiation</i> .....	16
A. <i>Proneural genes</i> .....	18
B. <i>Neurogenic genes</i> .....	19
(4) <i>Ion channels in neuronal development</i> .....	22
<b>1.2 MAJOR INTRINSIC PROTEIN (MIP) FAMILY</b> .....	<b>26</b>
(1) <i>Structure and function of MIPs</i> .....	27
A. <i>Sequence alignments</i> .....	29
B. <i>Mutagenesis and chimeric analysis</i> .....	30
C. <i>Crystallographic analysis of MIP channels</i> .....	33
(2) <i>Regulation of MIP function</i> .....	38
(3) <i>Developmental expression of aquaporins</i> .....	41
<b>1.3 GENERAL HYPOTHESIS AND AIMS</b> .....	<b>44</b>
 <b>CHAPTER 2. FUNCTIONAL CHARACTERISTICS OF BIB EXPRESSED IN XENOPUS OOCYTES</b>	
<b>2.1 INTRODUCTION</b> .....	<b>59</b>
<b>2.2 MATERIALS AND METHODS</b> .....	<b>60</b>
(1) <i>Molecular techniques</i> .....	60
(2) <i>Oocyte preparation</i> .....	62
(3) <i>Electrophysiological recordings</i> .....	62
(4) <i>Osmotically-induced swelling assay</i> .....	63
(5) <i>Cellular fractionation</i> .....	63
(6) <i>Immunoprecipitation and Western blotting</i> .....	64
(7) <i>Immunofluorescence of intact oocytes</i> .....	65
<b>2.3 RESULTS</b> .....	<b>66</b>
<b>2.4 DISCUSSION</b> .....	<b>76</b>

## TABLE OF CONTENTS (*continued*)

### CHAPTER 3. DIVALENT CATION BLOCK OF BIG BRAIN CHANNELS

3.1	INTRODUCTION.....	91
3.2	MATERIALS AND METHODS.....	92
	(1) <i>Molecular techniques</i> .....	92
	(2) <i>Oocyte preparation</i> .....	94
	(3) <i>Electrophysiological recordings</i> .....	94
	(4) <i>Cellular fractionation</i> .....	94
	(5) <i>Western blotting</i> .....	95
3.3	RESULTS.....	95
3.4	DISCUSSION.....	103

### CHAPTER 4. THE ROLE OF THE CARBOXY TAIL OF BIG BRAIN

4.1	INTRODUCTION.....	133
4.2	MATERIALS AND METHDOS.....	137
	(1) <i>Molecular techniques</i> .....	137
	(2) <i>Oocyte preparation</i> .....	138
	(3) <i>Electrophysiological recordings</i> .....	138
	(4) <i>Osmotically-induced swelling assay</i> .....	138
	(5) <i>Cellular fractionation</i> .....	139
	(6) <i>Immunoprecipitation and Western blotting</i> .....	139
4.3	RESULTS.....	139
4.4	DISCUSSION.....	142
	<b>SUMMARY AND CONCLUSIONS</b> .....	<b>158</b>
	<b>REFERENCES</b> .....	<b>161</b>

## LIST OF FIGURES

<b>Figure 1.1</b>	Developmental timeline of <i>Drosophila</i> embryos .....	46
<b>Figure 1.2</b>	Neurogenic regions of the <i>Drosophila</i> embryo .....	47
<b>Figure 1.3</b>	Neuroblasts arise from the neuroectoderm .....	48
<b>Figure 1.4</b>	Differentiation of a neuroblast .....	49
<b>Figure 1.5</b>	Proneural cluster formation is affected by anterior-posterior and dorsal ventral patterning genes .....	50
<b>Figure 1.6</b>	Basic Notch signaling pathway .....	51
<b>Figure 1.7</b>	Membrane topology of MIP channels.....	52
<b>Figure 1.8</b>	Sequence alignment of bovine AQP0, human AQP1, <i>Drosophila</i> BIB and <i>E. coli</i> GlpF .....	53
<b>Figure 1.9</b>	The hourglass model .....	54
<b>Figure 1.10</b>	Helical packing arrangement of AQP1 subunits .....	55
<b>Figure 1.11</b>	Tetrameric assembly of AQP1 and GlpF subunits .....	56
<b>Figure 1.12</b>	The central pore of GlpF .....	57
<b>Figure 1.13</b>	Sequence identity of BIB with members of the MIP family: AQP0, AQP1, AQP4 and Nodulin 26 .....	58
<b>Figure 2.1</b>	BIB is not a water permeable channel .....	79
<b>Figure 2.2</b>	Ion channel activity in BIB-expressing oocytes .....	80
<b>Figure 2.3</b>	BIB channels show non-selective monovalent cation selectivity .....	82
<b>Figure 2.4</b>	Mutation of HABIB (E71N) abolishes the ionic conductance response without preventing membrane localization of the heterologously expressed channel in oocytes.....	83
<b>Figure 2.5</b>	Regulators of kinase pathways differentially modulate the ionic conductance produced by electrode insertion and endogenous signaling in BIB-expressing oocytes .....	85
<b>Figure 2.6</b>	Summary of differential modulation of kinase pathways on the ionic conductance produced by electrode insertion and endogenous signaling in BIB-expressing oocytes .....	87
<b>Figure 2.7</b>	BIB channels are tyrosine phosphorylated .....	89
<b>Figure 2.8</b>	BIB channels have a large single channel conductance .....	90
<b>Figure 3.1</b>	Strategy for site-directed mutagenesis of BIB at D253, E274 and E71 .....	108
<b>Figure 3.2</b>	Calcium and barium block currents induced by HABIB expression in <i>Xenopus</i> oocytes .....	110
<b>Figure 3.3</b>	Dose and voltage-dependence of calcium and barium block of whole-cell conductance in oocytes expressing HABIB .....	112
<b>Figure 3.4</b>	Fraction of unblocked current for oocytes expressing HABIB in magnesium, calcium or barium saline .....	114
<b>Figure 3.5</b>	Net rates of unblock show no apparent voltage dependence .....	116
<b>Figure 3.6</b>	Net rates of block show no apparent voltage dependence .....	117
<b>Figure 3.7</b>	Fractional electrical field distance of calcium block .....	118
<b>Figure 3.8</b>	Schematic diagram of the amino acids in and surrounding Loops B and E of BIB .....	119

### LIST OF FIGURES (continued)

<b>Figure 3.9</b>	Amino acid structure of amino acids mutated in BIB to analyze divalent cation block .....	120
<b>Figure 3.10</b>	Summary of the effects of the mutations D253N, E274N, E71N, E71Q and E71K .....	121
<b>Figure 3.11</b>	Summary of the effect of E71D on properties of HABIB expressed in <i>Xenopus</i> oocytes .....	123
<b>Figure 3.12</b>	Current traces demonstrate that mutation of E71 to aspartic acid induces Mg <sup>2+</sup> block .....	124
<b>Figure 3.13</b>	Tail current traces demonstrate that mutation of E71 to aspartic acid induces Mg <sup>2+</sup> block .....	125
<b>Figure 3.14</b>	Fraction of unblocked current in oocytes expressing E71D or wild-type HABIB in magnesium, calcium or barium saline .....	126
<b>Figure 3.15</b>	Extracellular view of the GlpF tetramer showing the location of E14 .....	128
<b>Figure 4.1</b>	Carboxy tail domain of BIB with sites of potential phosphorylation and protein interactions highlighted .....	147
<b>Figure 4.2</b>	Alignment of carboxy tail domain of BIB with rat AQP4 and human AQP1 .....	149
<b>Figure 4.3</b>	Truncation strategy for BIB .....	150
<b>Figure 4.4</b>	Restriction digest analysis of full length and truncation mutants of HABIB cDNA and illustration of cRNA products .....	152
<b>Figure 4.5</b>	Truncation of the carboxy tail domain does not confer water permeability to BIB .....	153
<b>Figure 4.6</b>	Δ317 and Δ377 are expressed on the plasma membrane of <i>Xenopus</i> oocytes.....	154
<b>Figure 4.7</b>	Δ317 and Δ377 have a linear current-voltage relationship .....	155
<b>Figure 4.8</b>	Δ317 and Δ377 have reduced whole-cell conductance compared to full length BIB .....	156
<b>Figure 4.9</b>	Truncation of the carboxy tail removes detectable tyrosine phosphorylation of BIB .....	157

**LIST OF TABLES**

<b>Table 3.1</b> Dose and voltage-dependence of block by calcium on currents in oocytes expressing HABIB channels .....	129
<b>Table 3.2</b> Dose and voltage dependence of block by barium on currents in oocytes expressing HABIB channels .....	130
<b>Table 3.3</b> Fraction of unblocked current ( $I_{UF}$ ) for HABIB channels in the presence of 4.5mM magnesium, calcium or barium.....	131
<b>Table 3.4</b> Comparison of the fraction of unblocked current ( $I_{UF}$ ) in oocytes expressing wild-type and E71D HABIB channels in magnesium, calcium or barium saline .....	132

## ABSTRACT

*big brain* is a neurogenic gene which, when mutated causes defects in cell fate determination during *Drosophila* neurogenesis through an unknown mechanism. The protein Big Brain (BIB) has sequence identity with the Major Intrinsic Protein family including the water- and ion-conducting Aquaporin channels. We show here that BIB expressed heterologously in *Xenopus* oocytes is a non-selective monovalent cation channel with permeability to  $K^+ > Na^+ \gg TEA^+$ . BIB macroscopic conductance, activated in response to endogenous oocyte signaling pathways, was decreased after treatment with 20  $\mu$ M insulin and was enhanced with 10  $\mu$ M lavendustin A, a tyrosine kinase inhibitor. Current activation is not observed in control oocytes or in oocytes expressing a non-functional mutant BIB channel (E71N) that is expressed on the plasma membrane, as confirmed with confocal microscopy and western blotting. Cell-attached patch clamp experiments revealed a novel large conductance (300  $\pm$  30 pS) channel in BIB-expressing but not control oocytes.

Divalent cations, such as calcium, are important developmental signaling molecules. We found that calcium and barium partially block currents in BIB-expressing oocytes. We further demonstrated that a conserved glutamate (E71) located in transmembrane domain 1 is crucial for channel properties of BIB.  $Mg^{2+}$  block was introduced in currents from oocytes expressing the BIB mutant E71D. The carboxy tail of BIB comprises 61% of the channel (431 of 700 residues) and contains sites of potential serine/threonine and tyrosine phosphorylation, SH3 binding domains, PDZ binding domains and three polyglutamine stretches. The importance of the carboxy tail for BIB channel activity was demonstrated by truncation of the channel at two sites.

Truncated channels had reduced whole-cell conductance and at least one ( $\Delta 317$ ) was not tyrosine phosphorylated. In summary, the results presented in this dissertation provide a novel function of the *Drosophila* protein Big Brain as a regulated cationic channel, indicate that BIB can participate in tyrosine kinase-regulated transmembrane signaling, and suggest a role for membrane depolarization in the neurogenic function of BIB in early development.

## **CHAPTER 1. Background and Literature Review**

**Big Brain (BIB), the *Drosophila* channel that has been the focus of my research, was first identified in genetic screens for genes involved in early stages of nervous system development. Loss-of-function mutations in BIB result in an excess number of nervous system cells formed at the expense of the ventral epidermis, a lethal condition (Lehmann, et al., 1983). In 1990, the laboratories of Lily and Yeh Nung Jan at UCSF cloned the *bib* cDNA. The *bib* gene product was found to have sequence identity with a recently identified family of channel proteins, the Major Intrinsic Protein family (Rao et al., 1990). Since that time only three papers have been published in regards to *bib*; they have provided additional data supporting *bib*'s role in nervous system development but no explanation as to how *bib*, a transmembrane protein resembling a family of ion, water and glycerol channels might function to establish cell fate. In this dissertation I describe the results of experiments that provide novel characterization of BIB as a non-selective cation channel.**

**My interests in studying mechanisms of nervous system development are essentially two-fold. The first lies in the potential application of the results. Knowledge of developmental mechanisms may provide insight into developmental diseases of the nervous system or for neurodegenerative diseases which, in many cases, have similar underlying molecular components. The second has roots in the nature of science. Development is absolutely fascinating. How is it possible that from a single cell an entire living organism is created? From this one cell, how is the nervous system, a complex network of over  $10^{11}$  neurons and 10-50 times as many glial cells generated in a systematic way?**

## 1.1 DEVELOPMENT OF THE NERVOUS SYSTEM

### *(1) The use of model systems to study development*

Insects, including fruit flies (*Drosophila melanogaster*), grasshoppers (*Shistocerca* species), and moths (*Manduca sexta*) have been integral in assessing the interactions that determine cell fate as well as for determining specific gene products involved in developmental processes. In this regard, studies of the nematode, *C. elegans* have also been useful. Model organisms, such as *Drosophila*, are used to study development for many reasons, principally: (i) they have stereotyped patterns of development; (ii) mutations are easily introduced; (iii) they have a large number of offspring and rapid generation times; and (iv) ethical considerations.

In general, the genes involved in nervous system development in flies are similar to those in other insects as well as in mice, *Xenopus*, and humans (Kimble and Simpson, 1997; Greenwald, 1998). For example, Notch, a transmembrane receptor, involved in intercellular communication during cell fate decisions in *Drosophila* was discovered in the 1930's during genetic screens for genes involved in neuronal generation. Notch genes are found in *C. elegans*, *Xenopus*, mice, and humans where Notch seems to play a pivotal role throughout development into adulthood and in certain disease states (Reaume et al., 1992; Zagouras et al., 1995; Joutel et al., 1996; Gridley, 1997).

### *(2) Drosophila nervous system development*

Larval embryonic development of *Drosophila* takes 22 hours at 25°C and occurs in 16 stages (Doe, 1992). The first four steps in embryogenesis include (1) fertilization,

(2) blastoderm formation (stage 5), (3) cellularization of the blastoderm, and (4) gastrulation (stages 6 and 7; Figure 1.1; Ingham, 1988).

Before nervous system development begins, the major body plan of the embryo is established through determination of the anterior-posterior and dorsal-ventral axes. This is accomplished through expression of genes contributed by the mother (maternal effect genes) and those expressed by the embryo (Arenander and de Vellis, 1994). The anterior-posterior axis forms shortly after fertilization when maternal RNA encoding *bicoid* (anterior end) and genes of the *oskar* gene complex (posterior end) are expressed in the embryo. Segments along the anterior-posterior axis, which later give rise to specific body parts, are refined by expression of genes such as the gap genes (*hunchback*, *kruppel*, *knirps*), pair-rule genes (such as *runt* and *hairy*), segment polarity genes (such as *engrailed* and *wingless*), and homeotic genes (such as genes of the *antennepedia* complex; Ingham, 1988). The dorsal-ventral axis is initially established by expression of maternal RNAs (*snake*, *dorsal*, *tolloid*) and refined by zygotic genes such as *decapentaplegic* and *twist* (Ingham, 1988). Many of these genes are used again in nervous system development to impart unique neural identity according to positional information along the anterior-posterior and dorsal-ventral axes.

Once the major axes are established, nervous system development begins. The central nervous system of *Drosophila*, composed of the brain and ventral nerve cord, arises from the procephalic region and the ventral ectoderm, respectively (Figure 1.2). The peripheral nervous system comes from cells of the dorsal ectoderm (Bossing et al., 1996; Schmidt et al., 1997). The nervous system is established through specific processes, which can generally be broken down into six major steps (Jessell and Schacher, 1991): (1) neural precursor cells are generated in a specified pattern; (2)

specific cell types (neurons and glia) diversify from precursor cells; (3) cells migrate to their appropriate locations; (4) neurons extend axons to their targets; (5) synaptic connections between cells are formed; and (6) connections between neurons are modified, presumably through activity-dependent mechanisms. Big Brain activity aids in the first steps during the formation of neural precursor cells.

Neural precursor cells are "born" from a subset of the ectodermal cells, termed the neuroectoderm, which is positioned along the ventral midline of the embryo. Induction of neural potential in the neuroectoderm occurs by inhibition of *decapentaplegic* by *short gastrulation* in insects (Bier, 1997). Cells in the neuroectoderm are initially equivalent and must choose between one of two fates, neural precursors (neuroblasts) or epidermal precursors (epidermoblasts). The neural or epidermal fate is determined by the actions of two inter-related gene families, the proneural and neurogenic genes. The actions of these genes result in neuroblast formation in a spatially and temporally defined pattern. What are the molecular processes involved in neuroblasts formation? How are unique neuronal and glial cells differentiated from a neuroblast?

### ***(3) Neuroblast segregation and differentiation***

Each hemi-segment of a *Drosophila* embryo contains approximately 60-70 neuroectodermal cells. From these 60-70 cells, approximately 25 neuroblasts are generated (Doe, 1992). The molecular processes involved in neuroblast segregation have been extensively reviewed: Hartenstein and Campos-Ortega, 1984; Artavanis-Tsakonas and Simpson, 1999b; Greenspan, 1992; Doe, 1992; Campos-Ortega and Jan, 1991; and Doe and Goodman, 1985b. The first step in neuroblast segregation is

specification of a cluster of cells to have neural potential. This occurs through expression of a family of transcription factors, called the proneural genes (Figure 1.3). The further specification of one cell from within a proneural cluster to become the neuroblast occurs through an intercellular communication process, termed lateral inhibition. Experiments by Chris Doe and Corey Goodman suggested that inhibitory signaling between cells of a proneural cluster was responsible for selecting only one as the neuroblast. When a neuroblast from a grasshopper embryo is selectively removed by laser ablation, a surrounding cell within the proneural cluster replaces the neuroblast and gives rise to identical daughter cells (Doe and Goodman, 1985a). This result is consistent regardless of the location of the ablated neuroblast but is dependent on the presence of surrounding neuroectoderm cells. If the neuroblast and the surrounding neuroectoderm cells are removed, no replacement neuroblast is formed. These results suggest an interaction between cells of a proneural cluster to determine one as the neuroblast; the distinguished neuroblast then inhibits the remaining cells from acquiring the same fate (Doe and Goodman, 1985a). The neurogenic genes including *big brain* (Figure 1.3) govern lateral inhibition within a proneural cluster.

Each neuroblast is identified uniquely by its specific spatial location, temporal "arrival", pattern of expression of molecular markers (Schmid et al., 1999) and characteristic progeny (Doe and Skeath, 1996). Neuroblasts delaminate from the ectodermal surface and migrate dorsally within the embryo while the remaining cells of the cluster become epidermoblasts and give rise to the ventral epidermis (Doe and Goodman, 1985b). Neurons and glia are generated from the neuroblast through subsequent asymmetric divisions (Figure 1.4). The first divisions give rise to an average of five ganglion mother cells (GMCs; Doe, 1992). Ganglion mother cells each undergo

only one division to form specific neuronal or glial cells (Doe and Goodman, 1985b). In the peripheral nervous system, a similar process occurs with each neuroblast (termed a sensory organ precursor cell) dividing twice to yield one neuron and three support cells (Artavanis-Tsakonas and Simpson, 1999b).

#### (A) Proneural genes

Proneural clusters are specified through the actions of the proneural genes, including *extramachrochaete*, *ventral nervous system defective*, *atonal*, *single minded* and genes of the *achaete-scute* gene complex: *achaete*, *scute*, and *lethal of scute* (Campos-Ortega and Jan, 1991; Greenspan, 1992; Jan and Jan, 1994). Proneural genes are basic Helix-Loop-Helix (bHLH) transcription factors that can form heterodimers and influence cell fate by regulating transcription (Jan and Jan, 1994). Loss-of-function mutations in the proneural genes results in a reduced number of neuroblasts (Figure 1.3; Brand and Campos-Ortega, 1988) and conversely, introducing extra copies of proneural genes leads to an increase in the number of neuroblasts (Doe, 1992). Vertebrate homologues of *Drosophila* proneural genes have been identified and play similar roles in vertebrate neurogenesis (Chan and Jan, 1999; Chitnis, 1999).

The location of proneural cluster formation, defined by proneural gene expression will define subsequent patterns of expression of the neurogenic genes, including *big brain*. The actions of the neurogenic genes specify each neuroblast. Therefore, the processes that regulate the location of proneural cluster formation not only provide unique spatial identity to a neuroblast but also determine the spatial patterns of expression of the neurogenic genes. In each hemi-segment of the ventral nerve cord, proneural clusters are formed along the anterior-posterior and dorsal-ventral

axes in four columns (A-D) and three rows (medial, intermediate and lateral; Figure 1.5; Skeath et al., 1992). The proneural genes, *achaete*, *scute* and *lethal of scute* are expressed in a precise pattern in proneural clusters (Figure 1.5). Pair-rule but not segment polarity genes (used previously to establish the embryonic anterior-posterior axis) affect *achaete* and *scute* (but not *lethal of scute*) expression along the anterior-posterior axis within in each hemi-segment. For example, lack of function mutations in *fushi tarazu* and *paired* (two pair-rule genes) result in loss of proneural clusters in row D of even and odd numbered segments respectively (Figure 1.5; Skeath et al., 1992). Loss of *odd-skipped* function increases the clusters in row D posteriorly along the anterior-posterior axis (Figure 1.5; Skeath et al., 1992). Loss of the *Drosophila* EGF receptor results in expansion of *achaete* expression dorsally into the intermediate column of proneural clusters in columns B and D (Figure 1.5; Skeath, 1998; Udolph et al., 1998). Positional regulation of proneural gene function defines unique proneural clusters and therefore affects the specification of a neuroblast by the neurogenic genes. This is one mechanism to establish unique neuroblast identity.

### (B) Neurogenic genes

Once proneural clusters are defined, one cell differentiates as the neuroblast while the others are prevented from the same fate through the inhibitory actions of the neurogenic genes. Activation of the inhibitory signal confers epidermal precursor identity to the remaining cells of the cluster. Mutations in neurogenic genes that cause a lack-of-function result in a characteristic phenotype in flies: hypertrophy of the central and peripheral nervous system and lack of ventral epidermis (Figure 1.3; Lehmann et al., 1983). *big brain (bib)* was one of the earliest identified neurogenic genes along with

*Notch, Delta, mastermind, neuralized, and the Enhancer of split gene complex* (Lehmann et al., 1983). Based on genetic analysis of epistatic relationships *Notch, Delta, mastermind, neuralized* and *Enhancer of split genes* appear to act in a hierarchical manner (i.e. a pathway) but *bib* may regulate epidermal cell fate through a different or parallel pathway (de la Concha et al., 1988).

Cloning and biochemical studies have defined interactions between the neurogenic gene products. From these studies the framework for a lateral inhibition signaling pathway has been established and begins on the cell surface by interaction of Delta (on the presumptive neuroblast) with the Notch receptor (on the presumptive epidermoblast; Figure 1.6; Fehon et al., 1990). Activation of Notch by Delta, results in translocation of Suppressor of Hairless from the cytoplasm to the nucleus where it activates transcription of genes in the Enhancer of split complex (Figure 1.6; Fortini and Artavanis-Tsakonas, 1994; Artavanis-Tsakonas et al., 1995; Artavanis-Tsakonas et al., 1999a). Enhancer of split transcription factors down-regulate proneural genes.

However, Notch signaling is probably more complicated than this simple scheme predicts. Other neurogenic genes function to regulate this pathway. For example, *deltex* (a cytoplasmic protein) interacts with intracellular domains of Notch (Diederich et al., 1994). *Deltex* interaction with Notch prevents Suppressor of Hairless binding to Notch intracellular domains (Matsuno et al., 1995). Additional ligands for the Notch receptor have been identified (such as *Serrate*); and modification of ligand-receptor interactions occurs via *fringe*, which promotes the Notch-Delta interaction but inhibits the Notch-Serrate interaction (Artavanis-Tsakonas et al., 1999a). *kuzbanian* encodes a metalloprotease that appears to cleave intracellular domains of Notch at the plasma membrane (Pan and Rubin, 1997). Notch is also post-translationally cleaved in the

Golgi network and may exist as a heterodimer (between extracellular and intracellular domains) on the cell surface (Blaumueller et al., 1997). Regulation of Notch signaling by expression of different ligands or accessory proteins, post-translational processing and spatial distribution of both Notch and regulatory proteins is a mechanism to establish specific and unique cellular identities within a common signaling network. However, the functions of many known neurogenic genes, including *bib*, within this pathway remain unclear.

*big brain* is unique among the neurogenic genes in many aspects. In contrast to the other neurogenic genes, the *bib* gene product has sequence identity to the Major Intrinsic Protein family of channels (Rao et al., 1990). Mutations in genes of the *achaete-scute* gene complex have no effect on the neurogenic phenotype induced by lack-of-function mutations of *bib* (Brand and Campos-Ortega, 1988). No genetic interaction was found between *bib* and *Notch*, *Delta*, *Enhancer of split*, *mastermind* or *neuralized* (de la Concha et al., 1988). Although *bib* mutation causes a neurogenic phenotype in embryonic central and peripheral nervous systems, the phenotype is less extreme than for other neurogenic genes (Lehmann et al., 1983; Rao et al., 1992). From these studies, it seems that *bib* does not function within the Notch signaling pathway. However, the *bib* gene product (BIB) is expressed in domains overlapping with the other neurogenic genes, and on the plasma membrane of ectodermal cells during neuroblast differentiation (Doherty et al., 1997). Therefore, *bib* is expressed in the correct locations and at the correct times to be influencing cell fate determinations during neurogenesis. Clues to how *bib* expression might influence development can be found in how ion channels cause developmental changes in excitability and from studies on the structure and function of channels in the Major Intrinsic Protein family.

#### ***(4) Ion channels in neuronal development***

The importance of ion channels to developmental processes is evident by their expression in oocytes even before fertilization (Dascal, 1987; Moody, 1995). *Xenopus laevis* oocytes endogenously express calcium-dependent and hyperpolarization-activated chloride channels, as well as calcium, sodium and potassium channels (Dascal, 1987). After fertilization, a wave of depolarization spreads over the oocyte and may serve as an electrical block to polyspermy until mechanical barriers are in place. In amphibians, the depolarization wave is mediated by an outward chloride conductance (Dascal, 1987; Moody, 1995). In general, after the fertilization-induced depolarization, excitability decreases until cellular differentiation begins (Moody, 1998b).

Electrical excitability often occurs spontaneously (*i.e.* due to unknown mechanisms) and probably serves to enlist second messenger pathways important for development of mature cellular phenotypes, firing patterns and connectivity (Moody, 1998a). For example, in *Xenopus* primary spinal neurons, spontaneous increases in intracellular calcium occur with two different frequencies, classified as spikes and waves (Spitzer and Ribera, 1998). Calcium spikes occur with low frequency (~3/hr), are due to calcium dependent action potentials and regulate changes in transcription. Higher frequency (~8/hr) calcium waves result from calcium leak and typically occur in growth cones where they affect cytoskeletal properties important for axonal pathfinding (Spitzer and Ribera, 1998).

The electrical activity of a cell reflects underlying channel expression profiles. Neuroblasts and their progeny have changes in electrical excitability that may provide clues to the properties of the channels themselves or how they function to determine cell

fate. The dorsal unpaired median (DUM) neuroblast is located on the midline of grasshopper embryos in between the left and right hemi-segments and is surrounded by the ventral neuroblasts in each segment (Goodman and Spitzer, 1979). DUM neuroblasts have resting membrane potentials between -60 and -80mV, while the surrounding ectodermal cells are slightly more depolarized (-40 to -60mV). At day 8 of development, the DUM neuroblasts are electrically and dye-coupled to the surrounding neuroblasts and ectodermal cells suggesting the presence of gap junctional communication (Goodman and Spitzer, 1979). The neuroblasts stay coupled until they stop dividing and degenerate (around day 15). The neuroblast progeny lose coupling to the neuroblast at approximately the same time that they acquire the ability to elicit action potentials, around day 11, implying a loss of gap junctional communication (Goodman and Spitzer, 1979). Ion channel expression profiles reflect these activity changes; treatment of neuroblasts or neuronal progeny with veratradine (a sodium channel activator) does not cause depolarization until day 12 in the oldest DUM progeny (Goodman and Spitzer, 1979). This general pattern is the same for the progeny of another neuroblast, MP3 (Goodman and Spitzer, 1981). Two general conclusions can be made from these experiments. First, during neuroblast differentiation there may be a link between transmembrane signaling and changes in membrane potential. Secondly, changes in ion channel gene expression reflect changes in electrical properties.

Neural cells are able to generate action potentials once they become electrically uncoupled from their "parent" neuroblast. The action potential waveform is further refined during development. *Xenopus* spinal neurons elicit long duration (100ms), calcium dependent action potentials. Within one day the action potential duration decreases (to 1ms) and becomes sodium dependent (O'Dowd et al., 1988). Although

the contribution of calcium to the action potential diminishes, there are no changes in the calcium currents. The switch to sodium dependent fast action potentials reflects increases in sodium current density (via increased single channel conductance, increased open probability or the number of channels), increases in  $K_V$  and  $K_{Ca}$  currents, and development of faster inactivation in the  $K_V$  current (O'Dowd et al., 1988). Longer duration action potentials in immature neurons are a property of many cell types (Moody, 1998a). Depolarized membrane potentials of neurons early in development may reflect an underlying need to generate sufficient influx of calcium ions for intracellular signaling and establishment of adult patterns of protein expression. Changes in the subunit composition of acetylcholine receptors during development further support this idea.

In bovine fetal muscle, acetylcholine receptor channels are composed of  $\alpha$ ,  $\beta$ ,  $\delta$  and  $\gamma$  subunits but after birth are composed of  $\alpha$ ,  $\beta$ ,  $\delta$  and  $\epsilon$  subunits (Mishina et al., 1986). Fetal acetylcholine receptors, have longer open times but smaller single channel conductances (5ms, 40pS) than adult channels (1ms, 60pS; Mishina et al., 1986). These activity changes parallel development of muscle innervation at adult stages and may have functional consequences, since opening of fetal channels would result in larger depolarizations (Moody, 1998b).

In addition to the subunit composition of the ion channels themselves, developmental expression of regulatory proteins alters cellular excitability. Ion channels exist on the plasma membrane within protein complexes as evidenced from excised patches in which expressed channels are modified by levels of ATP as well as kinase and phosphatase inhibitors (Chung et al., 1991; Molokanova et al., 2000). Recently, a molecular complex of voltage-gated sodium channels and receptor tyrosine phosphatases was found in rat brain (Ratcliffe et al., 2000).  $Na^+$  channel  $\alpha$ -subunits

interact with the carbonic anhydrase domain of PTP $\beta$  while the  $\beta 1$  Na $^+$  channel subunit interacts with the catalytic D1 and D2 domains of PTP $\beta$  (Ratcliffe et al., 2000).

Interaction of PTP $\beta$  with Na $^+$  channels expressed in tSA-201 cells shifts the voltage-dependent inactivation to more depolarized membrane potentials thereby increasing Na $^+$  channel currents (Ratcliffe et al., 2000). PTP $\beta$  exists in three isoforms; the short and long forms (containing the catalytically active D1 and D2 domains) are expressed at postnatal day 1 but by postnatal day 16 only the phosphacan form (lacking D1 and D2) is expressed in rat brain (Ratcliffe et al., 2000). Expression of short and long forms of PTP $\beta$  enhances cellular excitability early in development but changes in PTP $\beta$  expression (to the phosphacan form) decrease excitability in mature rats.

In summary ion channels have three fates during development: (1) embryonic channels are retained in the mature cell; (2) expression of the channels is modified either by changes in subunit composition (as for the acetylcholine receptor) or associated regulatory proteins (as with the Na $^+$  channel-RPTP $\beta$  interaction); or (3) embryonic channels are down-regulated in the mature state (as with loss of gap-junctional coupling between the DUM neuroblast and its progeny (Goodman and Spitzer, 1979; Moody, 1998a).

If the *bib* gene product (BIB) functions as an ion channel, changes in membrane potential may be a regulatory mechanism in establishing cell fate. This idea fits logically with studies of electrical excitability in neuroblasts and surrounding non-neural cells in grasshopper embryos. Non-neural cells of the ectoderm have depolarized membrane potentials compared to differentiated neuroblasts (Goodman and Spitzer, 1979). How does an ion channel function for BIB fit in with established channel properties in the Major Intrinsic Protein family?

## 1.2 MAJOR INTRINSIC PROTEIN FAMILY

Since the cDNA cloning of *big brain* revealed a channel with sequence identity to channels of the Major Intrinsic Protein (MIP) family, the properties of these channels may provide insight into a function of Big Brain during neurogenesis. The MIP family was named after the major intrinsic protein of the bovine lens fiber (now called AQP0), which was cloned in 1984. The cloning of AQP0, revealed a 263 amino acid protein predicted to have six transmembrane domains and intracellular amino and carboxy termini (Gorin et al., 1984). AQP0 was initially thought to be a component of gap junctions in the lens (Girsch and Peracchia, 1985; Nikaido and Rosenberg, 1985). No similar proteins were identified by database searches in 1984 (Gorin et al., 1984). The existence of the MIP family was noted after the cloning of GlpF from *E. coli* and Nodulin 26 from soybean root nodules (Baker and Saier, 1990). Approximately ten years later the MIP family is known to encompass over 150 channels found throughout all phyla.

MIP channels are broadly classified based on their permeabilities and have traditionally been segregated into classes permeable to water (aquaporins) and those permeable to small chain hydrocarbons such as glycerol (aquaglyceroporins; Park and Saier, 1996). However, classification of permeability into two groups is probably shortsighted as early studies showed that AQP0 and Nodulin 26 reconstituted in lipid bilayers were ion channels (Ehring et al., 1990; Weaver et al., 1994). The mammalian aquaporins (AQPs) have been extensively studied and are distributed throughout the body in areas such as the eye, brain and kidney where water and solute movement are critical for proper organ function (King and Agre, 1996). The identification of AQP1 as an ion channel (Yool et al., 1996) while initially controversial brought ion permeation of

MIP channels into the forefront and generated significant interest in understanding mechanisms of selectivity and regulation of ion permeation. Several MIP channels have permeability to both water and small chain hydrocarbons. Notable in this group is AQP9, permeable to water, carbamides (urea and thiourea), polyols (glycerol, mannitol, sorbitol), uracil, adenine and monocarboxylates (lactate and  $\beta$ -HB; Tsukaguchi et al., 1998). The varying permeabilities of MIP channels have prompted investigations into how the unifying features of MIP channels provide for common functions, how the structure provides selectivity, and how channel activity is regulated.

#### ***(1) Structure and Function of MIP channels***

The predicted transmembrane topology of MIP based on the analysis of amino acid hydrophobicity is six transmembrane domains (TM1-6) with intracellular amino and carboxy termini (Figure 1.7). The three extracellular loops are referred to as Loop A, C and E, and the two intracellular loops are B and D (Preston and Agre, 1991). This subunit topology was confirmed by cleavage analysis of AQP1 engineered with novel chymotrypsin sites at various positions along the protein and also with antibodies generated against peptides from Loop C, E and the carboxy tail of AQP1 (Preston et al., 1994; Stamer et al., 1996).

Each channel is composed of four individual subunits that span the membrane six times (Smith and Agre, 1991; Borgnia and Agre, 2001). The functional significance of tetramerization is unclear. Results from early studies of oligomerization states with sucrose gradient sedimentation suggested that the aquaglyceroporins are monomers unlike the tetrameric aquaporins (Lagrée et al., 1998). Comparison of the amino acid sequence of Loop E between AQP<sub>cic</sub>, an insect water channel and GlpF, the *E. coli*

glycerol facilitator, demonstrated four amino acids that differed in this region between AQPcic and GlpF. Mutation of the amino acids in AQPcic to the corresponding amino acids in GlpF and expression of mutated AQPcic in *Xenopus* oocytes or yeast resulted in glycerol permeable AQPcic channels, AQPcic channels that had sucrose gradient sedimentation coefficients indicative of monomers (similar to GlpF), or both (Lagrée et al., 1998). Thus, a functional difference for tetrameric and monomeric channels was proposed: water permeable channels are tetramers while those permeable to glycerol are monomers.

However, two recent papers demonstrated that the oligomerization state of GlpF was sensitive to the composition of the sucrose gradient (Borgnia and Agre, 2001; Manley et al., 2000). Increasing the ionic strength of the sucrose gradient shifted the location of GlpF into higher density fractions indicative of tetramers (Borgnia and Agre, 2001). Extraction of GlpF with SDS resulted in predominantly monomeric channels, confirming the results by Lagrée and colleagues (1998), but when urea (4M) was included, a range of molecular weights was obtained corresponding to monomers, dimers, trimers and tetramers (Manley et al., 2000). Taken together these results suggest that the affinity of GlpF subunits for each other is lower than that of the aquaporins (such as AQPcic) and confirms that GlpF can form tetramers similar to the aquaporins. In summary, MIP channels are tetramers and each subunit spans the membrane six times. Within this common structural framework, the amino acid sequences of the channels show similarities in regions such as the transmembrane domains but differences in putative pore regions and amino and carboxy termini.

### **(A) Sequence alignments**

MIP channels have two highly conserved sequence motifs, N-P-A (asparagine – proline- alanine) in Loops B and E. Sequence analysis of the 18 members cloned in 1993, revealed that in addition to the conserved N-P-A motifs, two glutamates (E) in TM 1 and 4 and two glycines (G) in TM 3 and 6 are conserved (Reizer et al., 1993). Figure 1.8 shows an alignment of BIB, AQP0, AQP1 and GlpF with the conserved amino acids N, P, A, E, and G boxed. The conservation of these amino acid residues suggests they are critical for channel structure or selectivity; however, of these highly conserved residues only the NPA motifs and the residues immediately surrounding them have been mutated to determine the effect on channel permeability.

MIP channels have internal similarity; the primary structure between transmembrane domains 1-3 is similar to that of transmembrane domains 4-6 (homologous transmembrane domains are indicated by color in Figure 1.7). In distantly related MIP channels, transmembrane domains 1-3 are more similar to each other than transmembrane domains 4-6. In contrast, closely related MIP channels have greater amino acid sequence identity in transmembrane domains 4-6. This suggests that transmembrane domains 1-3 are important for common functions (*i.e.* for channel assembly, structure or membrane insertion) while transmembrane domains 4-6 confer unique features to channel function (*i.e.* channel specificity or regulation).

Sequence comparison of mammalian aquaporins, Nodulin 26 and BIB based on known channel permeabilities showed no substantial differences in Loop B based on grouping by permeability, emphasizing the potential importance of this region for common functions of MIP channels (Yool and Stamer, 2001). However, alignment of

residues in Loop E with respect to the last residue in the sequence NPARX (shaded in gray in Figure 1.8), sorted channels into three main groups: those with the sequence NPARS, NPARD or NPARA. The first group, with the sequence NPARS, included water and ion-conducting channels such as AQP1, bovine MIP, Nodulin 26 and Big Brain (Yool and Stamer, 2001). The second group, with the NPARD motif, contained the aquaglyceroporins, AQP3, AQP7 and AQP9. The third group, NPARA, contained only AQP8, a water permeable channel expressed in testis (Ishibashi et al., 1997). *Identification of novel MIP family members will likely add more proteins to this third group.*

The results of sequence comparisons show that the similar transmembrane topology and tetrameric channel structure of MIP channels is the result of underlying amino acid sequence identity. In contrast, unique channel properties are the result of specific amino acid residues in putative pore-lining regions and putative regulatory domains. Mutagenesis and domain swapping in these regions have supported their role in channel selectivity.

#### **(B) Mutagenesis and chimeric analyses**

Point mutations and chimeric analysis of channels is one way to test the role of specific amino acid residues that are important for conferring unique channel properties, such as selectivity for water or ions over glycerol. Sequence comparison of BIB with channels in which these analyses have been performed may provide information regarding the properties of Big Brain channels.

Mercurial reagents inhibit the water permeability of AQP1 (Preston et al., 1992). Mutations that alter mercury block were used to determine potential pore-lining residues

Site-directed mutagenesis of the four cysteine residues of AQP1 to serine (C87S, C102S, C152S and C189S; Figure 1.9) had a variety of effects on the ability of HgCl<sub>2</sub> to block water permeability of wild type and mutant AQP1 channels expressed in *Xenopus* oocytes (Preston et al., 1993). Since mercury binds to sulfhydryl groups, a mutation from cysteine to serine should abolish HgCl<sub>2</sub> block if the cysteine resides in or near the water pore. Mutation of C189, located in Loop E, to serine was the only mutant that no longer exhibited block by HgCl<sub>2</sub>, suggesting that C189 lines the water pore. Additional mutations of C189 to alanine (A), valine (V), methionine (M), tryptophan (W) and tyrosine (Y) had various effects. C189V, C189M, C189W and C189Y had altered glycosylation patterns on western blots suggesting a processing defect but C189V still exhibited water permeability, albeit reduced. Preston and colleagues proposed that C189 resides in or close to the water pore and that it is critical for proper function and processing of the channel.

Follow-up studies with cysteine scanning mutagenesis in Loops B and E gave rise to a possible structure for the water pathway for AQP1 (Jung et al., 1994). Using the C189S mutant as a background, amino acids in Loop E between 187-197 were individually mutated to cysteine and expressed in *X.* oocytes. All mutants had decreased water permeability (compared to oocytes expressing wild type or C189S AQP1) that was further reduced by 1mM HgCl<sub>2</sub> (Jung et al., 1994). Alanine 73, in Loop B is in an equivalent position to C189 in Loop E. HgCl<sub>2</sub> inhibited water permeability of oocytes expressing the double mutant A73C/C189S. Because A73 and C189 are at equivalent positions in each half of AQP1, the hourglass model was proposed in which the N-P-A motifs of Loops B and E form a constriction in a water pathway through each subunit (Figure 1.10; Jung et al., 1994).

Additional evidence for the involvement of the amino acids in Loop E in water conductance was further supported by novel findings of a non-mercurial blocker of AQP1 (Brooks et al., 2000). The similarity in subunit topology between aquaporins and K<sup>+</sup> channels was the basis for looking at the effect of the K<sup>+</sup> channel blockers, TEA (tetraethylammonium chloride), TMA (tetramethylammonium), TPA (tetrapropylammonium), and clofilium on AQP1 water permeability. 100μM TEA blocked water permeability of AQP1 by 20-40% to a level equivalent to that of 300μM HgCl<sub>2</sub> (Brooks et al., 2000). The molecular basis of this inhibition was investigated with site-directed mutagenesis at tyrosine 186, located three residues away from C189, the proposed site of mercury inhibition of water permeability. Three Y186 mutants were constructed: Y186F, Y186N, and Y186A. Y186N and Y186A lacked water permeability as well as appropriate glycosylation patterns on western blots; however Y186N appeared to be on the plasma membrane as determined with confocal microscopy (Brooks et al., 2000). Mutation of Y186 to phenylalanine, a more conservative substitution, resulted in functional water channels that lacked sensitivity to TEA but remained sensitive to block by HgCl<sub>2</sub> (Brooks et al., 2000). These results provided the first non-mercurial blocker for an aquaporin, supported the involvement of Loop E as a pore lining region of the water channel, and may provide a starting point for drug development.

AQP0 has low water permeability compared to other aquaporins (Chandy et al., 1997; Yang and Verkman, 1997). AQP2 has a single channel water permeability 13 times greater than that of AQP0 (Yang and Verkman, 1997). Kuwahara and colleagues (1999), capitalized on this fact and made chimeras between AQP0 and AQP2. Twelve chimeras with portions of Loops B, C, D and E of AQP2 spliced into the appropriate

regions of AQP0 were tested for osmotically induced swelling in *Xenopus* oocytes and yeast cells (Kawahara et al., 1999). Only AQP0 mutants that contained portions of Loop E from AQP2 exhibited water permeability greater than wild type channels. Water permeability equivalent to that of AQP2 was obtained in chimeric AQP0 channels that incorporated the cytoplasmic portion of helix 5 and the entire Loop E region of AQP2. Conversely, when the cytoplasmic portion of helix 5 of AQP0 was transferred to AQP2 chimeric channels exhibited water permeability equivalent to wild type AQP0 (Kawahara et al., 1999).

Amino acids in Loop B contribute to the anion selectivity of Aquaporin 6 (AQP6). *Xenopus* oocytes expressing AQP6 have no detectable water permeability. Acidic pH activates an anion selective conductance in oocytes expressing AQP6 ( $P_{Na^+}/P_{Cl^-} = 0.28$ ). Sequence scanning suggested that the positively charged lysine at position 72 (located in Loop B) might have an effect on ionic selectivity. Two mutants were constructed, K72E and K72H (Yasui et al., 1999a). Mutation of K72 to H had no effect on pH-stimulated ion currents in AQP6-expressing oocytes, whereas mutation of K72 to E shifted the relative ionic permeability of sodium and chloride ( $P_{Na^+}/P_{Cl^-}$ ) from 0.28 to 1.13 (Yasui et al., 1999a). These results suggest that Loop B influences the ion pore in AQP6 and thereby affect selectivity directly, or indirectly by affecting the structure of AQP6 within the bilayer.

Together, these examples of mutational and chimeric analyses of aquaporins in the MIP family determined that Loops B and E line a pathway for water or ions. Where are these regions located in the three-dimensional channel structure? Where is the location of the pore in these channels?

### (C) Crystallographic analysis of MIP channels

Crystallographic analysis of MIP channels has the potential to provide structural information at the molecular level. This type of information is particularly intriguing for MIP channels since structural information may provide information as to how the same basic structure can result in channels with a variety of permeabilities.

Despite the limitations involved in crystallizing membrane bound proteins (Walz and Grigorieff, 1998; Rigaud et al., 2000), X-ray and 2-D crystal structures have been solved for a number of MIP channels, particularly AQP1. Early studies were of sufficient resolution only to confirm that AQP1 exists as a tetramer (Walz et al., 1994b; Walz et al., 1994a; Jap and Li, 1995; Walz et al., 1996). Interestingly, each of these studies revealed the same point group symmetry (P4<sub>2</sub>,2) of AQP1 despite differences in lipid composition, source of AQP1 and the sugar used in the embedding medium. The predicted arrangement of the  $\alpha$ -helical transmembrane domains of each subunit is shown in Figure 1.10 (de Groot et al., 2000).

A 3.8Å resolution structure, sufficient to visualize protrusions corresponding to individual amino acid side chains, was recently obtained from 2D crystals embedded in trehalose. The resulting structure is shown in Figure 1.11A with transmembrane domains 1-3 colored gold, transmembrane domains 4-6 colored blue and Loops B and E in green (Murata et al., 2000). Within each subunit there is a pseudo two-fold symmetry axis that is the result of the internal sequence similarity between transmembrane domains 1-3 and transmembrane domains 4-6 (dashed white line in Figure 1.11A). At the center of AQP1 tetramer is a four-fold axis of symmetry (yellow circle; Figure 1.11A). Amino acids surrounding the four-fold axis are contributed by helices 2 and 5 of each subunit. van der Waal's interactions between prolines in the conserved N-P-A motifs are

predicted to stabilize the interaction between Loops B and E, confirming the hourglass model of water pore structure (Jung et al., 1994).

A major drawback to the crystallographic analysis by Murata and colleagues was the lack of resolution of water molecules in the electron density map used for the atomic model. However, using their atomic model and results of previously described mutagenesis studies, a model of water permeation through each subunit was predicted. In their model, the pore (approximately 5Å in diameter) has a constriction at the center (3Å, a size just slightly larger than a water molecule - 2.8Å; Murata et al., 2000) that would constrain water molecules into a single file column. The positive ends of helix dipoles of Loops B and E may induce a water molecule to reorient perpendicularly to the channel axis forcing it to break its hydrogen bonds with surrounding water molecules. To compensate for this bond breakage, N76 and N192 (from the NPA motifs of Loops B and E) may serve as a selectivity filter, forming hydrogen bonds with the oxygen of a water molecule. The hydrophobic nature of the other pore lining residues combined with the narrow diameter of the pathway were proposed to be critical for water selectivity and the high permeability of water through the channel (Murata et al., 2000; Unger, 2000).

Interestingly, the central area at the four-fold axis of symmetry was dismissed as a possible pathway for water (or any other solute) for AQP1. This "central pore" is surrounded by helices 2 and 5 and a 3.5Å opening at the extracellular surface opens up to 8.5Å at the center of the bilayer. The small opening at the extracellular surface and hydrophobic lining of the interior was proposed to occlude solutes (Murata et al., 2000).

Ren and colleagues proposed a similar model for AQP1 with results from a density map obtained at 3.7Å resolution, only slightly better than that obtained by Murata and colleagues. An atomic model was fit to the data based on AQP1 subunit topology

put forth in previous studies (de Groot et al., 2000) and refined with predictions on pore lining residues (Heymann and Engel, 2000). The four-fold symmetry axis was also bounded by helices 2 and 5 of each subunit. A curved pathway for water within each subunit, with a bend of approximately  $25^\circ$  near the asparagines at the pore constriction was predicted. This curved pathway was proposed to promote an increase in hydrogen bond strain, or disrupt the hydrogen-bonding network of adjacent water molecules, or both (Ren et al., 2000). Hydrogen bonds between E17 and Q101, and between H69 and T80 are thought to stabilize the interactions between Loops B and E (Ren et al., 2000).

In general, the conclusions drawn from crystallographic data on AQP1 are limited by the lack of resolution of water molecules and ions in the structure. The low resolution requires that any proposed atomic model be the result of fitting data with previously determined topologies and sequence analyses. While these methods are proving useful in aiding in the structural determinations of AQP1, elucidation of the water pathway, and ion pathway await further improvements in resolution that are typically seen only with 3D crystals used for X-ray crystallography.

Better resolution has been achieved for *E. coli* glycerol facilitator GlpF. The reported crystal structure of GlpF, at 2.2Å resolution, was obtained from crystals embedded in glycerol (Fu et al., 2000). GlpF crystallized with properties similar to those of AQP1: a tetramer with a four-fold axis of symmetry at the center and pseudo-two-fold axes in the plane of the bilayer through each subunit (Figure 1.11B). Two exciting findings resulted from this crystal structure. First, because glycerol was used in the embedding medium, and sufficient resolution was obtained, the glycerol pathway could be determined. Three molecules of glycerol were found in pores within each subunit. The selectivity for glycerol over water by GlpF is achieved by two elements. The

extracellular region of each subunit is lined by W48 (helix 2) and F200 (Loop E); these two residues appear to form a “hydrophobic corner” and may interact with the carbon backbone of glycerol. R206 (immediately following the NPA motif in Loop E) forms hydrogen bonds with 2 OH<sup>-</sup> groups of glycerol. The rest of the pore is amphiphilic and glycerol is proposed to move progressively through the pore with successive hydrogen bonding on one side, including interactions between the asparagines of the NPA motifs in each loop (N68 and N203; Fu et al., 2000). Water permeation is thought to be prevented due to energetic constraints. The 3.8Å pore diameter prevents a water molecule from interacting with other water molecules but the pore is too large to compensate for the cost of dehydration. This mechanism is similar to that which prevents Na<sup>+</sup> ions from permeating the KcsA channel (Doyle et al., 1998). Visualization of glycerol within each individual subunit is direct confirmation that each subunit contains a pore for glycerol.

The second exciting finding was two Mg<sup>2+</sup> ions located at the four-fold axis of symmetry. Members of the ion channel gene family (such as potassium and cyclic nucleotide-gated channels) form ion pores at the four-fold axis of symmetry (Hille, 1992; Doyle et al., 1998). Similar to the central pore area of AQP1, helices 2 and 5 line the central pore of GlpF (Figure 1.12A). Mg<sup>2+</sup> ions interact with W42 and E43 (of helix 2; Figure 1.12B; Fu et al., 2000). Electrophysiological experiments suggested that GlpF was not a voltage-gated ion channel (Maurel et al., 1994). However, other MIP channels have ion channel activity regulated by second messenger pathways or pH (see below). The finding of Mg<sup>2+</sup> at the four-fold axis could have several implications: (i) Mg<sup>2+</sup> is blocking an additional central glycerol conducting pathway; (ii) Mg<sup>2+</sup> ions in the central pore stabilize the tetrameric structure of GlpF (Borgnia and Agre, 2001); or (iii) the four-

fold axis is an ion conducting pathway but  $Mg^{2+}$  is not permeable in this conformation of GlpF.

Despite the different permeabilities of GlpF (glycerol) and AQP1 (water) as well as their organism of origin, *E. coli* (GlpF) and human (AQP1), both have striking similarities in composition (tetrameric) and pore sizes. Therefore, it is likely that BIB also has similar properties. Several questions remain unanswered: (i) What is the mechanism of water permeation through aquaporins? (ii) How do both water and glycerol permeate aquaglyceroporins? (iii) Where is the ion pore? (iv) What are the effects of gating mechanisms on structure? The answers to these questions are important for understanding the structural and functional relationships among MIP channels, but also for understanding how the regulation of channel activity might alter their structure or for insight into how BIB activity might be regulated.

## ***(2) Regulation of MIP function***

Regulation of channel activity for channels in the MIP family is accomplished through a variety of mechanisms: phosphorylation, pH, binding of cyclic-nucleotides and protein translocation. Phosphorylation regulates the function of many classes of ion channels (Levitan, 1994) and has a variety of effects on MIP channels. The  $\alpha$ -TIP aquaporin found in plant seeds contains five consensus sites for phosphorylation (S7, S23, S99, S125 and S131) by protein kinase A (PKA). When expressed in *X. oocytes*  $\alpha$ -TIP has an apparently constitutive water permeability. However, oocytes expressing  $\alpha$ -TIP mutants S7A, S23A and S99 exhibited decreased water permeability (Maurel et al., 1995). *In vitro* kinase assays with oocyte plasma membrane fractions and the catalytic subunit of PKA showed that wild-type  $\alpha$ -TIP channels were phosphorylated. Channels

with mutated PKA consensus sites, serines 7, 23 and 99 all mutated to alanine, were not phosphorylated. Mammalian aquaporins are also regulated by phosphorylation. Protein kinase C (PKC) has inhibitory effects on AQP4 expressed in *X. oocytes*.

Pharmacological activators of PKC, PDBu (phorbol 12,13-dibutyrate) and PMA (phorbol 12-myristate 13-acetate) inhibited water permeability in a dose-dependent manner (Han et al., 1998). AQP4 from rat brain homogenates was phosphorylated by PKC in an *in vitro* kinase assay (Han et al., 1998).

Water and ion permeability are regulated through different mechanisms for AQP0. AQP0 channels isolated from bovine lens are ion channels and have a single channel water permeability much less than that of other aquaporins (Chandy et al., 1997; Yang and Verkman, 1997). AQP0 channels reconstituted into lipid bilayers had two main ion conductance states in 100mM KCl, 380 and 160pS; depolarized membrane potentials shifted AQP0 to lower conductance states indicating a voltage dependent open probability (Ehring et al., 1990). Phosphorylation of AQP0 by PKA resulted in a shift to a voltage-independent state with no effect on single channel conductance (Ehring et al., 1991). Changes in pH and calcium concentration had no effect on ion channel properties (Ehring et al., 1990) but altered the water conduction properties (Németh-Cahalan and Hall, 2000). Decreasing extracellular calcium or lowering pH to <7.5 caused an increase in water permeability. Histidine 40, located in the first extracellular loop, was determined to be the pH sensitive residue since oocytes expressing the AQP0 mutants H40A, H40D and H40K were no longer sensitive to changes in pH or changes in extracellular calcium (Németh-Cahalan and Hall, 2000). The calcium effect is probably intracellular, since inhibitors of the calcium dependent protein, calmodulin, also increased water permeability. The regulation of both water and ion flux in AQP0 have

important physiological consequences since AQP0 is a major component of the lens (60% of the membrane protein content; Németh-Cahalan and Hall, 2000) and mutations in AQP0 cause cataract formation in mice (Shiels and Bassnett, 1996).

Aquaporin-1 forms non-selective cation channels in *X. oocytes* (Yool et al., 1996; Anthony et al., 2000). AQP1 ion channels are activated by cGMP binding and have large single channel conductance (150pS; Anthony et al., 2000). cGMP applied to excised patches induced a conductance in AQP1-expressing but not control oocytes. Specific binding of cGMP to membranes of Sf9 insect cells expressing AQP1 suggests that cGMP binds directly to AQP1 (Anthony et al., 2000). The carboxy tail of AQP1 has intriguing identity to binding regions in cyclic nucleotide-gated channels of retinal and olfactory cells (Anthony et al., 2000). Multiple regulators may affect AQP1 channels since an AQP1 carboxy tail fusion peptide is phosphorylated by PKA catalytic subunits *in vitro* (Yool et al., 1996) and AQP1 from rat kidney homogenates is also phosphorylated by PKA catalytic subunits (Han and Patil, 2000). Forskolin stimulation of oocytes expressing AQP1 causes an increase in water permeability (Yool et al., 1996; Patil et al., 1997).

AQP2 is translocated from intracellular vesicles to the apical plasma membrane of collecting duct cells in the inner medulla by the antidiuretic hormone arginine vasopressin (Sasaki et al., 1998). The trafficking of AQP2 requires the phosphorylation of S256 of AQP2 by PKA (Kawahara et al., 1995; Fushimi et al., 1997) as well as an interaction between PKA and protein kinase A anchoring proteins (Klussmann et al., 1999). Abnormalities in AQP2 trafficking to the apical membrane result in nephrogenic diabetes insipidus (King and Agre, 1996).

In addition to regulation of aquaporins through post-translational mechanisms, levels of expression of aquaporins can be regulated transcriptionally. The 5'-untranslated region of the AQP2 gene contains a cyclic-AMP response element (CRE) binding site as well as TATA and GATA boxes (Sasaki et al., 1998). AQP2 mRNA levels are increased following dehydration in rats (Sasaki et al., 1998). Growth factor stimulation induces transcription of two sets of genes in mouse fibroblast 3T3 cells; immediate-early response genes, activated within minutes after stimulation and delayed early response genes, activated after a few hours presumably by immediate early transcription factors (Lanahan et al., 1992). An mRNA with 94% identity to AQP1 was present by four hours after stimulation of 3T3 cells with fetal bovine serum, fibroblast growth factor and PDGF (Lanahan et al., 1992). Transcriptional regulation of aquaporins is also apparent during development and may provide insight into a vertebrate homologue of BIB.

### *(3) Developmental expression of aquaporins*

Aquaporins 1 and 4 are abundantly expressed in the brain; AQP1 is localized in the choroid plexus and AQP4 is predominantly found in glial cells (Nielsen et al., 1997; Nagelhus et al., 1998). Two AQP4 proteins, differing by the length of the amino terminus, have been identified (here referred to as AQP4-1 and AQP4-2; Smith et al., 1996; Zelenin et al., 2000). Reverse transcriptase-polymerase chain reaction analysis of adult and two-day old mice revealed differential expression of the two AQP4 isoforms. AQP4-1 mRNA was abundant in the brain and expressed as early as postnatal day 2 but was twice as abundant in adult (Zelenin et al., 2000). In contrast, low levels of AQP4-2 mRNA were found in the brain at all ages. High levels were found in lungs at postnatal

day 2 but the expression decreased into adulthood (Zelenin et al., 2000). A similar pattern was observed for AQP4-2 in the kidney (Zelenin et al., 2000).

Wen and colleagues studied the expression patterns of AQP4 protein in rat cerebellum. Immunoblots of total protein isolated from cerebellum showed the expression of only one isoform in one day old rats, and its expression increased from postnatal day 4 into adulthood (Wen et al., 1999). The second isoform was present beginning from postnatal day 14 and increased into adulthood. Immunofluorescence and immunogold labeling with antibodies to the common carboxy tail regions revealed a similar pattern of development. Thus, in the cerebellum, levels of AQP4 protein are present at low level by postnatal day 1 but increase into adulthood. AQP4 was not detected in neuronal cells at any of the developmental stages investigated but was seen in glial cell membranes, particularly those in contact with capillaries and pia (Wen et al., 1999). AQP1, 2, 3 and 5 were not detected in the cerebellum during these stages. The increase in AQP4 expression at or around postnatal day 7 coincides with increases in cellular numbers and decreases in the volume of the extracellular space in the brain suggesting that these processes may be functionally coupled (Wen et al., 1999).

Expression of AQP4 isoforms occurred much earlier in the optic tectum, telencephalon and cerebellum of chicks (Nico et al., 2001). AQP4 mRNA and protein were present as early as embryonic day 9. Labeling was seen only in ependymal and astroglial cells and significant levels occurred at embryonic day 14, later than the appearance of mRNA. This shift towards earlier expression in the chick (as compared to mice and rats) may reflect species differences in development since the chick brain is more developed at birth (Nico et al., 2001). Similar to the findings of Wen and colleagues, AQP4 expression in the chick seemed to follow glial cell expression and

correlated with development of the blood-brain barrier. There may be functional interdependence of AQP4 expression and water movement in astroglial cells with decreases in extracellular volume in the brain (Nico et al., 2001).

Aquaporins are developmentally regulated in other tissues, in addition to the brain. AQP2 is expressed as early as embryonic day 10 in the inner ear of the mouse, where maintenance of the endolymph composition is important for hearing and balance (Merves et al., 2000). In the kidney, where water and salt composition of the urine is maintained, many subtypes of aquaporins, including AQP1, 2, 3 and 4 are highly expressed but in general their expression is not apparent until the first week after birth (King and Agre, 1996; Horster, 2000). Of the aquaporins expressed in the lung, AQP1, 3, 4 and 5, only AQP1 is expressed in embryonic stages (King et al., 1997; Horster, 2000).

Although aquaporins are expressed in embryonic organ systems, to date no experiments have investigated their involvement in vertebrate neurogenesis. AQP4 is expressed in the brain and has high amount of identity with BIB but several features of the BIB protein are lacking in AQP4, notably the large carboxy tail with sites of potential regulatory interactions.

## **GENERAL HYPOTHESIS AND AIMS**

When BIB was cloned from *Drosophila melanogaster* in 1990, hydropathy analysis indicated six transmembrane domains, similar to AQP0 (then called the Major Intrinsic Protein), GlpF and Nod26 (Rao et al., 1990). The MIP family signature sequence, two N-P-A (asparagines-proline-alanine) motifs in the first intracellular loop (Loop B) and third extracellular loop (LoopE) are also present (Rao et al., 1990). Figure 1.13A shows the transmembrane topology of a BIB subunit. The percent sequence identity of BIB with other members of the MIP family is given in Figure 1.13B. BIB has 19–38% overall sequence identity with AQP0, AQP1, AQP4 and Nodulin26. AQP4 has been suggested to be the mammalian homologue of BIB based on overall amino acid identity (Adams et al., 1992). The identity between BIB and MIP channels is most apparent in the transmembrane domains and the putative pore-lining regions, Loops B and E (Figure 1.13B). Amino and carboxy tail domains have the most variability among MIP channels (Reizer et al., 1993), suggesting their importance as regulatory domains and BIB has the largest carboxy tail of all known MIP channels (the carboxy tail comprises amino acids 269-700). Based on the similarity of Big Brain with ion channels in the MIP family, I hypothesized that Big Brain is an ion channel.

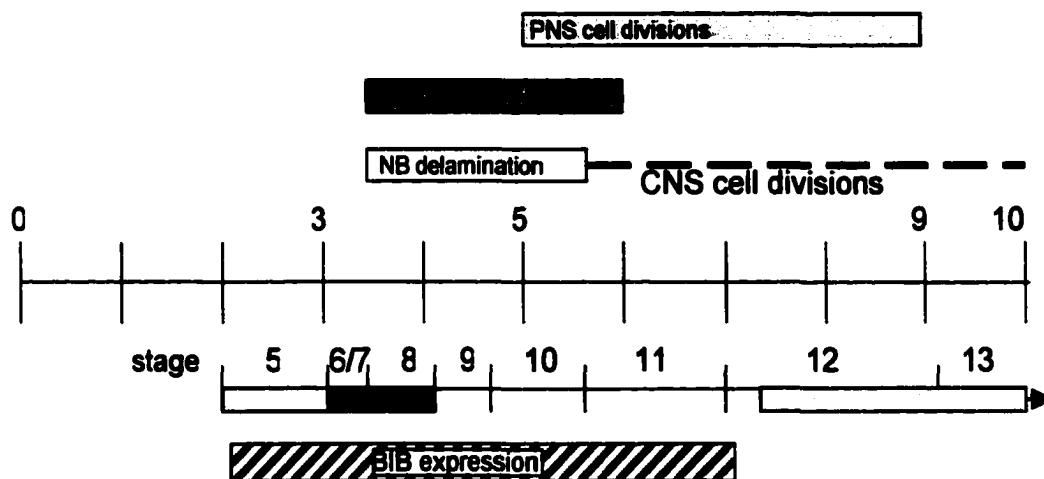
My first specific aim was to determine the functional characteristics of Big Brain expressed in *Xenopus* oocytes. Based on similarities with mammalian aquaporins, I tested for water channel properties with osmotically induced swelling assays. Ion channel properties were tested with two-electrode voltage clamp and cell-attached patch clamp. In Chapter 2 I describe experiments performed to determine the ion channel properties and potential regulatory mechanisms. These studies led to the novel discovery that Big Brain is a voltage-independent monovalent cation channel. Big Brain

channels are phosphorylated on tyrosine residues and appear to be activated in response to endogenous signaling pathways involving tyrosine kinases.

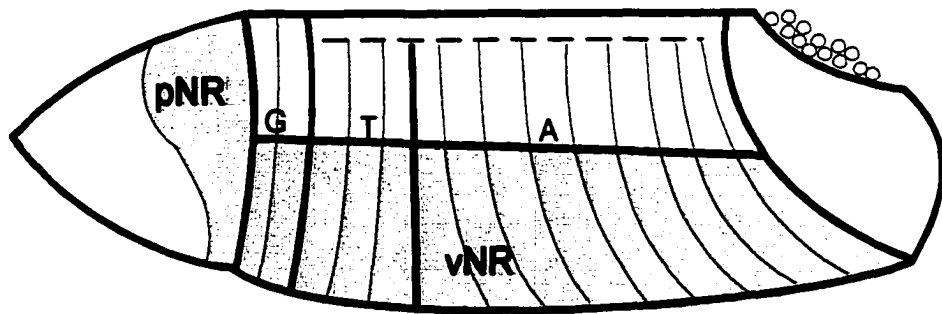
The importance of Big Brain to neural development and its novel characterization as an ion channel led to my second specific aim which was to determine the effect of divalent cations such as magnesium, calcium and barium on whole-cell currents in Big Brain-expressing oocytes. Results presented in Chapter 3 demonstrate that calcium and barium block currents in Big Brain-expressing oocytes. Mutation of a conserved glutamate (E71) in the first transmembrane domain to aspartic acid introduced block by  $Mg^{2+}$  and showed that E71 is critical for BIB cationic channel properties and confirmed that BIB is an ion channel.

My third specific aim was to explore the regulatory role of the carboxy tail of Big Brain. In Chapter 4 I describe experiments designed to test the effect of truncation of the carboxy tail on cationic channel properties of Big Brain. Truncation of the carboxy tail resulted in decreased whole-cell currents, and channels that were no longer tyrosine phosphorylated.

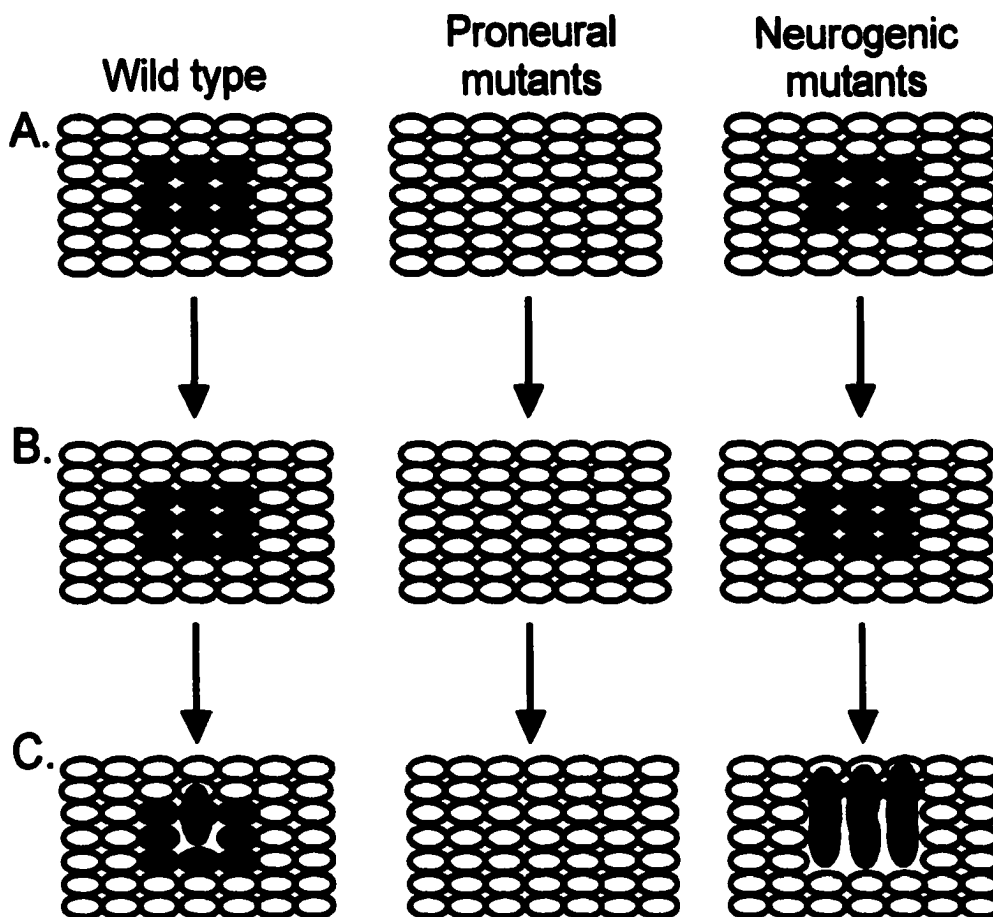
Results presented in this dissertation provide the first characterization of Big Brain as a cationic channel regulated by signaling pathways. These properties fit logically with established mechanisms of neuronal development that involve both transmembrane signaling pathways and changes in membrane potential. This work has provided a foundation from which the *in vivo* properties of Big Brain channels can be determined and is evidence for the diversity of function of channels in the MIP family.



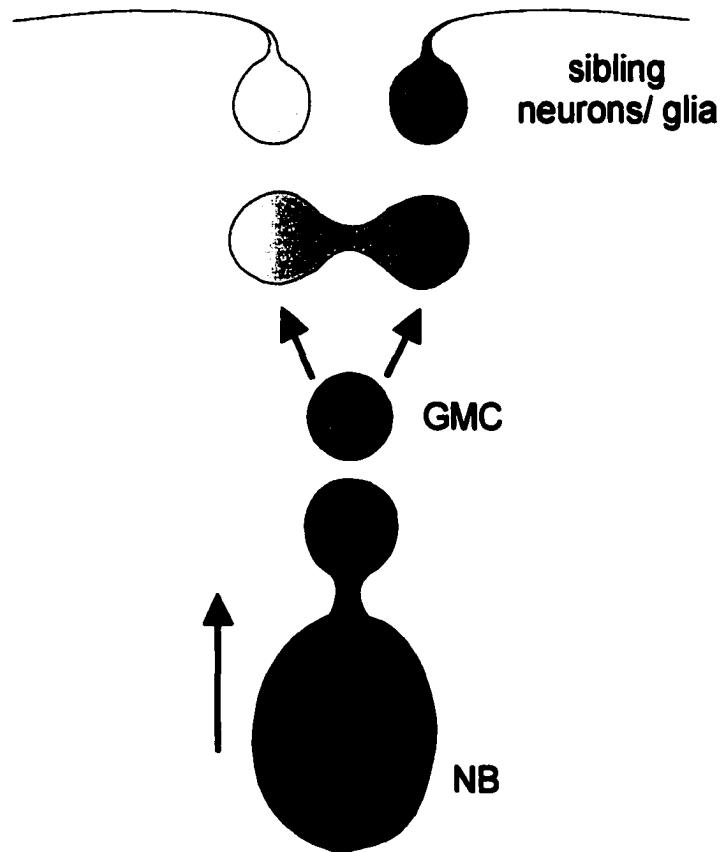
**Figure 1.1** *Developmental timeline of Drosophila embryos.* Neuroblasts begin to form after three hours of development at approximately stage 8. Cell divisions that give rise to the CNS begin after this at approximately stage 11. PNS cell divisions (upper gray) begin midway through stage 10 at about 5 hours of development. Yellow, blastoderm formation; green, gastrulation; black, germ band elongation; gray, germ band retraction. Adapted from Campos-Ortega and Jan, 1991.



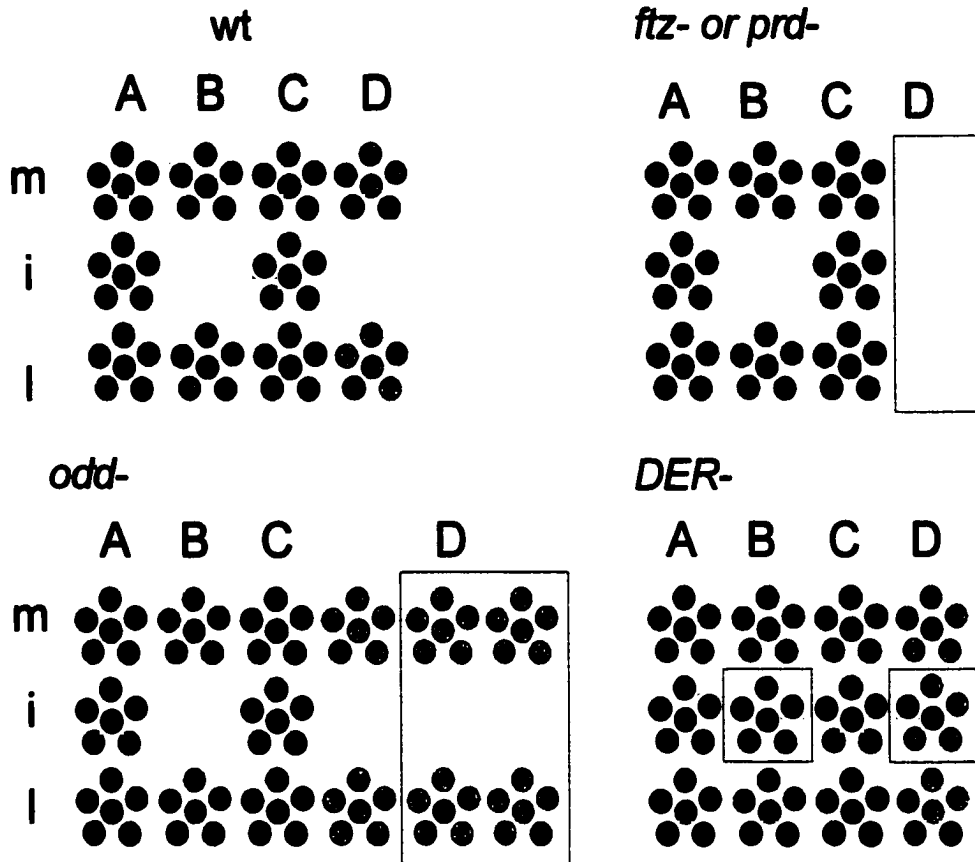
**Figure 1.2 Neurogenic regions of the *Drosophila* embryo.** Lateral view of a stage 11 embryo. Anterior is to the left and dorsal is up. Shaded regions indicate the ventral neurogenic (vNR) and procephalic neurogenic (pNR) regions which give rise to the central nervous system. Segments are indicated, G-gnathal, T-thoracic, and A-abdominal. Adapted from Bossing et al., (1996).



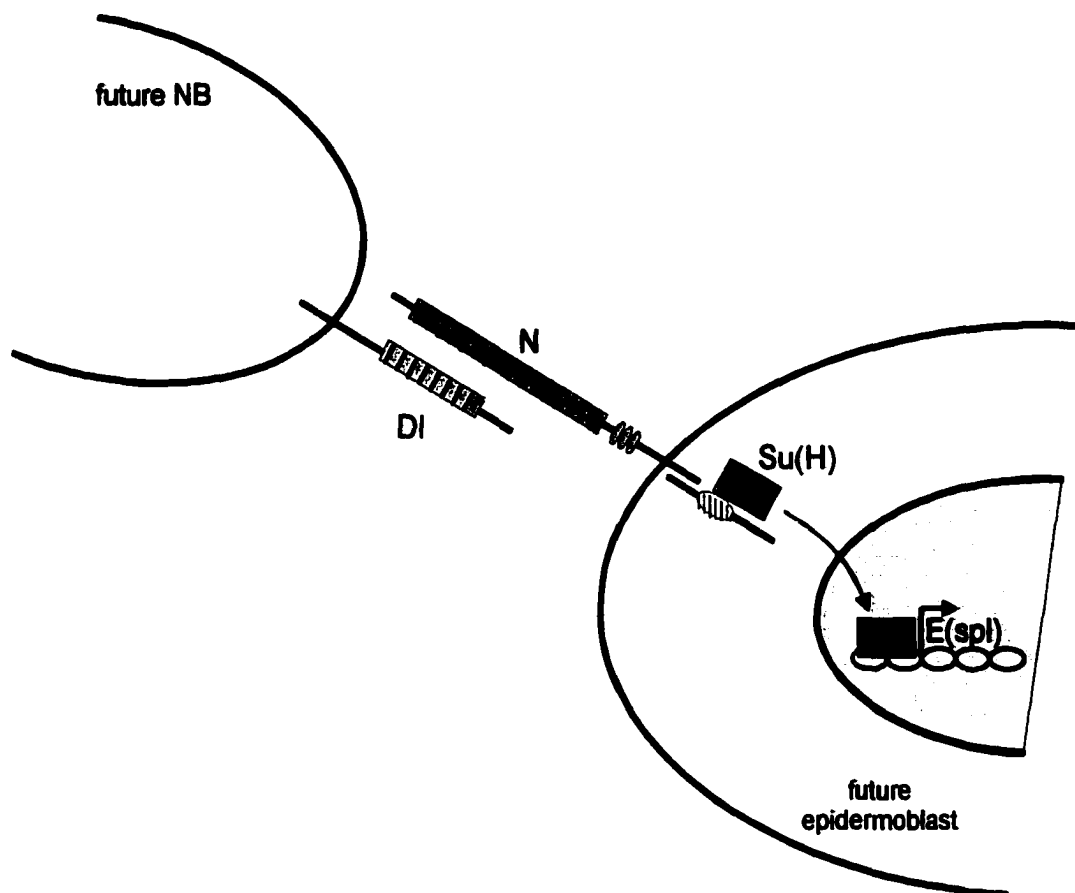
**Figure 1.3 Neuroblasts arise from the neuroectoderm.** A schematic diagram of neural precursors in the CNS. **Wild-type:** A. clusters of cells within the neuroectoderm acquire neural potential through expression of proneural genes (red); B. one cell in each cluster is singled out to become the neuroblast (red) and inhibits the remaining cells of the cluster from acquiring the same fate through lateral inhibition (green); C. the resulting neuroblast (blue) delaminates dorsally from the ventral surface. The other cells of the cluster give rise to epidermoplasts. **Proneural mutants:** lack-of-function mutations in proneural genes result in lack of proneural cluster formation (A.) and a decrease in neuroblast formation (C.). **Neurogenic mutants:** lack-of-function mutations in neurogenic genes result in an excess number of neuroblasts (C.) due to the lack of inhibitory signaling within proneural clusters (B.). Adapted from Artavanis-Tsakonas and Simpson, 1991.



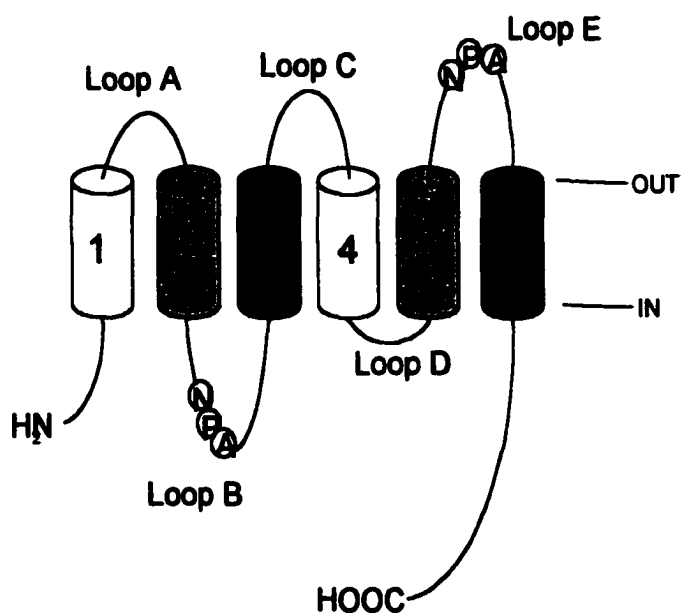
**Figure 1.4** *Differentiation of a neuroblast.* Each CNS neuroblast (NB) divides asymmetrically to yield several ganglion mother cells (GMC; only one is shown for clarity) which each divide once asymmetrically to yield neurons or glia. Different colors signify unique cellular identity; adapted from Goodman and Spitzer (1979).



**Figure 1.5 Proneural cluster formation is affected by anterior-posterior and dorsal-ventral patterning genes.** The first phase of proneural clusters form in four columns along the anterior (left) to posterior axis and three rows (medial, m; intermediate, i; lateral, l) along the dorsal (down) to ventral axis. Black indicates *lethal of scute* expression; green indicates *achaete* and *scute* expression; purple indicates expression *lethal of scute*, *achaete* and *scute*. Boxes enclose areas of altered proneural cluster formation or proneural gene expression as described in the text. *fushi tarazu* (*ftz*); *paired* (*prd*), *odd-skipped* (*odd*) and *Drosophila* epidermal growth factor receptor (*DER*); adapted from Skeath et al., 1992.

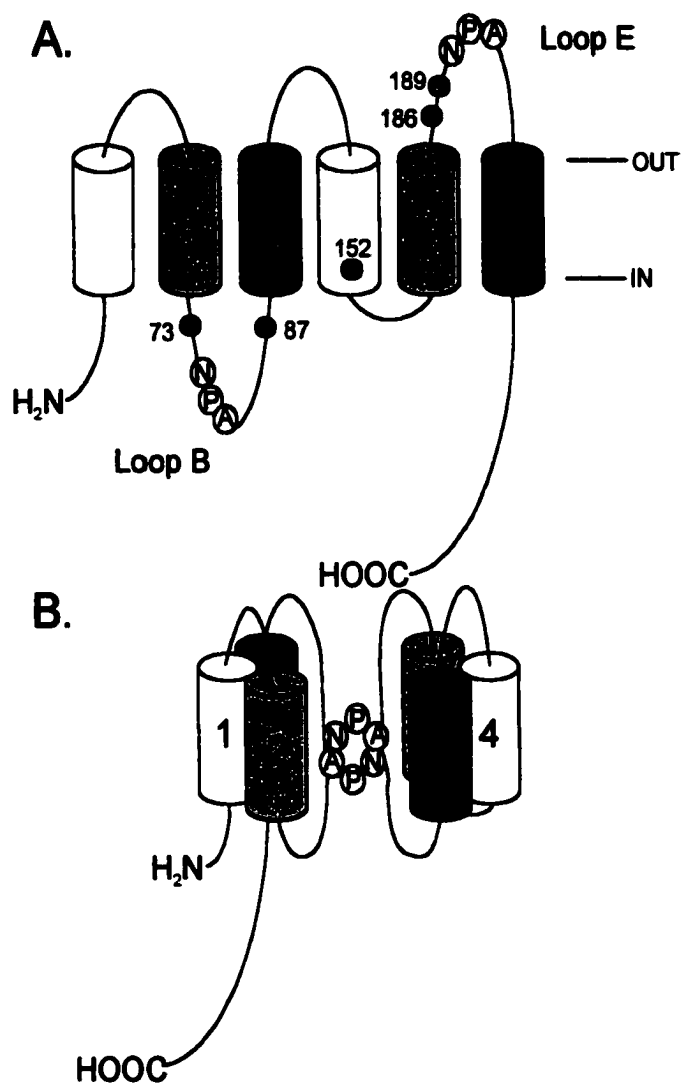


**Figure 1.6 Basic Notch signaling pathway.** Delta (DI) and Notch (N) interaction at the cell surface results in translocation of Suppressor of Hairless (Su(H)) from the cytoplasm (where it binds to intracellular domains of N) to the nucleus and activation of genes of the Enhancer of Split (E(spl)) complex. Additional regulators of this process are not shown. Adapted from Artavanis-Tsakonas, 1995 and Artavanis-Tsakonas et al., 1999.

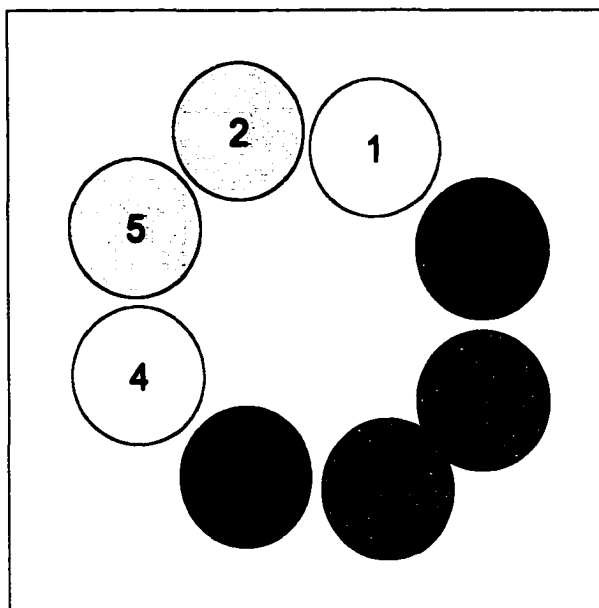


**Figure 1.7 Membrane topology of MIP channels.** MIP channels have six transmembrane domains (labeled 1-6). The conserved N-P-A motifs are shown in Loops B and E. The location of the lipid bilayer is indicated by a line showing the extracellular (out) and intracellular (in) locations. Internal similarity is indicated with similar transmembrane domains in the same color in each half of the protein.

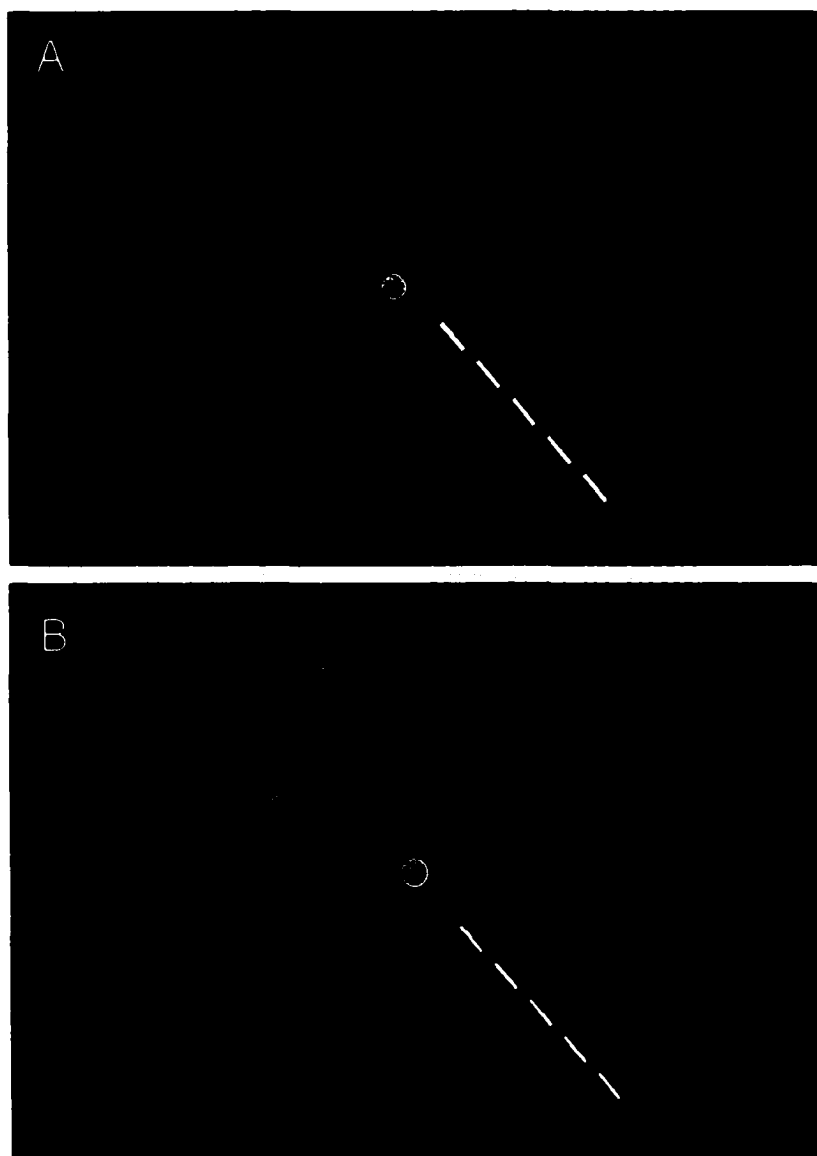




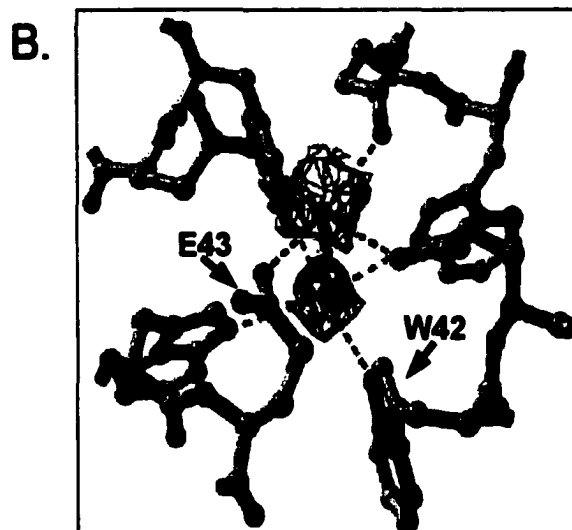
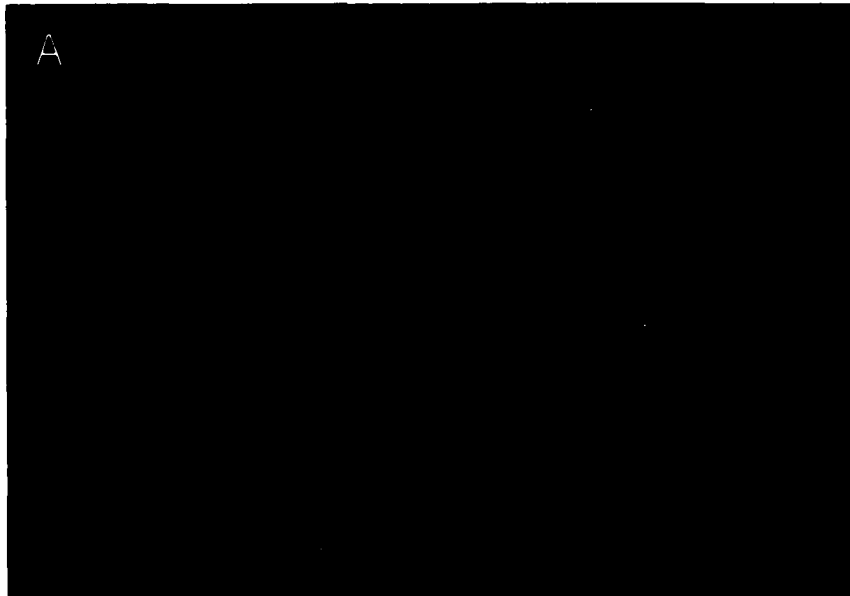
**Figure 1.9 The hourglass model.** **A.** Transmembrane topology of AQP1 (as in Figure 1.7) with sites of mutation which suggest that Loops B and E line the water pathway. N-P-A motifs in Loops B and E are indicated. The locations of mutated residues are indicated: cysteines (orange), tyrosine 186 (black), alanine 73 (green). **B.** The hourglass model predicted by Jung et al., 1994. Each subunit was predicted to be a water channel with Loops B and E (each containing the conserved N-P-A motifs) forming a narrow constriction for water passage through the membrane.



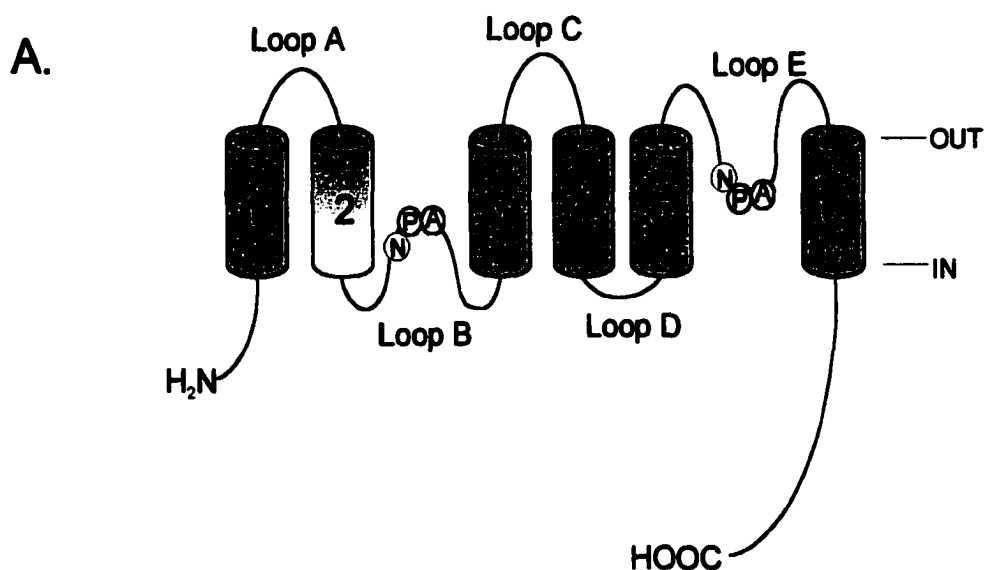
**Figure 1.10 Helical packing arrangement of AQP1 subunits.** The position of  $\alpha$ -helices in AQP1 was predicted by comparison of medium resolution crystallography data with the known orientation of helices in bacteriorhodopsin (de Groot et al., 2000). Internal similarity within AQP1 is indicated by similarly shaded helices (as in Figure 1.7) with the exception of Loops B and E (green).



**Figure 1.11 Tetrameric assembly of AQP1 and GlpF subunits.** Extracellular view of tetrameric AQP1 (A.; Murata et al., 2000) and GlpF channels (B.; Fu et al., 2000). Transmembrane domains 1-3 (gold), 4-6 (blue) and Loops B and E (green) are indicated for one subunit. The four-fold axis of symmetry is indicated by a yellow circle and the pseudo two-fold symmetry axis is indicated by a dashed white line for one subunit in both A. and B. The red space-filled molecules in B. represent glycerol molecules within each subunit. Pictures were generated with RASMOL from structural coordinates of AQP1 (1FQY) and GlpF (1FX8) deposited in RCSB protein databank.



**Figure 1.12** *The central pore of GlpF.* A. GlpF tetramer, helices 2 (green) and 5 (red) from each GlpF subunit line the central pore. Generated from RASMOL from GlpF structural coordinates (RCSB protein databank, accession code 1FX8). B. Two magnesium ions (purple) were found coordinated with W42 and E43 of helix 2 in the central pore of GlpF (adapted from Fu et al., 2000).



**B.**

	AQP0	AQP1	AQP4	Nod26
TM1	39	23	21	22
TM2	50	38	36	18
TM3	54	54	58	25
TM4	42	42	37	17
TM5	18	14	18	5
TM6	47	41	41	41
overall	38	32	32	19

**Figure 1.13 Sequence identity of BIB with members of the MIP family: AQP0, AQP1, AQP4 and Nodulin 26.** **A.** Predicted transmembrane topology of BIB with transmembrane domains (TM) and loops indicated. **B.** Percent sequence identity with BIB is shown in the table for each transmembrane domain and Loops B and E, the putative pore lining regions. Percent identity was obtained from sequence alignments of BIB (accession number X53275) with AQP0 (K02818), AQP1 (M77829), AQP4 (U63623) and Nodulin 26 (X04782) with ClustalW multiple sequence alignment ([www.clustalw.genome.ad.jp](http://www.clustalw.genome.ad.jp)).

## **CHAPTER 2. FUNCTIONAL CHARACTERISTICS OF BIB EXPRESSED IN XENOPUS OOCYTES**

### **2.1 INTRODUCTION**

Neurogenic genes separate neural precursors (neuroblasts) and epidermal precursors (epidermoblasts) from the *Drosophila* neuroectoderm through a process termed lateral inhibition (Greenspan, 1992). Loss-of-function mutations in these genes cause central and peripheral nervous system overgrowth (Lehmann et al., 1983; Brand and Campos-Ortega, 1988; Han et al., 1998a; Artavanis-Tsakonas et al., 1999). *big brain (bib)* is a neurogenic gene; however, the neurogenic phenotype induced by loss-of-function mutations of *big brain (bib)* is less severe than that for other neurogenic genes (Lehmann et al., 1983; Goriely et al., 1991; Rao et al., 1992). The molecular contributions of the neurogenic genes Notch (a transmembrane receptor) and Delta (a transmembrane ligand for Notch) have been identified (Fehon et al., 1990; Artavanis-Tsakonas et al., 1995). Suppressor of Hairless and the Enhancer of split gene complex contribute to a signaling pathway, regulating the signal from Notch to the nucleus (Delidakis and Artavanis-Tsakonas, 1992; Fortini and Artavanis-Tsakonas, 1994; Bailey and Posakony, 1995; Kimble and Simpson, 1997; Lai et al., 2000). Although the *bib* gene product, BIB, is located on the plasma membrane and can interact functionally with Notch and Delta, its mechanism of action within the established signaling pathway for Notch is unclear (de la Concha et al., 1988; Doherty et al., 1997). Rao et al. (1990) suggested that BIB directly mediates intercellular communication in the neuroectoderm.

The proposed membrane topology of BIB predicts six transmembrane domains with intracellular amino and carboxy termini (Rao et al., 1990). This structure is similar to members of the Major Intrinsic Protein (MIP) family that includes aquaporins,

mammalian channels for water as well as other solutes including ions (Ehring et al., 1990; Reizer et al., 1993; Yool et al., 1996; Tsukaguchi et al., 1998; Yasui et al., 1999). BIB has high amino acid sequence identity with aquaporins in transmembrane regions where it shows 38% overall identity with AQP0 (Rao et al., 1990), and 32% identity with AQP4 (Adams et al., 1992).

Despite the established involvement of *bib* in developmental pathways and its sequence identity to aquaporins, its function has previously remained unknown. We show here that the *bib* protein, BIB expressed in *Xenopus* oocytes functions as a regulated ion channel. Water and ionic permeability were investigated with osmotically induced swelling assays, two-electrode voltage clamp and cell-attached patch clamp recordings. Our results demonstrate that BIB is not appreciably permeant to osmotic water flux. Several lines of evidence support the idea that BIB does function as a kinase-regulated non-selective cation channel. Given the importance of tyrosine kinases in growth factor-mediated control of nervous system development (Pimentel et al., 1996; Skeath, 1998; Udolph et al., 1998; Chen et al., 1999), we suggest that the observed properties of BIB are consistent with a role in transmembrane voltage signaling as an essential early step in neurogenesis.

## 2.2 MATERIALS AND METHODS

(1) *Molecular Techniques.* *Drosophila big brain* cDNA was generously provided by Dr. Lily Jan (Rao et al., 1990). We subcloned the coding region of *bib* into the plasmid pX $\beta$ Gev, a *Xenopus* expression vector. For subcloning, the coding region of *bib* was amplified by the polymerase chain reaction (PCR) with PWO polymerase (Boehringer-Mannheim, Indianapolis, IN) using sense and antisense primers that introduced BglII

(Boehringer-Mannheim) restriction sites (underlined) into the 5' and 3'-untranslated regions of the *bib* cDNA:

"sense": 5'-AAC AAA TCG AGA TCT GAG TCC GAC ATG-3' (bp 277-303)

"antisense": 5'-ACC CCA GAT CTG CCG CTT TCA GTT GCG-3' (bp 2421-2395)

In order to visualize BIB channels by immunofluorescence microscopy an epitope tag consisting of nine amino acids (YPYDVPDYA) from the influenza hemagglutinin protein (HA) was inserted in the amino terminus of BIB. Incorporation of the HA peptide sequence required two rounds of PCR. The sense primer for the first reaction contained the last seven codons of the HA epitope (underlined) followed by a region of overlap with the *bib* sequence:

5'-TAC GAC GTG CCG GAC TAC GCT GCC GAC GAA AGT CTG-3' (bp 304–318).

The antisense primer was the same as used for *bib* subcloning (above). The sense primer for the second PCR reaction contained the remaining HA sequence (underlined), the start codon (*italics*), and a *Bgl*III restriction site (**bold**):

5'-TCG **AGA TCT** GAG TCC GAC *ATG* TAC CCG TAC GAC GTG CCG GAC-3' with

the same antisense primer as above. The entire coding sequences of all constructs were sequenced to verify that no inadvertent mutations were introduced.

Site directed mutagenesis was performed with Stratagene QuickChange site-directed mutagenesis kit (Stratagene, La Jolla, CA). Glutamate 71 was mutated to asparagine (E71N), using the following primer combinations (mutated base pairs underlined):

sense: 5'-GGA GAT CCA TCA TCA GCA ACT GTC TGG CCT CC-3' (bp 494–525)

antisense: 5'-GGA GGC CAG ACA GTT GCT GAT GAT GGA TCT CC-3' (bp 525-494)

Plasmid DNA was linearized with *SpeI* in the polylinker region and used to transcribe RNA *in vitro* with T3 RNA polymerase. Enzymes were purchased from Roche Molecular Biochemicals (Indianapolis, IN).

*(2) Oocyte preparation and injection.* Stage V-VI oocytes from adult female *Xenopus laevis* were obtained and defolliculated as described by Anthony et al. (2000). Prepared oocytes were injected with 50nl of sterile water (control oocytes) or 50nl of sterile water containing *bib* cRNA (0.4ng/nl unless otherwise indicated) and were incubated for 2-5 days at 18°C in ND96 culture medium (96mM NaCl, 2mM KCl, 1.8mM CaCl<sub>2</sub>, 1mM MgCl<sub>2</sub>, 5mM Hepes, 2.5mM pyruvic acid, 100U/ml penicillin, and 100µg/ml streptomycin, pH 7.6) to allow protein expression before recording.

*(3) Electrophysiological Recordings.* Two-electrode voltage clamp was used to investigate the macroscopic ion channel properties of BIB. Recordings were performed at room temperature with electrodes (0.5-3MΩ) filled with 3M KCl. Data were recorded with a GeneClamp 500 (Axon Instruments, Foster City, CA), filtered at 2 kHz, digitized at 50 to 2000 µs and analyzed with pClamp software (Axon Instruments). Recording salines for two-electrode voltage clamp contained (in mM): 100 NaCl, 2 KCl, 4.5 MgCl<sub>2</sub>, 5 Hepes, pH7.3. Reversal potentials were obtained from a polynomial fit (second order) of the current-voltage relationship for each oocyte and used to calculate relative ionic permeability. Relative ionic permeability was calculated from the reversal potential ( $E_r$ ) with a simplified equation for bi-ionic conditions (Hille, 1992):

$$P_X/P_K = ([K]_i/[X]_o) \exp^{(E_r/58)}$$

Where  $P_x/P_K$  is the relative permeability to the test ion  $X^+$ ,  $E_r$  is the reversal potential,  $[X]_o$  is the concentration of the test ion in the extracellular saline and  $[K]_i$  is the calculated internal  $K^+$  concentration. The internal  $K^+$  concentration was estimated for each oocyte from the Nernst equation by the reversal potential in bath saline with 100mM  $K^+$  (internal  $K^+$  ranged from 110-133mM). H7, insulin, lavendustin A and staurosporine were purchased from Sigma Chemical Company (St. Louis, MO); cycloheximide was purchased from Calbiochem (La Jolla, CA).

**(4) Osmotically-induced swelling assay.** Analysis of water permeability was performed as described in Rivers et al., 1997. Oocytes were placed in 50% hypotonic saline (1:1 dilution of ND96 with deionized water) and swelling was monitored by videomicroscopy. Images were taken every 15 seconds with COHU CCD camera and analyzed with IPLab spectrum software. The relative volume was calculated from the two dimensional area of the oocyte as a function of time of exposure to hypotonic saline and was used to determine the net osmotic water permeability.

**(5) Cellular fractionation.** 2-3 days after RNA injection, oocyte plasma membranes were isolated by a method adapted from Geering et al., 1989. Briefly, fifteen oocytes per group were isolated in 500 $\mu$ l lysis buffer (1% Triton X-100, 10mM Tris HCl, 50mM NaCl, 50mM NaF, 1% aprotinin) supplemented with leupeptin (10 $\mu$ g/ml), pepstatin A (10 $\mu$ g/ml), PMSF (10mM) and sodium orthovanadate (2mM), and lysed by trituration. Cell lysates were incubated on ice approximately 10 minutes followed by centrifugation (400 x g) for 10 minutes at 4°C to remove yolk granules. The supernatant was removed to a clean tube and samples were centrifuged again (400 x g) for 10 minutes at 4°C to yield a yolk-

depleted supernatant. A pellet enriched in plasma membranes was obtained following centrifugation of the supernatant (12000 x g), 20 minutes, 4°C. Pellets were resuspended in 50µl lysis buffer and used for immunoprecipitation or resuspended in 25µl Laemmli buffer (10% glycerol, 50mM Tris HCl, 2% SDS, 5% β-mercaptoethanol, 0.02% bromophenol blue) and resolved by SDS-PAGE for western blotting. Leupeptin, pepstatin A, PMSF and sodium orthovanadate were purchased from Sigma Chemical Company (St. Louis, MO).

*(6) Immunoprecipitation and Western Blotting.* Equivalent amounts of protein (20-30µg) were used for immunoprecipitation. Sample volumes were increased to approximately 1ml with lysis buffer followed by addition of the primary antibody (0.5µg of rat anti-HA high affinity clone 3F10, Boehringer-Mannheim, Indianapolis, IN or 0.5µg PY11120 antibody, Transduction Laboratories, Lexington, KY) and incubated overnight at 4°C with rotation. 0.5µg rabbit anti-rat IgG was added to samples immunoprecipitated with rat HA antibody, and incubated for one hour. 10µl of a 1:1 slurry of protein A sepharose (Sigma) was added to all samples, then rotated for one hour at 4°C. Proteins were precipitated by brief centrifugation steps (12000xg, 1min) and washed twice with lysis buffer and once in buffer containing 0.1% Triton). Laemmli buffer was added to each sample. Proteins resolved by 8% SDS-PAGE were transferred to nitrocellulose (.45µm; Bio-Rad, Hercules, CA) in transfer buffer (10% methanol, 10mM CAPS; 3-(cyclohexylamino)-1-propanesulfonic acid, Sigma) for one hour at 1Amp. Non-specific binding sites were blocked with 1.5% (w/v) evaporated milk in TBST (154mM NaCl, 10mM Tris-base, 0.2% Tween-20), and 0.01% thimerosal (for HA antibody) or with 3%

(w/v) bovine serum albumin in TBST and 0.01% thimerosal (for phospho-tyrosine and phospho-serine antibodies). After blocking, blots were exposed to primary antibodies: rat anti-HA antibody (clone 3F10, Roche, 50ng/ml), phospho-serine antibody, (clone PSR-45, Sigma, 1µg/ml) or phospho-tyrosine antibody, PY11120, 1µg/ml) for one hour at room temperature or overnight at 4°C followed by three 15-minute washes at room temperature in TBST. To visualize proteins recognized by primary antibodies blots were incubated with goat anti-rat (0.25µg/ml; Zymed Laboratories, San Francisco, CA) or goat anti-mouse HRP-conjugated antibodies (0.3µg/ml; Zymed) for 1 hour at room temperature followed by three 15-minute washes. Bands were visualized by enhanced chemi-luminescence (Pierce, Rockford, IL).

*(7) Immunofluorescence labeling of intact oocytes.* Intact oocytes on day 2 or 3 following cRNA injection were fixed in 4% para-formaldehyde for 2-3 hours at 4°C, followed by brief rinses in 30mM SSC (300mM sodium chloride, 20mM sodium citrate) and 100mM glycine. Oocytes were permeabilized for one hour in 30mM SSC containing 0.1% Triton X-100, followed by overnight incubation with rat anti-HA antibody (Boehringer-Mannheim, Indianapolis, IN) at 1:200 dilution (0.5µg/ml) in antibody dilution buffer (30mM SSC, 2% goat serum, 1% bovine serum albumin, 0.05% Triton X-100, 0.02% sodium azide). Oocytes were washed in antibody wash buffer (30mM SSC, 0.05% Triton X-100) for one hour and then incubated one hour with FITC-conjugated goat anti-rat antibody (1µg/ml in antibody dilution buffer). Oocytes were rinsed with antibody wash buffer for one hour, and imaged with a 10X objective (pinhole size 100) on a Leica TCS-4D laser scanning confocal microscope.

All data summaries are reported as mean  $\pm$  standard deviation. Statistical significance was tested with a two-tailed Student's t-test. p values  $<0.05$  were considered to indicate significance.

### 2.3 RESULTS

BIB has amino acid sequence identity with aquaporins of the MIP family (Rao et al., 1990; Adams et al., 1992; Reizer et al., 1993). Therefore, we compared the water permeability of oocytes expressing HABIB with that of oocytes expressing aquaporin-1 (AQP1), a well-characterized water channel (Preston et al., 1992). Figure 2.1 shows the results from a representative experiment that has been replicated in 4 batches of oocytes. By five minutes of exposure to 50% hypotonic saline, the relative volume of oocytes expressing AQP1 increased by an average of 12.5%, yielding a calculated water permeability factor ( $P_f$ ) value of  $26 \pm 13 \mu\text{m/s}$  ( $n=5$ ). In contrast, the relative volume of oocytes expressing HABIB did not increase and remained similar to control oocytes during five minutes in hypotonic saline or longer;  $P_f$  values were  $-1 \pm 5 \mu\text{m/s}$  ( $n=4$ ), and  $2 \pm 1 \mu\text{m/s}$  ( $n=4$ ) respectively. These data show that despite the sequence similarity between BIB and aquaporins, BIB is not a water channel under the conditions tested.

Several members of the MIP family have ion channel activity (Ehring et al., 1990; Weaver et al., 1994; Yool et al., 1996; Yasui et al., 1999; Anthony et al., 2000). Two-electrode voltage clamp was used to test for ionic conductance properties of BIB channels. Figure 2.2 (A-E) shows the activation of channels in BIB-expressing oocytes measured as an increase in whole-cell conductance. We initially tested BIB-expressing oocytes by placing them into recording saline, immediately inserting recording electrodes and assessing the response (if any) to a series of voltage steps from +60 to -90mV from

a holding potential of  $-40\text{mV}$ . BIB-expressing and control oocytes consistently showed no appreciable conductance immediately after electrode insertion (Figure 2.2Aa and d). However, we noticed during sustained recordings that BIB-expressing oocytes showed an increase in current beginning approximately 5 minutes after the initial electrode insertion; this response was absent from control oocytes. The current-voltage relationship of the activated current was linear ( $+60$  to  $-90\text{mV}$ ; Figure 2.2Ae) in contrast to a lack of response in control oocytes (Figure 2.2Ab). The net responses (Figure 2.2Ac and f) were obtained by subtracting the set of initial traces from the final.

Figure 2.2B shows the time-dependent spontaneous activation of channels triggered by electrode penetrations of BIB-expressing oocytes. The current response was monitored with repeated steps to  $+40\text{mV}$  (800ms duration) every five seconds from a holding potential of  $-40\text{mV}$ . In oocytes expressing BIB channels, the current began to activate approximately five minutes after electrode insertion, and reached a plateau between 30–40 minutes after electrode insertion (Figure 2.2B). In contrast, control oocytes did not display any comparable increase in current over equal durations or longer. The rate of activation (Figure 2.2C) was calculated from a linear fit of current plotted as a function of time, for the interval between 5 and 13 minutes. Control oocytes had a significantly lower rate of change in membrane conductance ( $8\pm 12\text{nA/min}$ ,  $p < 0.05$ ) than did BIB-expressing oocytes ( $30\pm 25\text{nA/min}$ ). Spontaneous activation in BIB-expressing oocytes was not affected by holding potential or voltage steps. Tests of different voltage steps ( $-40$ ,  $0$ ,  $+60$ ,  $+80\text{ mV}$ ) indicated no apparent effect of voltage on the rate or magnitude of channel activation (data not shown). Simply placing oocytes into recording saline for equivalent time periods did not elicit a current response,

indicating that spontaneous activation was initiated by the pricking effect of electrode insertion. Possible activation mechanisms are addressed further in Figures 2.5 and 2.6.

Averaged current-voltage relationships measured for control and BIB-expressing oocytes are shown in Figure 2.2D. The linear relationship shows a voltage-independent conductance, with a reversal potential consistent with a non-selective cationic conductance (see Figure 2.3 below). The box plot (Figure 2.2E) summarizes the net conductance at 30 minutes after electrode insertion for control and BIB-expressing oocytes, calculated from linear fits of the net current-voltage relationship for each oocyte. Control oocytes had a mean net conductance of  $1 \pm 4 \text{ nA/mV}$  ( $n=10$ ). Wild type BIB-expressing oocytes had a mean net conductance of  $17 \pm 11 \text{ nA/mV}$  ( $p < 0.0001$ ,  $n=19$ ) that was significantly greater than that of control oocytes.

In order to visualize BIB channels with immunofluorescence and western blots, we inserted an HA epitope (see Methods for details) into the amino terminus of BIB (HABIB) and tested the effect of epitope insertion on BIB channel properties. Representative current traces shown in Figure 2.2A show the effects of BIB and HABIB expression are indistinguishable in general properties. HABIB-expressing oocytes (Figure 2.2C) were not significantly different from oocytes expressing wild-type BIB in the rate of activation ( $30 \pm 25 \text{ nA/min}$ ,  $n=22$  and  $42 \pm 42 \text{ nA/min}$ ,  $n=19$  respectively), or in net conductance (Figure 2.2E). These results showed that insertion of the HA epitope did not affect the activation of ionic conductance or current-voltage relationship of the response.

The current in BIB-expressing oocytes showed non-selective monovalent cation permeability (Figure 2.3), analyzed by iso-osmotic substitution of NaCl in the bath recording saline. Figure 2.3A shows current-voltage relationships for HABIB-expressing

oocytes in various salines. Figure 2.3B summarizes the reversal potentials measured for individual oocytes in each bath saline. Substitution of 100mM NaCl with equimolar KCl resulted in a significant depolarizing shift of the reversal potential from  $-14 \pm 3$  mV (NaCl, n=8) to  $-4 \pm 2$  mV (KCl, n=9,  $p < 0.001$ ). Substitution of NaCl with 100mM tetraethylammonium chloride (TEACl, n=7) significantly shifted the reversal potential to  $-32 \pm 2$  mV (n=7,  $p < 0.001$ ). Partial substitution of NaCl with 60mM sodium gluconate had no significant effect on reversal potential ( $-11 \pm 5$  mV, n=11) indicating no appreciable anionic permeability. Relative ionic permeability was calculated as described (see Methods) from the reversal potential and resulted in the following selectivity sequence:  $P_K/P_K (1.0) > P_{Na}/P_K (0.71) \gg P_{TEA}/P_K (0.32)$ .

Figure 2.4 shows that the expression of non-functional mutant HABIB channel protein in plasma membrane does not induce an increased membrane conductance in oocytes. The box plot data (Figure 2.4A) summarize the responses of control oocytes, oocytes expressing HABIB wild type, and HABIB E71N mutant channels. The mutation of glutamate at position 71 in BIB to asparagine (E71N) was one of a series of glutamate substitutions used to investigate putative cation binding sites (see Chapter 3). E71N abolished the ionic conductance associated with BIB channels ( $6 \pm 5$  nA/mV, n=17) as compared with wild type HABIB ( $47 \pm 31$  nA/mV, n=13,  $p < 0.001$ ) but did not prevent trafficking to plasma membrane. Figure 2.4B shows the net current-voltage relationships measured in oocytes expressing HABIB wild type (n=13), HABIB E71N (n=17) and in control oocytes (n=7). The current-voltage relationship of oocytes expressing E71N channels was not different from that of control oocytes. Figure 2.4C shows representative responses for current activation as a function of time in oocytes expressing HABIB wild type, HABIB E71N, and a control oocyte. Only the HABIB-

expressing oocytes showed development of current by spontaneous activation. Control oocytes and HABIB E71N-expressing oocytes showed no channel activation. The absence of a conductance response in HABIB E71N-expressing oocytes shows the BIB-associated current is not an indirect consequence of heterologous protein expression in oocytes.

Immunofluorescent microscopy of intact oocytes was used to confirm the expression of HABIB E71N channels in the oocyte plasma membrane (Figure 2.4D). Oocytes were labeled with a rat anti-HA antibody and a FITC-conjugated goat anti-rat secondary antibody. Images are shown in reverse field so that positive labeling is visualized as black staining. Control oocytes show no labeling. Both HABIB-expressing oocytes and HABIB E71N-expressing oocytes had intense labeling on the plasma membrane indicating that although E71N channels are not functional they are successfully translated, transported and expressed on the plasma membrane of the oocyte. Absence of labeling in control oocytes showed that the signal detected by the antibody is specific for epitope-tagged HABIB wild type and HABIB E71N channels.

Figures 2.2–2.4 established that the currents activated in BIB-expressing oocytes have monovalent cationic selectivity that is not a consequence of heterologous protein expression but is attributable to BIB channels in the plasma membrane. We next sought to investigate possible mechanisms of current activation in BIB-expressing oocytes. Since neither voltage nor exposure to recording saline induced spontaneous activities, we hypothesized that insertion of recording electrodes was activating a signaling pathway. A simple leak current was ruled out by the observation that control oocytes had no response (Figure 2.2). Oocytes are known to be induced to progress through the cell cycle artificially by pricking (Wolf, 1974; Kubota et al., 1987; Wangh, 1989), or

fertilization, processes which involve kinase-mediated pathways (Sato et al., 1998; Glahn et al., 1999; Sato et al., 1999). MIP family channels are targets of kinase-mediated cell signaling (Ehring et al., 1991, Maurel et al., 1995, Fushimi et al., 1997, Han et al., 1998b, Han and Patil, 2000). BIB contains consensus sites for phosphorylation (Burris et al., 1998; and discussed in depth in Chapter 4). Therefore, we tested whether BIB was a target of endogenous signaling pathways present in the oocyte by pretreating oocytes with pharmacological agents that modify serine/threonine and tyrosine kinase pathways. The results of these experiments are shown in Figure 2.5 and 2.6.

Figure 2.5 shows traces of HABIB-expressing and control oocytes after exposure to pharmacological agents that modify kinase-mediated signaling pathways and protein synthesis in oocytes. Insulin activates endogenous insulin receptor tyrosine kinases (Scavo et al., 1991); lavendustin A inhibits tyrosine kinases (O'Dell et al., 1991; Lawrence and Niu, 1998); H7 inhibits cAMP and cGMP dependent protein kinases (Hidaka et al., 1984); staurosporine inhibits protein kinase C (Kim et al., 2000; Volk et al., 2000); sodium orthovanadate inhibits protein tyrosine phosphatases (Molokanova et al., 1997); and cycloheximide inhibits protein synthesis (Gotoh et al., 1995). The initial traces represent the current responses immediately after electrode insertion and the net response shows the current activated after 30 minutes of recording. Net conductance values were calculated from linear fits of the net response current-voltage relationships.

Figure 2.6 summarizes the net whole cell conductance responses compiled for the same treatment conditions illustrated in Figure 2.5. Oocytes were pretreated with 1 $\mu$ M staurosporine for 1 hour (Kim et al., 2000; Volk et al., 2000) or in 10 $\mu$ M H7 for 1-4 hours, or were maintained in parallel without staurosporine or H7. Pretreatment with

staurosporine had no effect on the net conductance response of BIB-expressing oocytes (Figure 2.6A). A similar lack of effect was seen with incubation times up to 5 hours. Similarly, pretreatment with H7 had no effect on the net conductance response of HABIB-expressing oocytes (Figure 2.6A). No significant differences were observed when compared to the net conductance of untreated HABIB-expressing oocytes.

In contrast, pretreatment with insulin (20 $\mu$ M, 1 hour) had a significant inhibitory effect on current activation in HABIB-expressing oocytes (Figure 2.6B). The net whole cell conductance after insulin ( $3\pm 5$  nA/mV, n=14) remained at less than 15% of that seen for untreated HABIB-expressing oocytes ( $24\pm 10$  nA/mV, n=17, p<0.001). The effect of insulin was not due indirectly to block of native oocyte currents. On the contrary, pretreatment with insulin activated a small conductance in HABIB-expressing oocytes that was also evident for control oocytes and thus attributed to endogenous oocyte channels. The insulin-induced native current showed an outwardly rectifying current-voltage relationship, with a reversal potential of  $-19\pm 4$  mV (n=16); both features distinguished it from the HABIB-related conductance which had an approximately linear current-voltage relationship and a reversal potential of  $-13\pm 4$  mV (n=17, p<0.001). Insulin effectively suppressed the current in HABIB-expressing oocytes to the level of control oocytes. The effect of insulin was dose dependent (Figure 2.6C). Pre-treatment of HABIB-expressing oocytes with 10 $\mu$ M insulin also significantly decreased the net whole-cell conductance 40% ( $10\pm 4$  nA/mV, n=6, p<0.05), while pre-treatment with 2 $\mu$ M insulin had no significant effect compared to untreated HABIB-expressing oocytes ( $27\pm 12$  nA/mV, n=5).

Lavendustin A is a membrane permeable tyrosine kinase inhibitor that is effective in oocytes (Molokanova et al., 1997). Pretreatment for one hour with 10 $\mu$ M lavendustin

A significantly increased the net conductance of HABIB-expressing oocytes by approximately 85% ( $27 \pm 15 \text{ nA/mV}$ ,  $n=18$ ) as compared with untreated HABIB-expressing oocytes ( $15 \pm 13 \text{ nA/mV}$ ,  $n=21$ ,  $p < 0.05$ ), but had no appreciable effect on control oocytes (Figure 2.6D). Thus, the endogenous signaling pathway triggered by electrode insertion appears to involve tyrosine phosphorylation or dephosphorylation, consistent with studies of prick and sperm activation in oocytes (Sato et al., 1998; Glahn et al., 1999)

However, pre-treatment of  $100 \mu\text{M}$  sodium orthovanadate, a protein tyrosine phosphatase inhibitor (Molokanova et al., 1997), had no effect on BIB whole cell conductance ( $19 \pm 11 \text{ nA/mV}$ ,  $n=13$  compared to untreated BIB,  $20 \pm 15 \text{ nA/mV}$ ,  $n=20$ ; Figure 2.6E). This lack of effect is likely to be due to the inability of sodium orthovanadate to cross the oocyte plasma membrane (Molokanova et al., 1997).

To confirm that the conductance of BIB-expressing oocytes was the result of kinase-mediated signaling pathways and not a result of new protein synthesis we tested the effect of cycloheximide, a membrane permeable inhibitor of protein synthesis in *Xenopus* oocytes (Gotoh et al., 1995). Not surprisingly, pre-treatment of oocytes with  $15 \mu\text{g/ml}$  cycloheximide for 30 minutes before injection of HABIB cRNA prevented the conductance response normally seen at two days after cRNA injection showing that the cycloheximide was active. However, pre-treatment with  $15 \mu\text{g/ml}$  cycloheximide for 30 minutes before voltage-clamp experiments had no effect on the conductance of BIB-expressing oocytes (Figure 2.6F). Therefore, new protein synthesis after electrode insertion is not the mechanism for spontaneous activation of currents in BIB-expressing oocytes.

Figure 2.7 demonstrates that BIB is a substrate for tyrosine kinase phosphorylation. Proteins from control and HABIB-expressing oocytes were

immunoprecipitated with rat-anti-HA antibody. After resolution by SDS-PAGE, proteins were transferred to nitrocellulose and probed with the rat-anti-HA antibody (top panel, to visualize BIB channels), anti-phosphotyrosine antibody (middle panel) or anti-phosphoserine antibody (bottom panel). As seen in the top panel, BIB channels are identified at the expected size of 80kD; whereas no proteins were visualized with HA antibody for proteins isolated from control oocytes. After stripping the blot and reprobing with anti-phosphotyrosine antibody a band at approximately 80kD (middle panel, arrow) was visualized in protein preparations from HABIB-expressing oocytes but was absent from control oocytes. A second band visualized with the phosphotyrosine antibody from HABIB-expressing oocytes was also seen in control oocytes and is likely to be due to non-specific interactions. No bands were visualized at approximately 80kD for HABIB-expressing or control oocytes after probing with the anti-phosphoserine antibody (lower panel).

In order to confirm the tyrosine phosphorylation of HABIB channels we repeated these experiments by immunoprecipitating proteins from control (lanes 1 and 3) or HABIB-expressing oocytes (lanes 2 and 4) with either the anti-HA antibody or the phosphotyrosine antibody. A representative blot is shown in Figure 2.7B. After resolution by SDS-PAGE and transfer to nitrocellulose, proteins were visualized with the HA antibody. A band corresponding to approximately 80kD (the predicted size of HABIB channels; arrow) is seen only from HABIB-expressing oocytes after immunoprecipitation with the HA and the phosphotyrosine antibody. No bands resolved at this size for protein from control oocytes. BIB channels are specifically phosphorylated at tyrosine residues. Possible sites of tyrosine phosphorylation are described in Chapter 4.

Figure 2.8 shows data from a cell-attached patch from a wild type HABIB-expressing oocyte. Single channel data were obtained after HABIB channel activation, as monitored with two-electrode voltage clamp (see Figure 2.2). Unitary channel conductance was obtained from a linear fit of the single channel current-voltage relationship. Figure 2.8A shows the current amplitudes at different voltages for data obtained from the three patches used to calculate unitary channel conductance. The current amplitudes at each voltage were obtained from Gaussian fits of amplitude histograms generated with pClamp Fetchan software. Wild type HABIB channels showed a single channel slope conductance of  $300 \pm 30 \text{ pS}$  (mean  $\pm$  S.D.,  $n=3$  patches from 3 different oocytes). The mean reversal potential was  $2 \pm 8 \text{ mV}$ , in agreement with the value measured by two-electrode voltage clamp in KCl bath saline. Only patches in which data were obtained at more than one voltage were used for unitary slope conductance calculations. The overall frequency of channel openings was low in patches with active channels, estimated at  $<5\%$  open time during the duration of the recording. However, a modal shift to high probability of opening was observed intermittently, as illustrated in Figure 2.8 that allowed measurement of unitary conductance and mean open time. In oocytes injected with 180ng of HABIB cRNA, 4 of 19 patches (from 9 different oocytes) contained the unique large conductance channels. In oocytes injected with 20ng of HABIB cRNA, 1 of 48 patches (from 24 oocytes) contained large conductance channels. Figure 2.8B shows sixteen consecutive traces of channel activity at a membrane potential of  $+40 \text{ mV}$  (pipette command potential multiplied by  $-1$ ). The open (O) and closed (C) amplitudes of a single channel are indicated. At  $+40 \text{ mV}$ , open state dwell time histograms were best fit by double exponential, with fast and slow tau values of 15ms and 1722ms, respectively. Control

**oocytes did not express these unique high conductance channels either before or after the two-electrode voltage clamp recordings (n=7). The channel events are uniquely associated with the expression of HABIB and the frequency of detection of active channels correlates with the amount of HABIB cRNA injected.**

## **2.4 DISCUSSION**

**The results presented in this chapter demonstrate that *Xenopus* oocytes expressing *Drosophila* BIB acquire a non-selective cation channel function. Channel activation is regulated by a mechanism involving endogenous signaling pathways and tyrosine phosphorylation but not serine/threonine phosphorylation. BIB is shown by western blot analysis to be a target for tyrosine phosphorylation, supporting the conclusion that the ionic conductance is mediated directly by the BIB protein.**

**Four lines of evidence demonstrate that the current we have observed in BIB-expressing oocytes is mediated by BIB channels and not by unidentified oocyte channels: (1) the lack of a conductance response from control oocytes; (2) mutation of glutamate at position 71 to asparagine (E71N) resulted in non-functional channels that were expressed on the plasma membrane, but did not recruit any ionic conductance response; (3) mechanisms of activation differ for the ionic conductance responses mediated by various channels in the MIP family, including AQP1 (activated by cGMP), AQP6 (activated by acidic pH) and BIB (regulated by tyrosine phosphorylation) when expressed in oocytes (Yasui et al., 1999; Anthony et al., 2000; and data presented here). (4) In addition, results from cell-attached patch clamp experiments of BIB-expressing oocytes revealed a large, novel single channel conductance ( $300 \pm 30$  pS, mean  $\pm$  SD). Large single channel conductances and long open times have been observed in other**

MIP family ion channels: 145pS for AQP1 (Anthony et al, 2000), 380pS for AQP0 (Ehring et al., 1990).

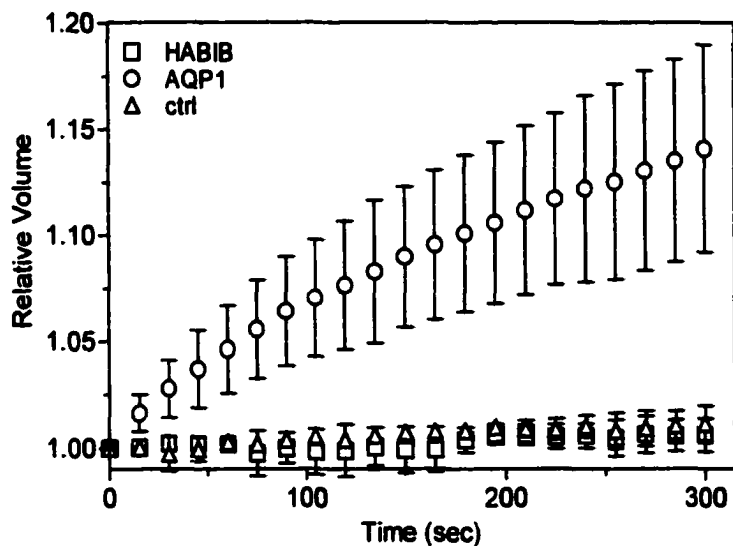
Although the nature of the regulation of BIB during neurogenesis in *Drosophila* is not known, we have shown that BIB protein is a target of tyrosine phosphorylation, and that the conductance associated with BIB expression is enhanced by lavendustin A, a tyrosine kinase inhibitor, and decreased by insulin, which acts on endogenously expressed insulin receptor tyrosine kinases (Scavo et al., 1991). We suggest that signals promoting dephosphorylation enhance BIB ion channel activation.

Serine/threonine kinase pathways do not appear to be involved based on the lack of effects of H7 and staurosporine.

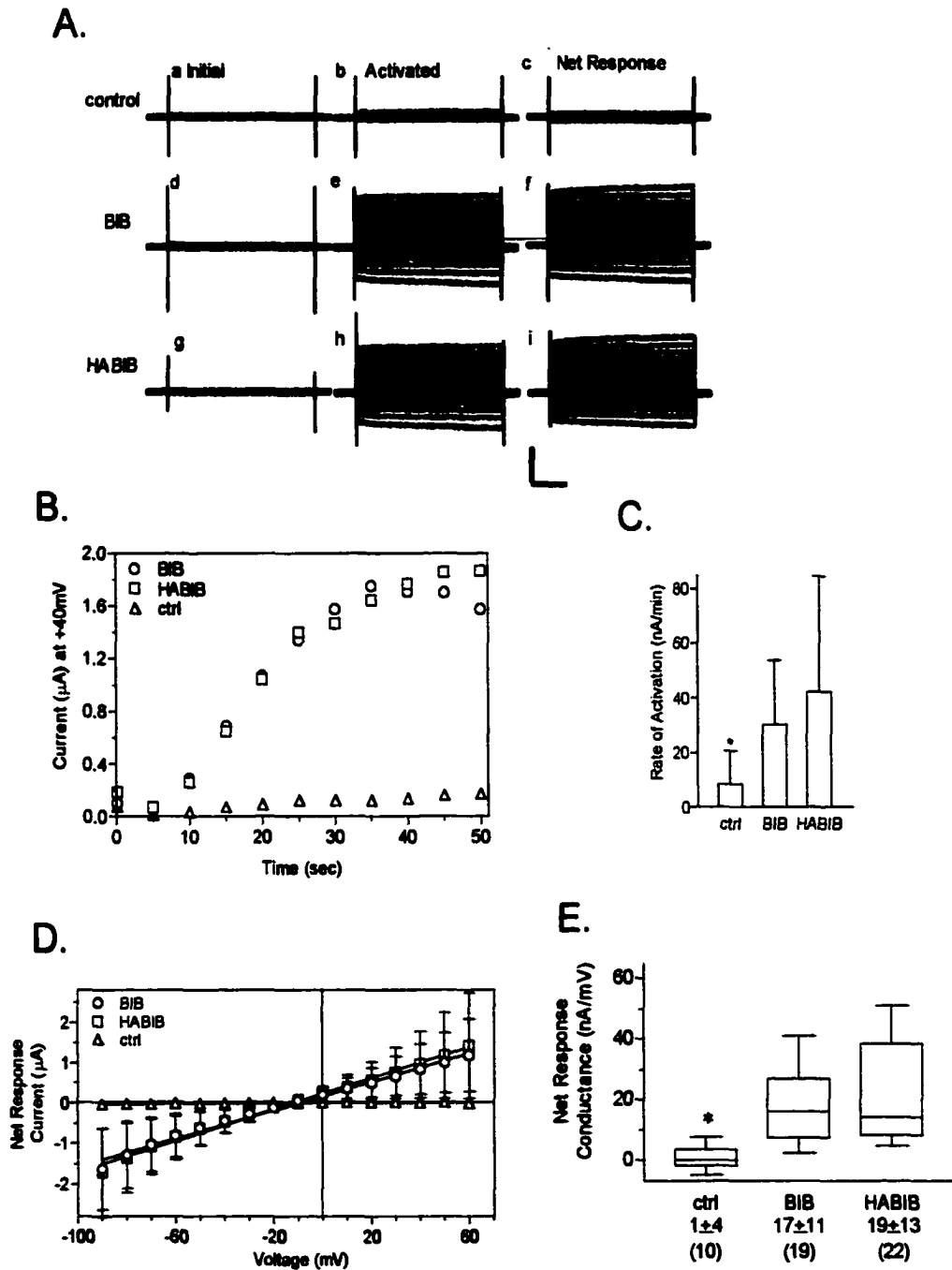
Tyrosine kinases and serine/threonine kinases are important for neuronal development in *Drosophila* (see for example Skeath, 1998; Ruel et al., 1993). The EGF receptor tyrosine kinase is important for determining neuroblast clusters along the dorsal-ventral axis of *Drosophila* embryos (Udolph et al., 1998; Skeath, 1998). *Drosophila* embryos carrying mutations in the insulin receptor were viable only when some kinase activity of the insulin receptor was preserved; lethality was observed in embryos that completely lacked insulin receptor tyrosine kinase activity (Chen et al., 1999). Interestingly, insulin receptor (*inr*) mutant embryos lacked populations of both neurons and glia that suggested a further role of *inr* in neurogenesis (Fernandez et al., 1995). Further experiments are needed to determine the importance of the putative ion channel function of BIB in *Drosophila* neuronal development and the Notch signaling pathway.

The data presented in this chapter support the hypothesis that BIB forms a non-selective cation channel when expressed in *Xenopus* oocytes. Our novel finding that the

**BIB-associated conductance is regulated by a mechanism involving tyrosine kinase pathways fits logically with the role of BIB in neurogenesis, a process that is governed by signaling pathways involving growth factors and other transmembrane receptor signaling through the Notch receptor (see chapter 1). Future experiments to investigate the native regulation of BIB during neurogenesis, the relationship between ion channel activity and the Notch signaling pathway and of the functional domains of the BIB protein should provide more clues to the unique involvement of *bib* in neurogenesis, and further evidence of the diversity of function in the MIP family of channels.**

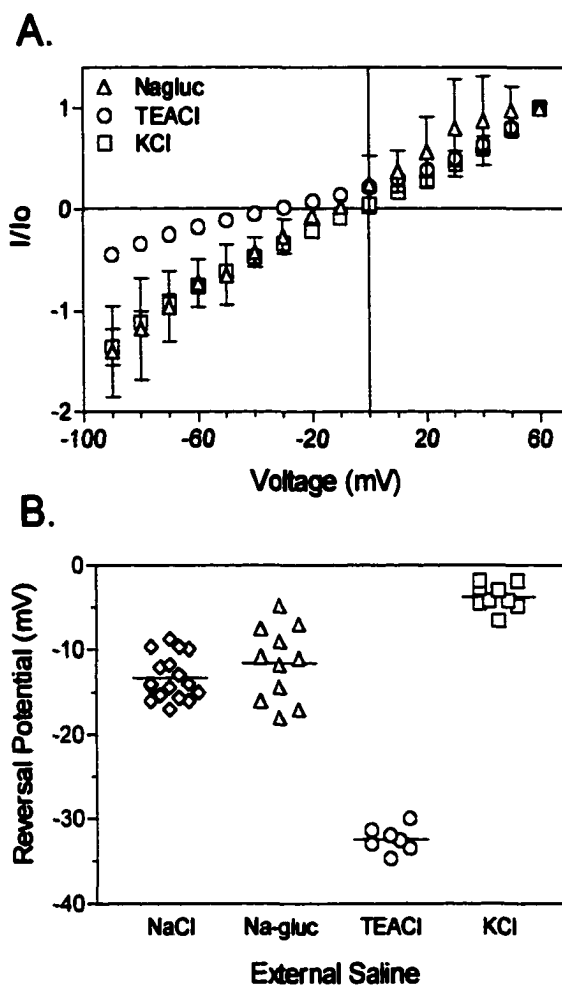


**Figure 2.1 *BIB is not a water permeable channel.*** Osmotic water permeability was analyzed with a swelling assay (see Methods). Oocytes expressing Aquaporin-1 (circles, n=5), or HABIB (squares, n=4) and control oocytes (triangles, n=4) were exposed to hypotonic saline at time zero and the relative volume change with time was measured from the video-imaged cross sectional area. Data are mean±S.D. from a representative experiment; n=4-5 oocytes per group.

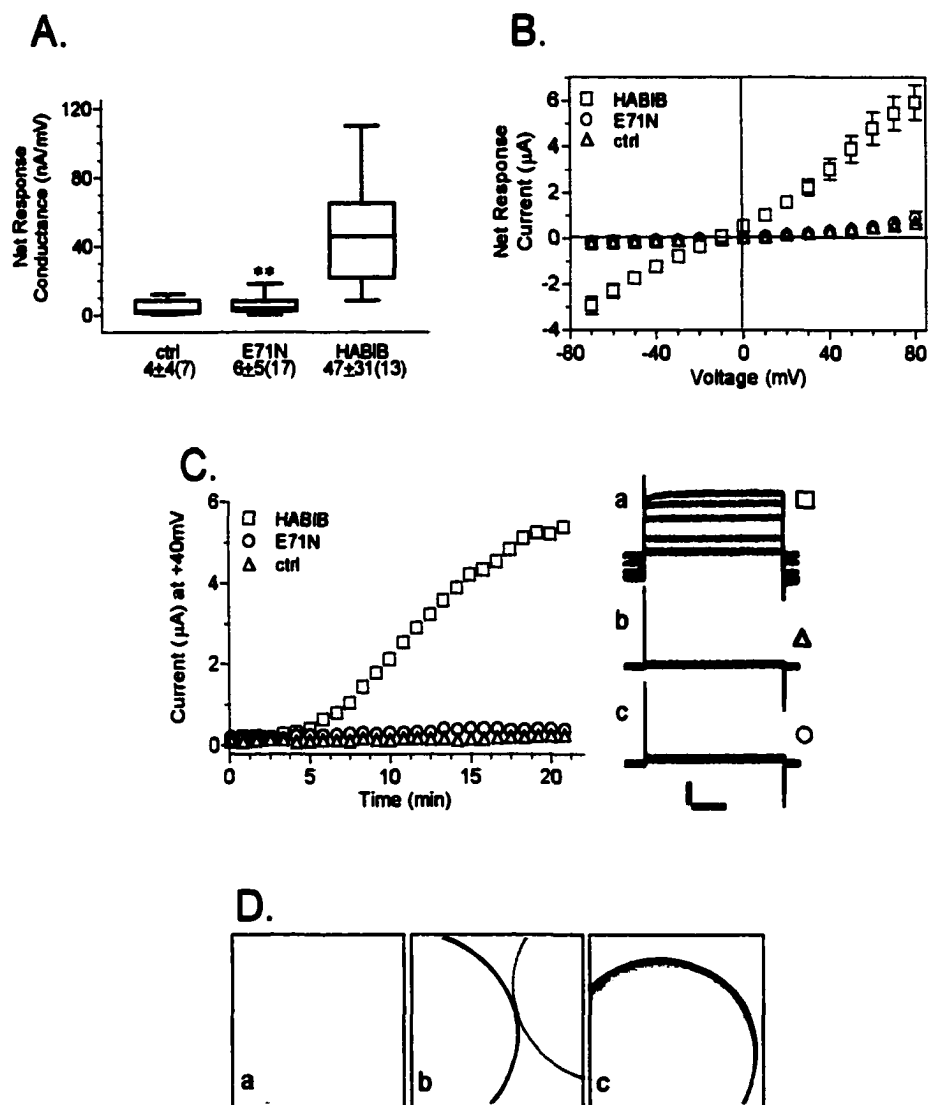


**Figure 2.2 Ion channel activity in BIB-expressing oocytes.** See next page for details.

**Figure 2.2 Ion channel activity in BIB expressing oocytes.** **A.** Representative traces from control (a, b, c), BIB- (d, e, f) and HABIB-expressing (g, h, i) oocytes. Traces show the current evoked by stepping to a series of voltages from +60mV to -90mV in 10mV increments from the holding potential of -40mV. The "initial" current response was obtained before channel activation (a, d, g). The "activated" current response (b, e, h) was obtained after BIB and HABIB channels were activated by endogenous signaling pathways as in C. The net current response (c, f, i) was obtained by subtracting the set of initial traces from the final. Scale bars represent 2 $\mu$ A and 200ms. **B.** Time dependent current activation in control, BIB- and HABIB-expressing oocytes. Data points show the current at +40mV in response to repeated steps to +40mV (800ms duration) every 5 seconds from the holding potential of -40mV. For clarity data points are shown at 5-minute intervals. **C.** The rate of activation was calculated in the approximately linear range between 5 and 13 minutes from the slope of a linear fit of the current plotted as a function of time. \* indicates that the rate of activation (nA/min) calculated for control oocytes ( $8 \pm 12$  nA/min, n=10, p<0.05) was significantly less than that of BIB-expressing ( $30 \pm 24$  nA/min, n=19) and HABIB-expressing oocytes ( $42 \pm 42$  nA/min, n=22). Rates of activation for BIB and HABIB-expressing oocytes were not significantly different. **D.** The net current-voltage relationship of control (triangles, n=10), BIB (circles, n=19) and HABIB expressing oocytes (squares, n=22). **E.** Box plot showing the net conductances of control, BIB-expressing and HABIB-expressing oocytes. The boxes enclose 50% of the data points; bars show the maximum and minimum data points and the horizontal bar represents the median data value. Numbers of oocytes (n) are indicated below each column.

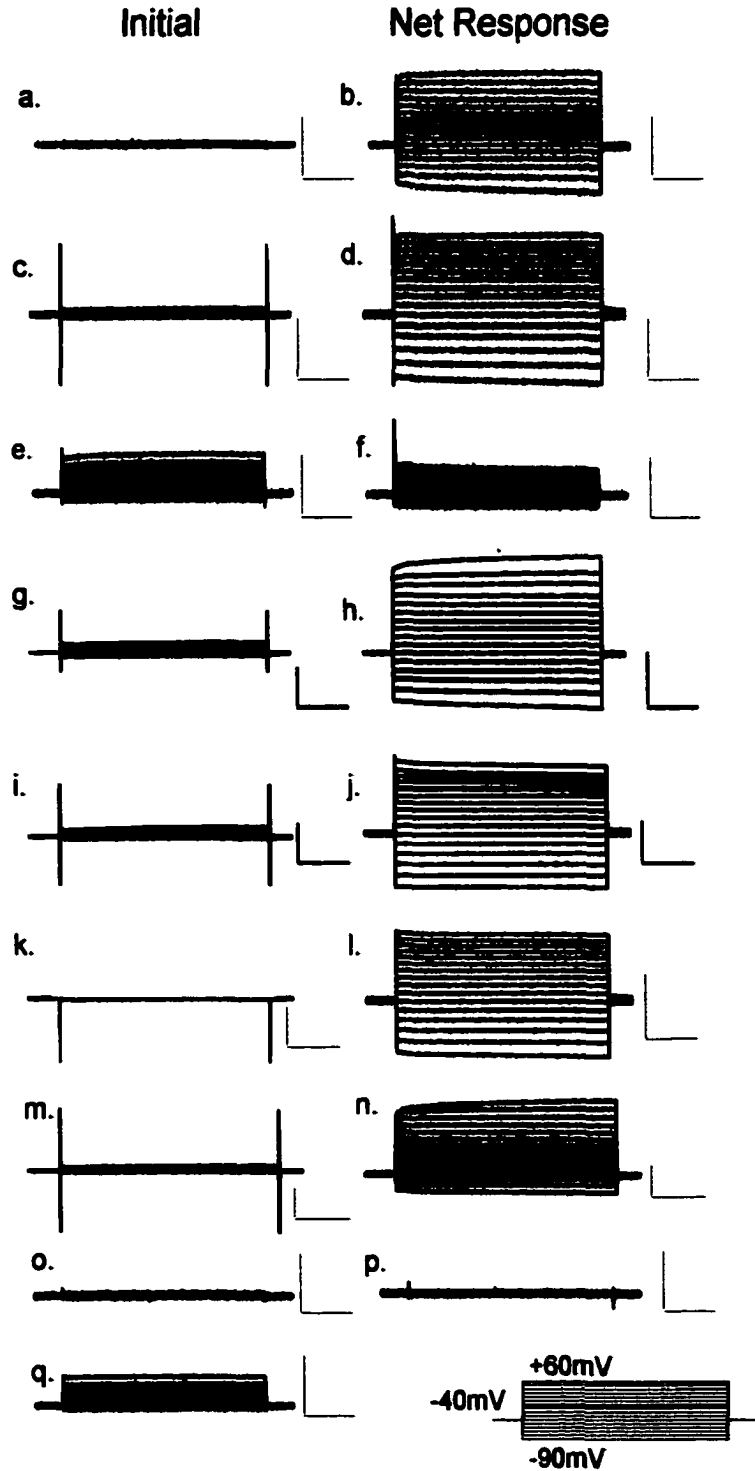


**Figure 2.3 *BIB* channels show non-selective monovalent cation selectivity.** **A.** Ionic selectivity was determined from the reversal potential of the current-voltage relationship of HABIB expressing oocytes with iso-osmotic substitution of 100mM NaCl in bath saline with 100mM KCl (squares, n=9), 100mM TEACl (circles, n=7), or 60mM Na-gluconate +40mM NaCl (triangles, n=9). Currents ( $I/I_o$ ) were standardized to the outward current at +60mV. **B.** Calculated reversal potentials of BIB whole cell currents in bath salines containing NaCl, Na-gluconate (Na-glu), TEACl and KCl, showing a selectivity sequence  $K^+ > Na^+ > TEA^+$ .



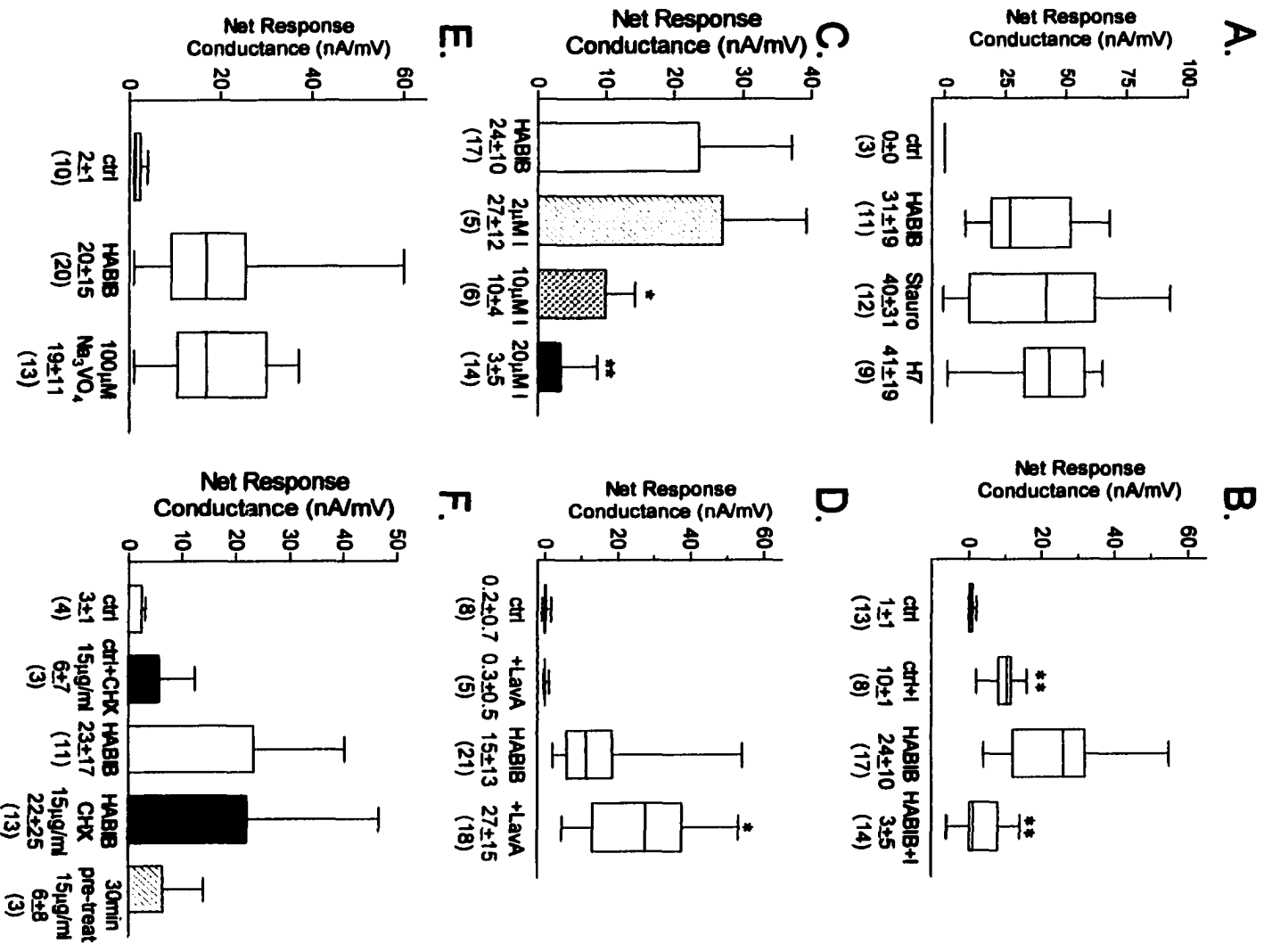
**Figure 2.4 Mutation of HABIB (E71N) abolishes the ionic conductance response without preventing membrane localization of the heterologously expressed channel in oocytes. See next page for details.**

**Figure 2.4 Mutation of HABIB (E71N) abolishes the ionic conductance response without preventing membrane localization of the heterologously expressed channel in oocytes.** **A.** The net conductance responses of control oocytes, or oocytes expressing HABIB wild type or E71N mutant channels are summarized as box plots. Net conductance values were obtained from the linear fits of the net current-voltage relationships. \*\* indicates that E71N-expressing oocytes had significantly reduced net conductance compared to HABIB-expressing oocytes ( $p < 0.01$ ) but not different than that of control oocytes. **B.** Mean net current-voltage relationships for wild type HABIB-expressing (squares,  $n=13$ ), HABIB E71N-expressing (circles,  $n=17$ ) and control oocytes (triangles,  $n=7$ ). Data are mean  $\pm$  S.D. **C.** Activation of ionic current as a function of recording time in an oocyte expressing wild type HABIB (squares,  $n=13$ ), but not in HABIB E71N-expressing (circles,  $n=17$ ) and control oocytes (triangles,  $n=7$ ). Data represent the current amplitude at +40mV evoked by repeated steps (800ms duration) every five seconds from a holding potential of -40mV and are shown at one-minute intervals for clarity. (Inset) Panels a-c show corresponding current traces, evoked by repeated steps to +40mV and shown at approximately four-minute intervals for an HABIB-expressing (a), control oocyte (b) and E71N expressing oocyte (c). **D.** Panels a-c show confocal images of a control oocyte (a), and oocytes expressing HABIB (b) or E71N (c), all labeled with a rat anti-HA antibody (Roche) and visualized by a fluorescein isothiocyanate-conjugated secondary antibody, with confocal microscopy. Images are shown as reverse field negatives for clarity.



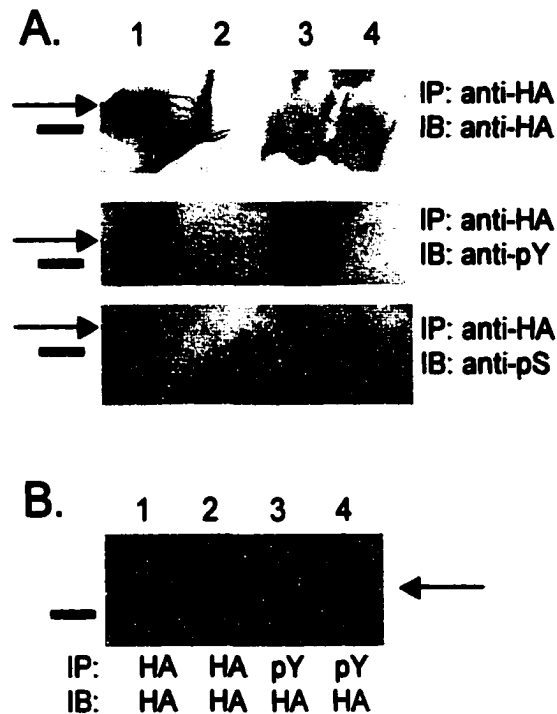
**Figure 2.5** *Regulators of kinase pathways differentially modulate the ionic conductance produced by electrode insertion and endogenous signaling in BIB-expressing oocytes. See next page for details.*

**Figure 2.5 Regulators of kinase pathways-differentially modulate the ionic conductance produced by electrode insertion and endogenous signaling in BIB-expressing oocytes.** Representative current traces from HABIB-expressing oocytes evoked by stepping to voltages from +60mV to -90mV in 10mV increments from a holding potential of -40mV, except for m and n which were evoked with steps from +80 to -70. Scale bars are 2.5 $\mu$ A and 200ms. Traces represent the initial current responses immediately following electrode insertion, (a,c,e,g,i,k,m,o,q) and the net response at 30 minutes after channel activation (b,d,f,h,j,l,n,p). Initial and net responses are shown for HABIB-expressing oocytes: (a,b) under standard conditions without pharmacological agents; (c,d) after one hour pre-incubation in 10 $\mu$ M lavendustin A; (e,f) after one hour pre-incubation with 20 $\mu$ M insulin; (g,h) after one hour pre-treatment with 1 $\mu$ M staurosporine; (i,j) after two hour pre-incubation with 10 $\mu$ M H7; (k,l) after one hour pre-incubation with 100 $\mu$ M sodium orthovanadate; (m,n) after 30 minute pre-incubation with 15 $\mu$ g/ml cycloheximide. Initial and net responses are shown for a control oocyte: (o,p) under standard conditions; and initial response is shown in (q) after one hour pre-incubation with 20 $\mu$ M insulin.

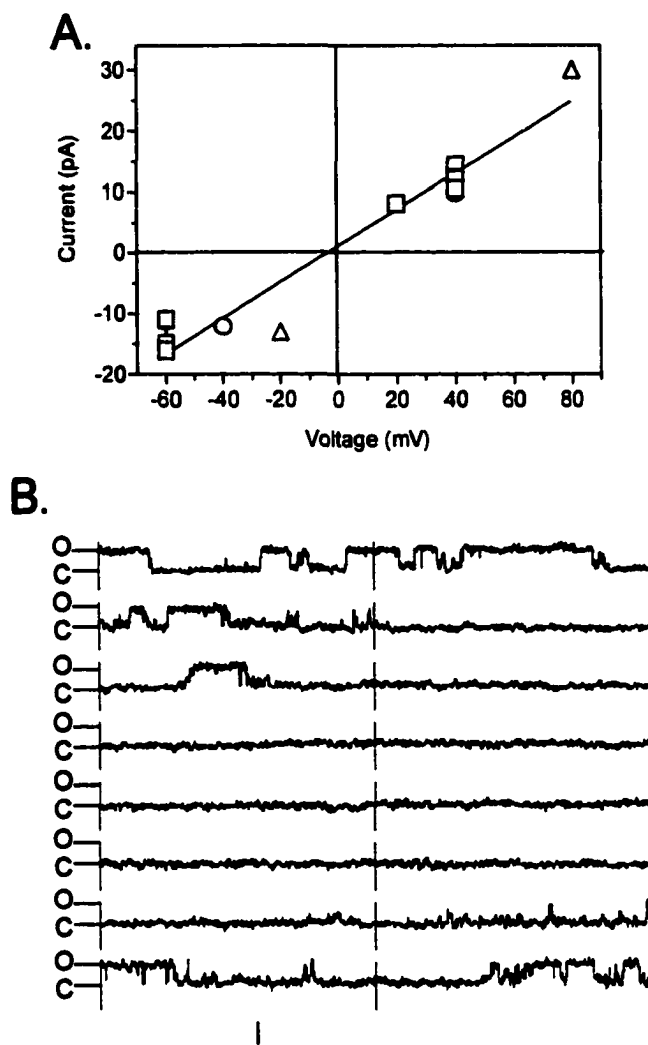


**Figure 2.6 Summary of differential modulation of kinase pathways on the ionic conductance produced by electrode insertion and endogenous signaling in BIB-expressing oocytes. See next page for details.**

**Figure 2.6 Summary of differential modulation of kinase pathways on the ionic conductance produced by electrode insertion and endogenous signaling in BIB-expressing oocytes.** A. Box plots summarize the effects of pre-incubation of HABIB-expressing oocytes with 1 $\mu$ M staurosporine (Stauro) or 10 $\mu$ M H7 (H7) on the net conductance of HABIB-expressing and untreated control oocytes. The boxes enclose 50% of the data points; vertical bars show the maximum and minimum data points and the horizontal bar represents the median value. Data values also are given as mean $\pm$ S.D. (n) below each column. No significant differences were observed for treated and untreated HABIB-expressing oocytes. B. Box plots show the effect of pre-incubation of HABIB-expressing oocytes with 20 $\mu$ M insulin (HABIB+I) for one hour. Asterisks indicate insulin treated HABIB-expressing oocytes had significantly reduced net conductance response compared with untreated HABIB-expressing oocytes ( $p < 0.01$ ) or that control oocytes treated with 20 $\mu$ M insulin have increased net conductance compared to untreated controls ( $p < 0.01$ ) reflecting insulin activation of endogenous channels (described in text). C. Bar graph showing the dose-dependent effect of insulin pre-treatment (2 $\mu$ M, 10 $\mu$ M and 20 $\mu$ M) on the net conductance of HABIB-expressing oocytes. Bar height indicates mean; error bars indicate standard deviation. Asterisks indicate HABIB-expressing oocytes treated with 10 or 20 $\mu$ M insulin had net conductance significantly reduced compared to untreated HABIB-expressing or those treated with 2 $\mu$ M insulin (\*,  $p < 0.05$  and \*\*,  $p < 0.01$  respectively). D. Box plot summary of the responses of control and HABIB-expressing oocytes to one hour pre-treatment with 10 $\mu$ M lavendustin A (+LavA). Asterisk indicates the net conductance of HABIB-expressing oocytes pre-incubated with 10 $\mu$ M Lavendustin A was significantly increased compared to untreated HABIB-expressing oocytes ( $p < 0.05$ ). E. Box plots show the effect of pre-incubation of 100 $\mu$ M sodium orthovanadate ( $\text{Na}_3\text{VO}_4$ ) for one hour. No significant differences were observed between treated and untreated HABIB-expressing oocytes. F. Bar graphs show the effect of pre-incubation of 15 $\mu$ g/ml cycloheximide for 30 minutes before voltage-clamp experiments (black bars) or before cRNA injection (hatched bar). The net conductance of HABIB-expressing oocytes incubated for 30 minutes with 15 $\mu$ g/ml cycloheximide before voltage-clamp experiments (black filled bar) was not significantly different than untreated HABIB-expressing oocytes (open bar). Pre-incubation of oocytes with 15 $\mu$ g/ml cycloheximide before cRNA injection reduced net conductance of oocytes injected with HABIB cRNA but the difference was not significant compared to untreated HABIB-expressing oocytes.



**Figure 2.7** *BIB channels are phosphorylated on tyrosine residues.* Solid bars represent the position of the 75kD molecular weight marker. Arrows show the location of BIB channels at the expected size of approximately 80kD. **A.** Oocyte plasma membrane fractions from HABIB-expressing oocytes (lane 1) or control oocytes (lane 3) were immunoprecipitated (IP) with anti-HA antibody. Proteins immunoprecipitated with anti-HA antibody from cytosolic fractions are shown in lane 2 (HABIB-expressing oocytes) and lane 4 (control oocytes). The blot was probed by immunoblotting (IB) with antibodies to HA (top panel); phosphorylated tyrosine residues (PY11120; middle panel); and phosphorylated serine residues (bottom panel). **B.** Oocyte plasma membrane fractions from control (lanes 1 and 3) or HABIB-expressing oocytes (lanes 2 and 4) were immunoprecipitated with either the HA antibody or PY11120 antibody (indicated below). The blot was probed with the HA antibody to show the presence of BIB channels.



**Figure 2.8 *BIB* channels have a large single channel conductance.**

Ion channel activity obtained in cell-attached patches from activated HABIB-expressing oocytes. Cell-attached patches were made on oocytes after the activation of HABIB channels as monitored with two-electrode voltage clamp. **A.** HABIB channels show a linear current-voltage relationship. Data from three patches from different oocytes are indicated by different symbols (squares, circles and triangles). Data points for single channel current amplitudes are mean±S.D., calculated from Gaussian fits of amplitude histograms at different holding potentials for each patch. Repeated symbols per voltage reflect analyses made at different times during the recording. Unitary conductance was 300±30pS, mean±S.D. for slope conductance from individual patches, and 297±22pS for the combined data as shown in A. **B.** Sixteen consecutive traces (demarcated by vertical bars) at +40mV are shown for a cell-attached patch from an HABIB-expressing oocyte. The open (O) and closed (C) states of a single level event are indicated. Scale bars are 10pA, 384ms.

## **CHAPTER 3. DIVALENT CATION BLOCK OF BIG BRAIN CHANNELS**

### **3.1 INTRODUCTION**

Calcium and magnesium ions have important physiological roles during development and into adulthood that result from both permeation and block of specific ion channels. Entry of calcium through voltage-gated calcium channels mediates the fertilization-induced depolarization potential in amphibian oocytes and prevents fertilization by multiple sperm (Dascal, 1987; Moody, 1995). Spontaneous calcium influx in developing neurons regulates gene transcription and causes cytoskeletal reorganization during growth cone navigation (Spitzer and Ribera, 1998). Calcium permeation of cyclic-nucleotide gated ion channels in rods and cones of the retina maintains the membrane potential in the dark as well as regulating levels of intracellular calcium (Hille, 1992).

Block of ion currents by calcium and magnesium is also important, especially in the brain. NMDA receptors are ligand-gated ion channels endogenously activated by the neurotransmitters glutamate and glycine (Hille, 1992). These channels also exhibit voltage dependence because at rest they are blocked by  $Mg^{2+}$ . In addition to ligand binding, sufficient depolarization is needed to unblock the pore, thereby allowing influx of calcium and enhancement of intracellular signaling through calcium-mediated pathways (Hille, 1992). In addition to ligand binding and membrane potential, NMDA receptors are regulated by tyrosine phosphorylation. Application of a soluble tyrosine kinase (src) potentiated calcium currents through NMDA receptors in spinal dorsal horn neurons (Yu et al., 1997). Thus, NMDA receptors provide a good example of an ion channel with multiple modes of regulation.

Results presented in the previous chapter indicated that in *Xenopus* oocytes expressing HABIB channels, a non-selective monovalent cation conductance was activated in response to endogenous signaling pathways. Due to the importance of calcium signaling in development and the established role of Big Brain mediating fate determinations during neurogenesis, we investigated the effects of divalent cations,  $\text{Ca}^{2+}$ ,  $\text{Ba}^{2+}$  and  $\text{Mg}^{2+}$  on whole-cell currents in *Xenopus* oocytes expressing HABIB. We found that whole-cell conductance of oocytes expressing HABIB is blocked by  $\text{Ca}^{2+}$  and  $\text{Ba}^{2+}$  but not by  $\text{Mg}^{2+}$ . We investigated the contribution of negatively charged amino acids of HABIB to  $\text{Ca}^{2+}$  and  $\text{Ba}^{2+}$  block with site-directed mutagenesis of D253, E274 and E71. We found that mutation of positions 253 and 274 has little effect, but mutation of E71 has profound effects on HABIB monovalent cation conductance. Several non-conservative substitutions eliminated ion channel function without preventing trafficking to the plasma membrane, or disrupted proper channel assembly. The conservative mutation of E71 to aspartic acid created sensitivity in HABIB-expressing oocytes to  $\text{Mg}^{2+}$ . E71 is a highly conserved amino acid in the MIP family of channels. Our analysis shows that it is crucial in determining channel properties. Furthermore, the change in divalent cation sensitivity with mutation of E71 confirms that BIB is an ion channel.

## 3.2 MATERIALS AND METHODS

*(1) Molecular techniques.* Site-directed mutagenesis was performed on HABIB constructs in the *Xenopus*  $\beta$ -globin expression vector (pX $\beta$ Gev) with the Stratagene QuickChange site-directed mutagenesis kit (Stratagene, La Jolla, CA). Aspartic acid 253, glutamate 274 and glutamate 71 were mutated to asparagine (D253N, E274N,

E71N). Glutamate 71 was also mutated to lysine (E71K), glutamine (E71Q) and aspartic acid (E71D), using the following primer combinations (mutated base pairs underlined):

**D253N**

sense: 5'-GTGCTTAACAAATGGACAGCCATTGGGTGACTGG-3' (bp 1042-1077)

antisense: 5'-CCAGTACACCCAATGGCTGTCCATTTGTTAAGCAC-3' (bp 1077-1042)

**E274N**

sense: 5'-GGCCTGGTGTACAACTTACATCTTCAACTCGCGC-3' (bp 1108-1140)

antisense: 5'-GCGCGAGTTGAAGATGTAGTTGTACACCAGGCC-3' (bp 1140-1108)

**E71N**

sense: 5'-GGAGATCCATCATCAGCAACTGTCTGGCCTCC-3' (bp 494-525)

antisense: 5'-GGAGGCCAGACAGTTGCTGATGATGGATCTCC-3' (bp 525-494)

**E71K**

sense: 5'-GGAGATCCATCATCAGCAGTGTCTGGCCTC-3' (bp 494-524)

antisense: 5'-GAGGCCAGACACTTTGCTGATCATCGATCTCC-3' (bp 524-494)

**E71Q**

sense: 5'-GGAGATCCATCATCAGCCAGTGTCTGGCCTC-3' (bp 494-524)

antisense: 5'-GAGGCCAGACACTGGGCTGATGATGGATCTCC-3' (bp 524-494)

**E71D**

sense: 5'-CCATCATCAGCGACTGTCTGGCCTCCTTC-3' (bp 500-528)

antisense: 5'-GAAGGAGGCCAGACAGTCGCTGATGATGG-3' (bp 528-500)

The mutation strategy is outlined in Figure 3.1. The entire coding sequences of all constructs were sequenced to verify that no inadvertent mutations were introduced.

Plasmid DNA was linearized with *SpeI* in the polylinker region and used to transcribe RNA *in vitro* with T3 RNA polymerase. Enzymes were purchased from Roche Molecular Biochemicals (Indianapolis, IN).

**(2) Oocyte preparation and injection.** Stage V-VI oocytes from adult female *Xenopus laevis* were obtained and defolliculated as described in Chapter 2.

**(3) Electrophysiological recordings.** Two-electrode voltage clamp was used to investigate the macroscopic ion channel properties of HABIB as described in Chapter 2. The effects of divalent cations ( $\text{Ca}^{2+}$  and  $\text{Ba}^{2+}$ ) were tested by iso-osmotic substitution of  $\text{CaCl}_2$  or  $\text{BaCl}_2$  for  $\text{MgCl}_2$  in the standard recording saline. All salines were buffered with 2mM EGTA. Free  $\text{Ca}^{2+}$  and  $\text{Ba}^{2+}$  concentrations were calculated using MaxChelator (<http://www.stanford.edu/~cpatton/maxc.html>). Channel activation was monitored by repeated steps to +40mV (800ms duration) every 5 seconds from a holding potential of -40mV. Conductance was measured as the slope of a linear fit of the current-voltage relationship between +40 and -70mV after channel activation in standard saline containing 4.5mM  $\text{MgCl}_2$  and after perfusion with saline containing  $\text{CaCl}_2$  or  $\text{BaCl}_2$ . The percent block was calculated as  $[(G_0 - G)/G_0] \times 100$ , where  $G_0$  is the conductance measured in recording saline with 4.5mM  $\text{MgCl}_2$  and  $G$  is the conductance measured in the test saline. The fraction of unblocked current ( $I_{UF}$ ) was calculated as:  $[(I_{ss} - I_{init})/I_{init}]$ , where  $I_{ss}$  is the steady-state current value obtained 4ms before the end of the voltage pulse and  $I_{init}$  is the initial current value approximately 2ms after the capacitance artifact. Current traces were best fit by a double exponential (Clampfit8.0, Axon Instruments, Foster City, CA).

**(5) Cellular fractionation.** Oocyte plasma membrane fractions were obtained as described in Chapter 2.

**(6) Western Blotting.** Western blots were performed as described in Chapter 2.

Data values are presented as mean±SD. Significance was tested by a Student's t-test, with significance indicated by  $p < 0.05$  unless otherwise indicated.

### **3.3 RESULTS**

The effects of divalent cations on the channel properties induced by expression of HABIB in *Xenopus* oocytes were tested by equimolar substitution of 4.5mM  $MgCl_2$  in the standard recording saline with  $CaCl_2$  or  $BaCl_2$ . For the purposes of this chapter, standard recording saline (102mM NaCl, 4.5mM  $MgCl_2$ , 2mM EGTA, 5mM Hepes, pH7.3) will be referred to as "magnesium saline" and saline substituted with 4.5mM  $CaCl_2$  will be referred to as "calcium saline"; standard saline with 4.5mM  $BaCl_2$  substituted will be referred to as "barium saline".

The effects of substitution of  $MgCl_2$  with equimolar  $CaCl_2$  or  $BaCl_2$  are shown in Figure 3.2. HABIB channel activation was monitored with steps to +40mV from a holding potential of -40mV as described in chapter 2. After HABIB channel activation in magnesium saline, saline containing calcium or barium was perfused into the recording chamber. Representative examples of perfusion with saline containing 4.5mM  $CaCl_2$  (top panel) or 4.5mM  $BaCl_2$  (bottom panel) are shown in Figure 3.2A. In Figure 3.2B traces show currents evoked over a range of voltages after HABIB channel activation in magnesium saline (top), and following perfusion with calcium (middle) or barium saline (bottom). Figure 3.2C shows the current-voltage relationship of HABIB channels in magnesium, calcium or barium salines for the traces shown in Figure 3.2B. Inward currents in HABIB-expressing oocytes in calcium and barium saline are dramatically

reduced in amplitude as compared to those in magnesium saline. Reversal potentials magnesium ( $-17 \pm 5$  mV,  $n=14$ ), calcium ( $-18 \pm 9$  mV,  $n=6$ ) and barium saline ( $-16 \pm 5$  mV,  $n=13$ ) were not significantly different.

Calcium and barium reduced the whole-cell conductance of HABIB-expressing oocytes in a dose-dependent manner. Figure 3.3A shows the percent conductance block, calculated as the change in conductance after perfusion with the test saline ( $G_0$ ; where  $G_0$  is the conductance in magnesium saline and  $G$  is the conductance in test saline) divided by the conductance in magnesium saline.

Figures 3.3B and C show the influence of voltage on the blocking effects of calcium and barium for HABIB currents standardized to the response in magnesium saline. The current at each voltage in calcium ( $I_{Ca}$ ) or barium saline ( $I_{Ba}$ ) was normalized to the current in magnesium saline ( $I_{Ca}/I_{Mg}$  and  $I_{Ba}/I_{Mg}$ ) and plotted as a function of step potential. Data for  $I_{Ca}/I_{Mg}$  and  $I_{Ba}/I_{Mg}$  are summarized in Tables 3.1 (calcium) and 3.2 (barium). Values of  $I_{Ca}/I_{Mg}$  and  $I_{Ba}/I_{Mg}$  less than one indicate that the current in magnesium saline was blocked by calcium or barium, conversely, values of  $I_{Ca}/I_{Mg}$  and  $I_{Ba}/I_{Mg}$  greater than or equal to one indicate the current in magnesium was not blocked.

Perfusion of either calcium or barium salines resulted in decreased HABIB currents at hyperpolarized membrane potentials. At voltage steps between  $-70$  and  $-40$  mV, the ratios  $I_{Ca}/I_{Mg}$  and  $I_{Ba}/I_{Mg}$  remained at less than one (indicating block) for all doses. In addition, the ratios remained constant between  $-70$  and  $-40$  mV. In contrast, at depolarized potentials, the ratios  $I_{Ca}/I_{Mg}$  and  $I_{Ba}/I_{Mg}$  increased with depolarization between ( $+30$  to  $+80$  mV). The blocking effects of calcium and barium are relieved with sufficient depolarization, indicating the block is voltage-dependent.

Current traces show voltage-dependent differences in magnesium, calcium and barium salines (Figure 3.4A and B). Traces in magnesium saline show unblocking at both depolarized and hyperpolarized potentials. In contrast, traces in calcium and barium saline only exhibit unblocking at depolarized potentials. We quantified these differences by calculating the fraction of unblocked current ( $I_{UF}$ , see Methods). Calculation of  $I_{UF}$  allowed quantitative comparison of blocking and unblocking of currents in magnesium, calcium and barium salines in a manner independent of the actual current amplitudes, which are influenced by levels of expression of HABIB. Unblocking occurs when the current at the end of the voltage step ( $I_{ss}$ ) is greater than the current at the beginning of the voltage step ( $I_{init}$ ), and will yield a calculated  $I_{UF}$  that is greater than zero. If currents are blocked then the current at the end of the voltage step will be less than that at the beginning of the voltage step and will yield a calculated  $I_{UF}$  that is less than zero.

The calculated fraction of unblocked current ( $I_{UF}$ ) is plotted as a function of membrane potential in Figure 3.4C and values are shown in Table 3.3. From this analysis two properties are apparent for currents in BIB-expressing oocyte in magnesium, calcium and barium salines. First, at depolarized potentials, monovalent cation currents in HABIB-expressing oocytes are unblocked in magnesium, calcium and barium salines. Unblocking at depolarized potentials is voltage-dependent. Calculated  $I_{UF}$  values increase with increasing depolarization, reaching maximum values at +80mV for currents in magnesium, calcium and barium. Second, at hyperpolarized potentials, currents in HABIB-expressing oocytes are unblocked in magnesium saline. Calculated  $I_{UF}$  values reach maximal levels at -120mV in magnesium saline. In contrast, currents in HABIB-expressing oocytes are blocked in barium saline.  $I_{UF}$  values calculated for

currents in barium saline remain at approximately  $-0.6$  at voltage steps between  $-120$  and  $-40$ mV. At hyperpolarized potentials, currents in calcium saline have properties intermediate between those of magnesium and barium. Values of  $I_{UF}$  for currents in HABIB-expressing oocytes in calcium saline remain at less than zero at voltage steps between  $-120$  and  $-40$ mV indicating that monovalent cation currents in oocytes expressing HABIB are blocked by calcium. However, unlike the  $I_{UF}$  values for currents in barium saline,  $I_{UF}$  values in calcium saline do increase with hyperpolarization and reach maximal levels at  $-120$ mV but they are not greater than zero. From this analysis we conclude that the blocking effects of calcium and barium are voltage-dependent. At depolarized potentials, currents in HABIB-expressing oocytes are unblocked in a voltage-dependent manner whereas, at hyperpolarized potentials, currents are blocked in calcium and barium salines.

Since the magnitude of current blocking and unblocking was voltage-dependent, we determined the effects of voltage on the rates of blocking and unblocking. The net rates of unblock (at depolarized potentials) and block (at hyperpolarized potentials) are plotted as a function of membrane potential in Figures 3.5 and 3.6. Tau values were obtained from double exponential fits of current traces such as those shown in Figure 3.4A and B. Both fast and slow tau values for unblocking show no apparent voltage dependence in magnesium, calcium or barium saline. Similarly, rates of block were not voltage-dependent. The lack of voltage dependence on the rate of block appears contradictory to our results indicating voltage dependence of blocking and unblocking. However, the rates of unblocking may be influenced by conformational changes that affect the accessibility of binding sites for calcium and barium at depolarized potentials. Fast and slow tau values for blocked currents were obtained by

fitting current traces from  $-120$  to  $-40$ mV after an initial step to  $+40$ mV where we hypothesized channels to be unblocked. However, our analysis of the fraction of unblocked current at depolarized potentials suggests that maximal unblocking occurs at  $+80$ mV. The apparent lack of voltage-dependence of fast and slow tau values at hyperpolarized potentials may be a result of the channels already being partially blocked since the step to  $+40$ mV does not completely unblock HABIB channels in oocytes.

In 1973, Woodhull proposed a model of voltage-dependent block based on experiments that tested the block by extracellular protons of sodium channel currents (Woodhull, 1973). Her analysis predicted that if the block was voltage dependent then protons must be interacting with the sodium channel from a site within the electrical field. The distance of the binding site from the extracellular side of the membrane is termed the fractional electrical field distance ( $\delta$ ). We calculated the apparent fractional electrical field distance of block by calcium using methods as described by Park and MacKinnon, 1995. The first step is to calculate the concentration of calcium that inhibits 50% of the current at each voltage ( $K_i$ ). Figure 3.7A shows a graph of relative calcium current amplitudes plotted as a function of free calcium concentration for different voltages. These graphs were fit by a sigmoidal dose response curve to obtain  $K_i$  values for each voltage. The  $K_i$  values were plotted as a function of membrane potential in Figure 3.7B and fit with the equation  $K_{1/2} = K_{1/2}(0\text{mV}) \exp(z\delta FV/RT)$ , where  $V$  is the membrane voltage,  $z$  is the valence of the blocking ion,  $R$  is the gas constant,  $T$  is temperature in Kelvin and  $K_{1/2}(0\text{mV})$  is the concentration required to produce 50% inhibition at  $0\text{mV}$ . (Park and MacKinnon, 1995). The fit of the line through the data was  $y = 0.28115 \exp(0.0011261x)$ ,  $R = 0.92$ . Therefore, for calcium  $K_{1/2}(0\text{mV})$  is  $0.28\text{mM}$ , yielding a value for the fractional electrical field distance of  $\delta = 0.14$  from the outside. These results predict

that *if* calcium ions block BIB currents by binding to a site that is located within the electrical field, then the binding site is at a location in the extracellular side of the HABIB channel. However, calcium and barium could be blocking currents in HABIB-expressing oocytes by mechanisms other than interacting with a binding site in the electrical field.

Divalent cation block of ion channels is affected by negatively charged amino acids in pore lining regions (see for example, Park and MacKinnon, 1995). Since Loops B and E are predicted to be pore lining regions of MIP channels (see Chapter 1), we examined these regions for negatively charged amino acids as possible candidates for cation binding sites. Three negatively charged amino acids (two aspartic acid, one glutamate) are located in or around Loop E while none are found in Loop B (Figure 3.8). The HABIB mutants D253N, E274N, E71N, E71Q, E71K and E71D were generated and expressed in *Xenopus* oocytes for analysis of the effects of divalent cations. Figure 3.9 shows the structures of aspartic acid, glutamic acid, asparagine, glutamine, and lysine for comparison.

A summary of the results for D253N, E274N and E71N, Q and K are shown in Figure 3.10. Panel A summarizes the net conductance responses of oocytes expressing the HABIB mutants. Results obtained for E274N ( $35 \pm 18 \text{ nA/mV}$ ,  $n=19$ ) and D253N ( $21 \pm 13 \text{ nA/mV}$ ,  $n=21$ ) were not significantly different than those for wild type HABIB, compared within the same batches of oocytes. Wild type responses were  $47 \pm 30 \text{ nA/mV}$ ,  $n=13$  (left) and  $30 \pm 22 \text{ nA/mV}$ ,  $n=19$  (right). In contrast, oocytes expressing E71N, E71Q and E71K showed significant reductions in net conductance responses as compared to oocytes expressing wild type HABIB, and were not different from control oocytes (E71N,  $6 \pm 5 \text{ nA/mV}$ ,  $n=17$ ,  $p < 0.01$ ; E71Q,  $0 \pm 2 \text{ nA/mV}$ ,  $n=3$ ,  $p < 0.05$ ; E71K,  $0.4 \pm 0.3 \text{ nA/mV}$ ,  $n=3$ ,  $p < 0.05$ , HABIB,  $47 \pm 31 \text{ nA/mV}$ ,  $n=13$ ; control  $4 \pm 4 \text{ nA/mV}$ ,  $n=7$ ). There are many

reasons for absence of a response, including lack of expression. Because oocytes expressing E71N, E71Q and E71K had no current responses, they were not tested further for changes in permeability or sensitivity to divalent cations.

The dose-dependent block of conductance by calcium in oocytes expressing D253N, and E274N was equivalent to that in wild type channels (Figure 3.10B). We also found that monovalent cation selectivity for these mutants was equivalent to that of wild type channels. The calculated relative permeability ratios for oocytes expressing mutant E71N, E274N and D253N HABIB channels are listed in Figure 3.10C. Relative ionic permeability was tested by iso-osmotic substitution of NaCl in the bath recording saline with KCl or tetraethylammonium chloride (TEACl). No effect on  $P_{Na}/P_K$  or  $P_{TEA}/P_K$  was observed by mutation of D253 or E274 to asparagine.

The expression of mutant channels on the plasma membrane was confirmed by western blot analysis of oocyte plasma membrane fractions. Wild type, E71N, E71Q, D253N and E274N channels were identified at the expected size of approximately 80kD (Figure 3.10D). However, no proteins were visualized from oocytes expressing E71K or control oocytes. These results indicated that the lack of conductance response in oocytes expressing E71K channels was likely to be due to lack of expression of these mutant channels in the membrane.

Glutamate 71 is conserved in over 90% of channels in the MIP family (see Chapter 1). Although several mutations of E71 were non-functional we found an interesting alteration in channel properties with a more conservative mutation to aspartic acid (E71D). Figure 3.11 summarizes the conductance responses obtained from oocytes expressing E71D, wild type HABIB channels and control oocytes. Oocytes expressing E71D had significantly reduced whole-cell conductance ( $6 \pm 4$  nA/mV,  $n=11$ ,

$p < 0.01$ ) as compared to that in oocytes expressing HABIB ( $36 \pm 22 \text{ nA/mV}$ ,  $n=12$ ), but the response with E71D was significantly greater than that of control oocytes ( $1 \pm 1 \text{ nA/mV}$ ,  $n=6$ ,  $p < 0.05$ ). Western blots confirmed the expression of E71D in the plasma membrane (Figure 3.12B). Bands at approximately 80kD were visualized from plasma membrane fractions of oocytes expressing HABIB and E71D, and not seen in control oocytes. The band intensity of E71D channels is less than that of HABIB, suggesting that even though E71D channels are routed to the plasma membrane, decreased expression levels may account for the decreased conductance of oocytes expressing E71D. Other possibilities for the decreased whole-cell conductance are decreased in single channel conductance, decreased open probability, or an increased sensitivity to  $\text{Mg}^{2+}$ .

Figures 3.12 and 3.13 show that in contrast to currents expressing wild type HABIB channels, currents from E71D-expressing oocytes exhibit block by  $\text{Mg}^{2+}$ . Currents evoked at different voltages are shown in Figure 3.12. Tail currents measured at  $-120$  to  $+40 \text{ mV}$  after an initial step to  $+40 \text{ mV}$  are shown in Figure 3.13. Dramatic differences in currents are seen between oocytes expressing wild type HABIB and E71D channels in magnesium saline, particularly at hyperpolarized potentials (compare the top panels in Figure 3.13). In contrast to the unblocking seen at hyperpolarized potentials in oocytes expressing wild type HABIB, currents from oocytes expressing E71D exhibited blocking at hyperpolarized potentials in magnesium saline.

To compare the differences in currents from oocytes expressing wild type HABIB and those from oocytes expressing the E71D mutant in a manner independent of the level of expression, we calculated the fraction of unblocked current ( $I_{UF}$ ) at different voltages.  $I_{UF}$  was plotted as a function of membrane potential for wild-type HABIB and E71D channels in magnesium, calcium and barium saline in Figure 3.14 and values for

wild type and E71D-expressing oocytes also are given in Table 3.4. As described for Figure 3.3, an  $I_{UF}$  value greater than zero indicates unblocking whereas blocking is indicated by an  $I_{UF}$  value less than zero. The  $I_{UF}$  value at hyperpolarized potentials for oocytes expressing E71D channels remained constant around  $-0.5$  (shaded area in Table 3.4), similar to the  $I_{UF}$  values for E71D and wild type channels in barium saline. These results show that mutation of E71 to aspartic acid introduces  $Mg^{2+}$  block. E71 is highly conserved in over 90% of channels in the MIP family and these results indicate that it is critical for determining channel properties.

### 3.4 DISCUSSION

Calcium and barium block monovalent cation currents in oocytes expressing HABIB. There are several possible mechanisms to describe the observed blocking properties of calcium and barium. (1) Calcium and barium block currents by interacting with a site in the channel that is located within the electrical field. At depolarized potentials we observed voltage dependence of the unblocking of currents from oocytes expressing HABIB. At hyperpolarized potentials, currents in HABIB-expressing oocytes were blocked approximately 50%. The voltage dependence is consistent with calcium and barium blocking within the electrical field. Also consistent with this possibility is the calculated value for the fractional electrical field distance of block by calcium ( $\delta=0.14$ ). (2) Calcium and barium interact with a binding site on the extracellular surface that is not within but is affected by changes in the electrical field. In this case, at hyperpolarized potentials binding of calcium and barium at an extracellular site might alter the conformation of the channel to a closed conformation. If the availability of the binding site changes with membrane potential an apparent voltage-dependence would be

observed. Our results of voltage dependent blocking and unblocking are also consistent with this possibility. The lack of voltage dependence on the rates of unblocking and blocking by calcium and barium are consistent with a site affected by but not within the electrical field. (3) The increased surface to charge ratio of divalent cations compared to monovalent cations results in slower rates of ionic dehydration (Hille, 1992). Calcium and barium may be able to move through HABIB channels expressed in *Xenopus* oocytes, but their slow rates of dehydration results in slow movement through the pore and effectively block currents carried by  $\text{Na}^+$  and  $\text{K}^+$  (Hille, 1992). (4) Block is occurring through an intracellular mechanism. Calcium entry may induce intracellular signaling or bind to a site on the intracellular surface that results in channel closure. This possibility could account for the blocking effects of calcium but not barium.

In the experiments presented in this chapter both calcium and barium were applied from the extracellular side. The possible mechanisms of block outlined above suggest that a site with the pore or on the extracellular surface of the channel may interact with divalent cations. Negatively charged amino acids in pore lining regions are known to affect the blocking properties of divalent cations (see for example Park and MacKinnon, 1995). We used site-directed mutagenesis to explore cation binding sites in putative pore lining regions of HABIB. Mutation of aspartic acid 253, located in the putative extracellular pore lining region, to asparagine had no effect on calculated relative permeability ratios ( $P_{\text{Na}}/P_{\text{K}}$  and  $P_{\text{TEA}}/P_{\text{K}}$ ) or current block by calcium. Similarly, oocytes expressing E274N channels had properties identical to those of oocytes expressing wild-type HABIB. Despite their negative charge and locations in the putative pore region, aspartic acid 253 and glutamic acid 274 do not appear to contribute to cationic selectivity or block of HABIB channels.

In contrast mutations of glutamate (E71) located in transmembrane domain 1 (near Loop B) had dramatic effects. Mutation of E71 to asparagine or glutamine resulted in non-functional channels and channels mutated to lysine were not expressed on the plasma membrane. The net conductance response was also reduced for oocytes expressing channels with the more conservative substitution of E71 to aspartic acid, however, measurable differences in sensitivity to  $Mg^{2+}$  were observed. Changes in  $Mg^{2+}$  sensitivity are most striking at hyperpolarized potentials. The  $I_{UF}$  values for currents in oocytes expressing wild type HABIB increase from  $-0.3$  at  $-40mV$  to  $0.1$  at  $-120mV$ , indicating that currents are unblocked in magnesium saline. In contrast,  $I_{UF}$  values for currents in E71D-expressing oocytes remain constant at  $-0.5$  between  $-40$  and  $-110mV$  and increase only slightly  $-0.4$  at  $-120mV$  indicating that the currents are blocked by magnesium (see Table 3.4).

The decreased whole-cell conductance of E71D-expressing oocytes could be due to decreased expression levels, decreased single channel conductance, decreased open probability or increased sensitivity to  $Mg^{2+}$  resulting in block of monovalent cation currents. Single channel studies are needed to address changes in single channel conductance and open probability. Our data show that compared to wild type HABIB, there is both decreased expression of E71D and increased sensitivity to  $Mg^{2+}$ .

Glutamate 71 of HABIB is in an analogous position to glutamate 14 of the *E. coli* glycerol facilitator, GlpF, which is also a member of the MIP family. In GlpF, E14 is located at a "buried position" and is not modeled to be a pore-lining residue but appears to be critical in maintaining the shape or size of the pore (Figure 3.15; Fu et al., 2000). Our data support a crucial role for E71 in determination of channel properties of HABIB.

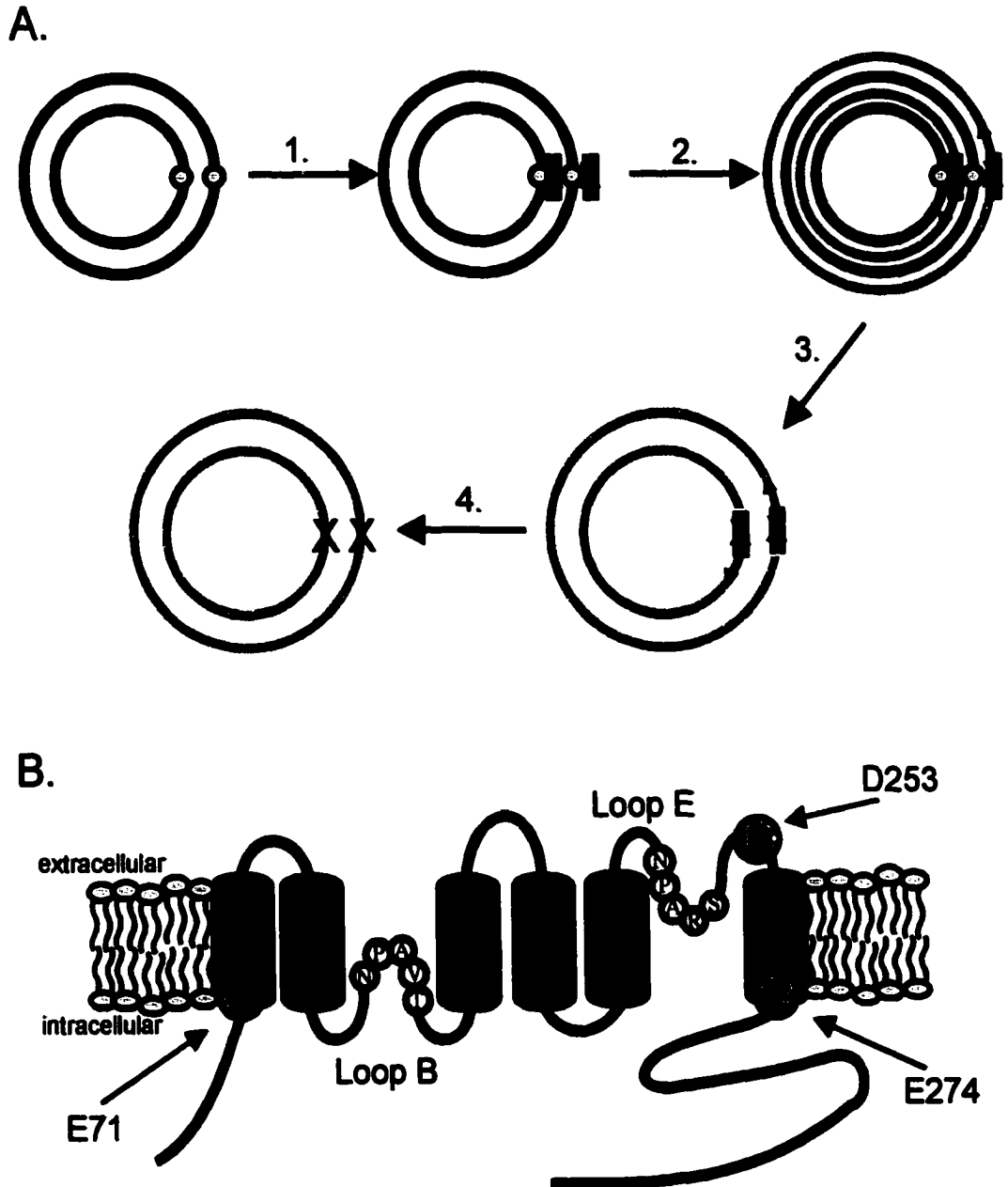
Factors including pore size, relative rates of dehydration, electrostatic interactions (between the permeant ion and amino acids of the pore as well as between other ions in a multi-ion pore) and energetic constraints work in concert to determine ionic permeability and selectivity in ion channels (Hille, 1992; Doyle et al., 1998). These factors must also contribute to ion permeation through HABIB channels. Relative permeability calculations for sodium (ionic radius 0.95Å), potassium (1.33Å), and tetraethylammonium ions (~5Å) resulted in the following selectivity sequence for currents in HABIB-expressing oocytes:  $K^+$  (1.0) >  $Na^+$  (.76) >  $TEA^+$  (0.48). Thus, the radius of the pore of HABIB channels should be large enough to accommodate  $TEA^+$ , ~5Å and pore size alone cannot account for the current block by  $Ca^{2+}$  (0.99Å) and  $Ba^{2+}$  ions (1.35Å) in oocytes expressing wild type HABIB. Increased sensitivity to  $Mg^{2+}$  (0.65Å) could be accounted for by a decreased pore size, but changes in permeability of monovalent cations would better test this possibility. Other factors could account for increased  $Mg^{2+}$  sensitivity such as conformational changes that unmask a  $Mg^{2+}$  binding site.

Although the mechanisms of selectivity of HABIB remain to be determined, crystallographic analysis of the related channels, AQP1 and GlpF provide a general understanding of the factors affecting selectivity in MIP channels. Both AQP1 and GlpF are homotetramers with a central pore at

the four-fold axis of symmetry (see Chapter 1). Each individual subunit contains a pathway for glycerol lined by Loops B and E in GlpF channels. These studies predict that the radius of the pore through each subunit is 4Å for AQP1 and 7.5Å for GlpF (Ren et al., 2000; Fu et al., 2000). The central pore at the four-fold axis of symmetry has a radius of 1.5Å for AQP1 and 5Å for GlpF (Ren et al., 2000; Fu et al., 2000). Selectivity for water and glycerol was determined to involve hydrogen bonding between permeant

molecules and pore-lining residues, as well as energetic constraints (Ren et al., 2000; Fu et al., 2000; Unger, 2000). Channels in the MIP family have a number of regions with highly conserved sequences of amino acids. Crystallography has revealed strikingly similar general structures even for MIP channels with very different substrate selectivities (such as for GlpF and AQP1). Further analysis of the ionic pore through Big Brain is needed to understand the cationic permeability in relation to structural components and will provide further knowledge of the basis for diversity in functions for channels in the MIP family.

In summary we have found that currents in oocytes expressing HABIB channels are blocked by extracellular divalent cations, calcium and barium. Calcium block is another means of regulating BIB cationic channel activity since block would reduce monovalent cation currents and therefore, reduce the magnitude of membrane depolarization induced by BIB activation.



**Figure 3.1 Strategy for site-directed mutagenesis of BIB at D253, E274 and E71.**  
See next page for details

**Figure 3.1 Strategy for site-directed mutagenesis of BIB at D253, E274, and E71.**

**A.** BIB channels with point mutations converting aspartic acid 253 (D253) to asparagine (D253N), glutamate 274 (E274) to asparagine (E274N), and glutamate 71 (E71) to asparagine, glutamine, lysine and aspartic acid (E71N, E71Q, E71K, E71D) were generated with the Quik-change site-directed mutagenesis kit from Stratagene (La Jolla, CA). 1. Primers were generated incorporating the desired mutation (see below, mutated base pairs underlined). 2. Using *PfuTurbo* DNA polymerase the mutagenic primers were extended. 3. The methylated template DNA was digested with methylation sensitive *DpnI* restriction enzyme leaving the non-methylated amplified DNA containing the mutation. 4. XL-1-Blue *E. coli* were transformed with the nicked double-stranded mutated DNA. **B.** Proposed topology of a BIB subunit with sites of mutation (D253, E274 and E71) indicated.

Cycling parameters:

12X  $\left\{ \begin{array}{l} 95^{\circ}\text{C } 30\text{sec} \\ \rightarrow 95^{\circ}\text{C } 30\text{sec} \\ 55^{\circ}\text{C } 1 \text{ minute} \\ 68^{\circ}\text{C } 10 \text{ minutes (2min/kb plasmid length: } \textit{bib}(2\text{kb})\text{-pX}\beta\text{G}(3\text{kb})=5\text{kb}) \\ 4^{\circ}\text{C} \end{array} \right.$

**D253N**

sense: 5'-GTGCTTAACAAATGGAACAGCCATTGGGTGACTGG-3' (bp 1042-1077)

antisense: 5'-CCAGTACACCCAATGGCTGTICCATTTGTTAAGCAC-3' (bp 1077-1042)

**E274N**

sense: 5'-GGCCTGGTGTACAACTACATCTTCAACTCGCGC-3' (bp 1108-1140)

antisense: 5'-GCGCGAGTTGAAGATGTAGTGTACACCAGGCC-3' (bp 1140-1108)

**E71N**

sense: 5'-GGAGATCCATCATCAGCAACTGTCTGGCCTCC-3' (bp 494-525)

antisense: 5'-GGAGGCCAGACAGTIGCTGATGATGGATCTCC-3' (bp 525-494)

**E71K**

sense: 5'-GGAGATCCATCATCAGCAAGTGTCTGGCCTC-3' (bp 494-524)

antisense: 5'-GAGGCCAGACACTIGCTGATCATCGATCTCC-3' (bp 524-494)

**E71Q**

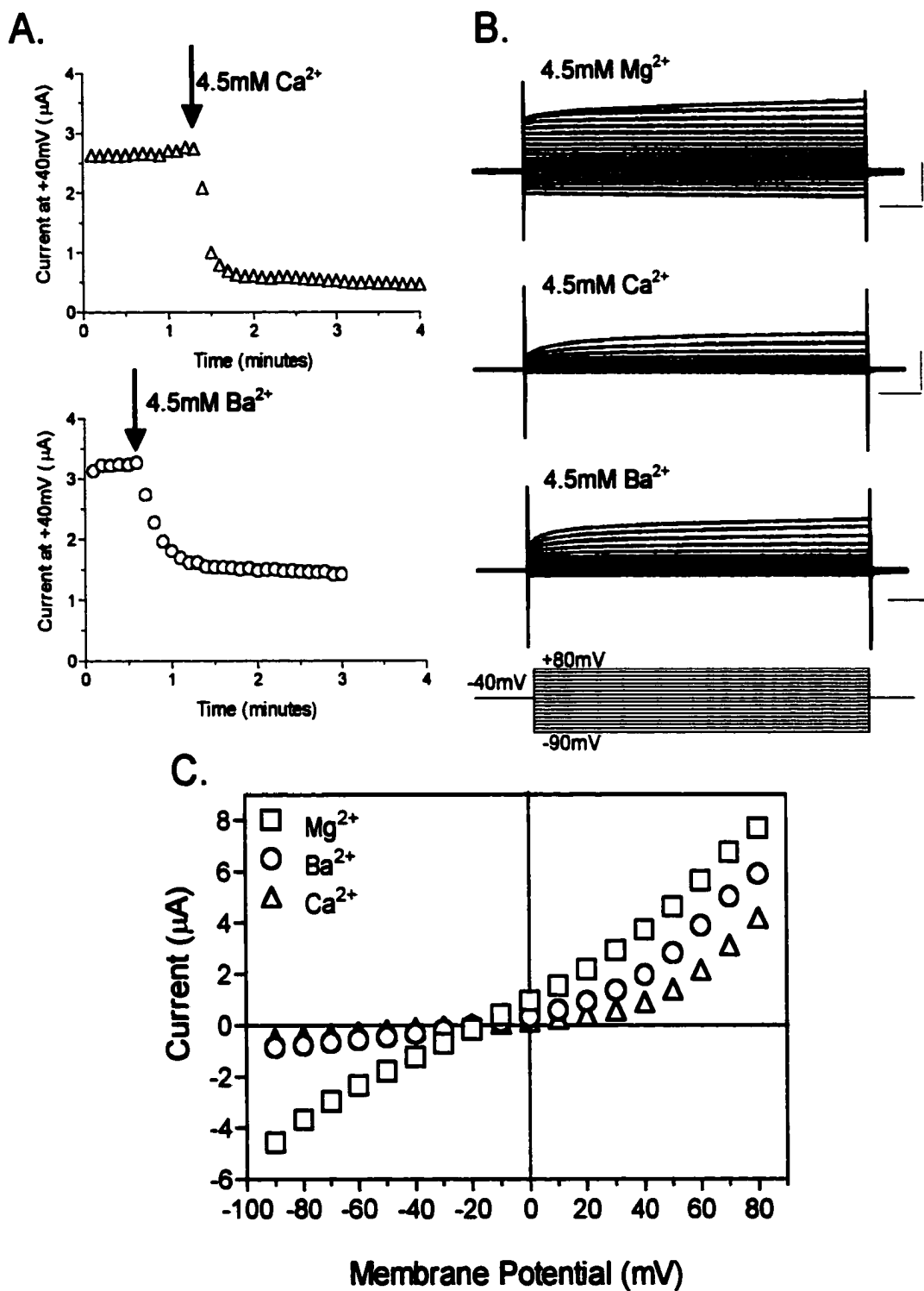
sense: 5'-GGAGATCCATCATCAGCCAGTGTCTGGCCTC-3' (bp 494-524)

antisense: 5'-GAGGCCAGACACTGGCTGATGATGGATCTCC-3' (bp 524-494)

**E71D**

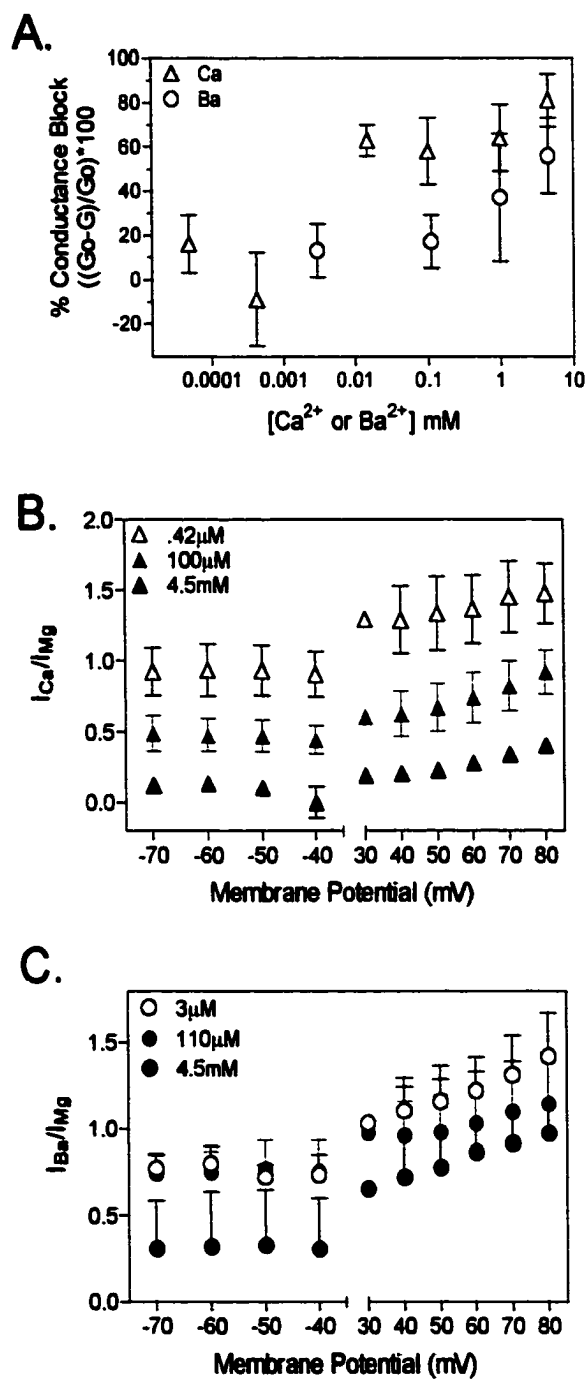
sense: 5'-CCATCATCAGCGACTGTCTGGCCTCCTTC-3' (bp 500-528)

antisense: 5'-GAAGGAGGCCAGACAGTCGCTGATGATGG-3' (bp 528-500)



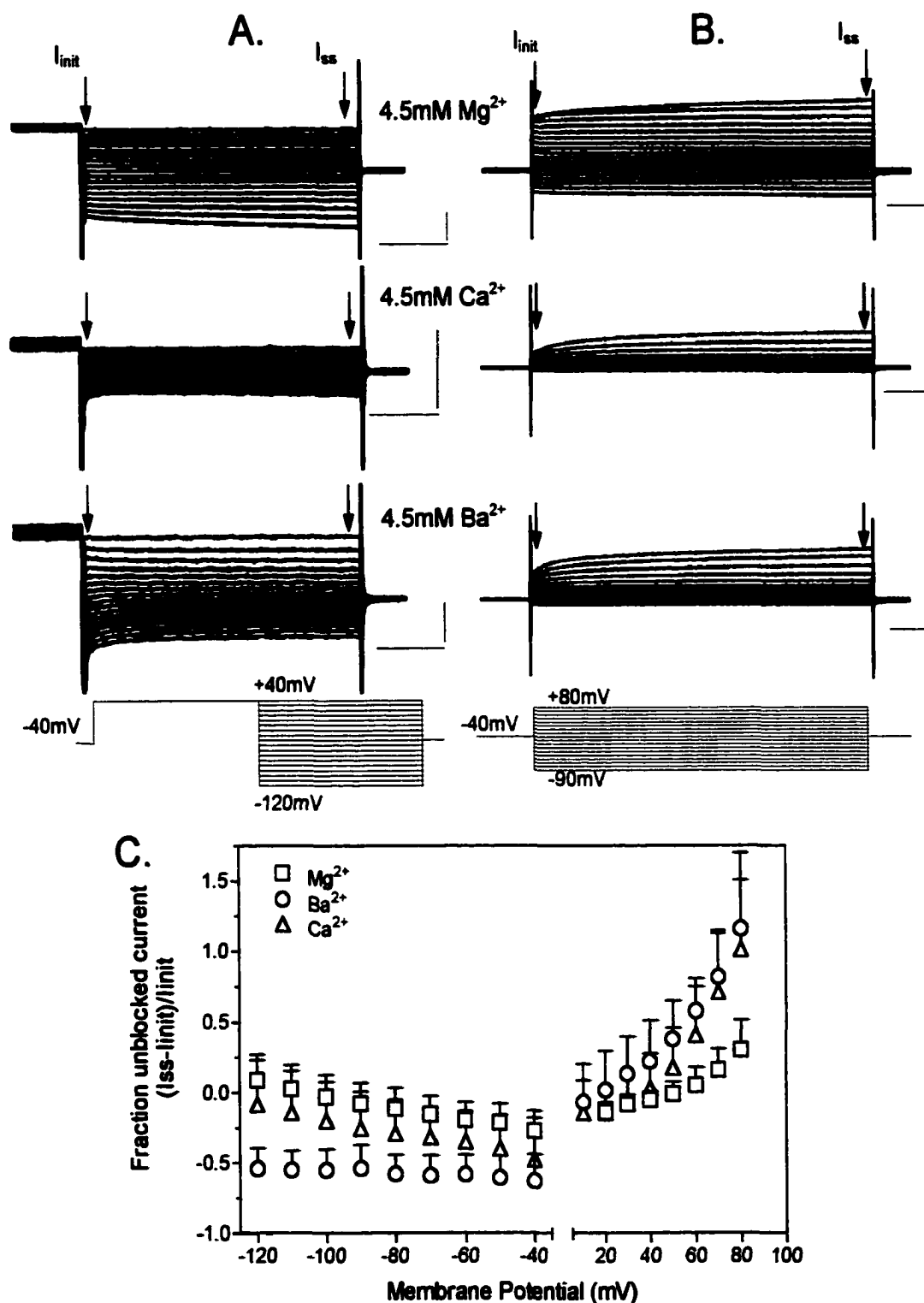
**Figure 3.2 Calcium and barium block currents induced by HABIB expression in *Xenopus oocytes*. See next page for details**

**Figure 3.2 Calcium and barium block currents induced by HABIB expression in *Xenopus* oocytes.** **A.** Current amplitude in magnesium saline, monitored at +40mV, decreases following perfusion of recording saline containing 4.5mM CaCl<sub>2</sub> (top) or BaCl<sub>2</sub> (bottom). **B.** Representative current traces evoked with 800ms steps from +80 to –70mV in 10mV increments from a holding potential of –40mV for an HABIB-expressing oocyte after channel activation in magnesium saline (4.5mM MgCl<sub>2</sub>; top) or following perfusion of the recording chamber with calcium saline (4.5mM CaCl<sub>2</sub>; middle) or barium saline (4.5mM BaCl<sub>2</sub>; bottom). Scale bars indicate 5μA and 100ms. **C.** Current-voltage relationships for data illustrated in B. No significant differences in reversal potential were observed for currents in magnesium (-17±5mV, n=14), calcium (-18±9mV, n=6) or barium saline (-16±5, n=13).



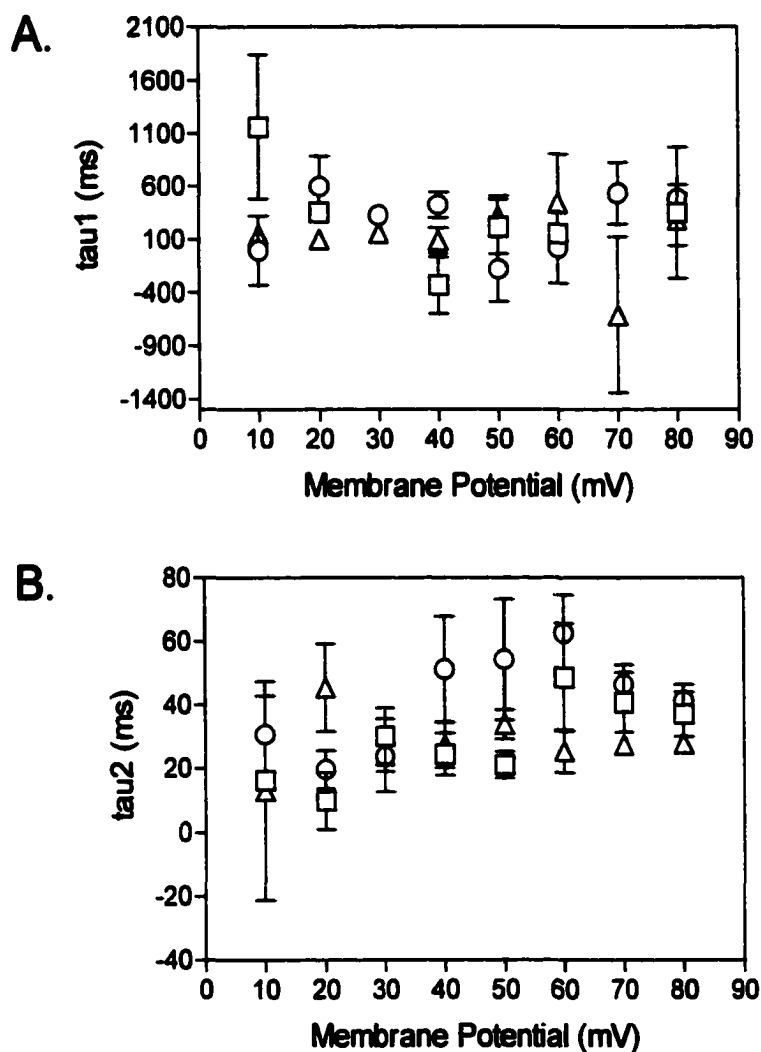
**Figure 3.3 Dose- and voltage-dependence of calcium and barium block of whole-cell conductance in oocytes expressing HABIB. See next page for details.**

**Figure 3.3 Dose- and voltage-dependence of calcium and barium block of whole-cell conductance of oocytes expressing HABIB. A.** Calcium and barium decreased the whole-cell conductance of oocytes expressing HABIB channels in a dose dependent manner. The percent conductance block,  $[(G_0 - G)/G_0]$ , where  $G_0$  is the conductance in magnesium saline calculated from linear fits of the current-voltage relationship between +40 and -70mV,  $G$  is the conductance in test saline calculated in the same manner. Percent block was plotted as a function of free calcium or barium in the extracellular recording saline. **B.** Voltage-dependent block by calcium of currents in HABIB-expressing oocytes. Currents after calcium saline perfusion ( $I_{Ca}$ ) were normalized to the currents in magnesium saline ( $I_{Mg}$ ) before perfusion ( $I_{Ca}/I_{Mg}$ ).  $I_{Ca}/I_{Mg}$  was plotted as a function of membrane potential. Values of  $I_{Ca}/I_{Mg}$  also are given in Table 3.1. **C.** Voltage-dependent block by barium of currents in HABIB-expressing oocytes. Currents after barium saline perfusion ( $I_{Ba}$ ) were normalized to the currents in magnesium saline ( $I_{Mg}$ ) before perfusion ( $I_{Ba}/I_{Mg}$ ).  $I_{Ba}/I_{Mg}$  was plotted as a function of membrane potential. Values of  $I_{Ba}/I_{Mg}$  also are given in Table 3.2.

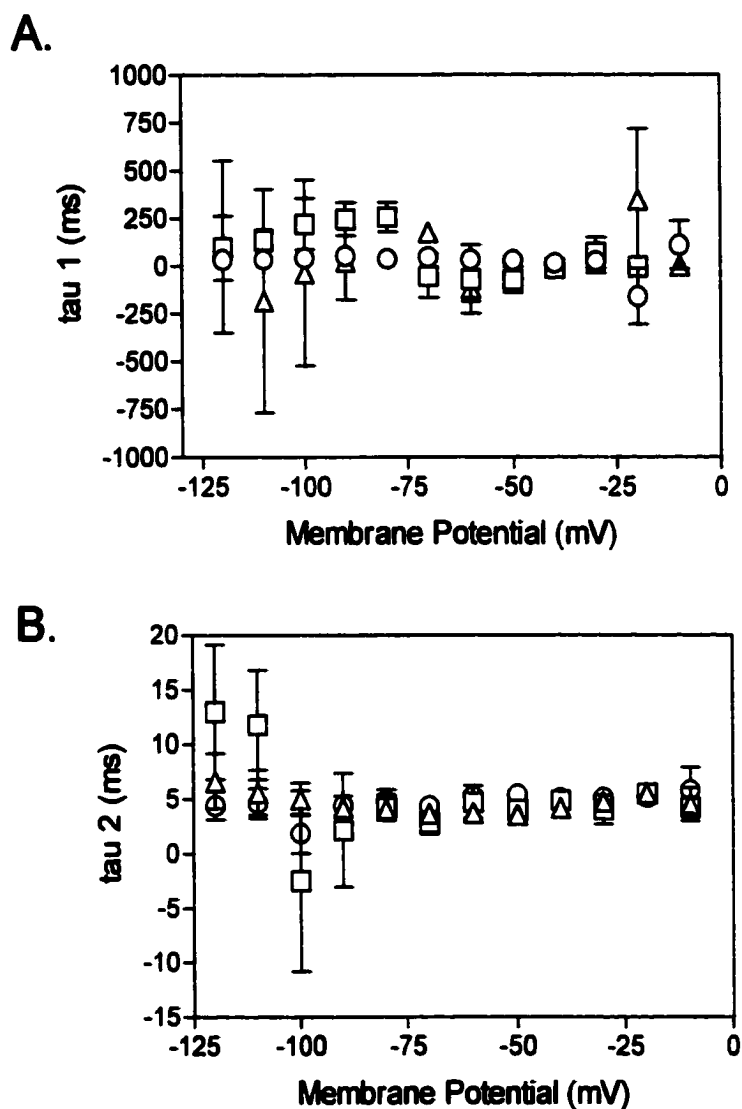


**Figure 3.4** Fraction of unblocked current for oocytes expressing HABIB in magnesium, calcium or barium saline. See next page for details.

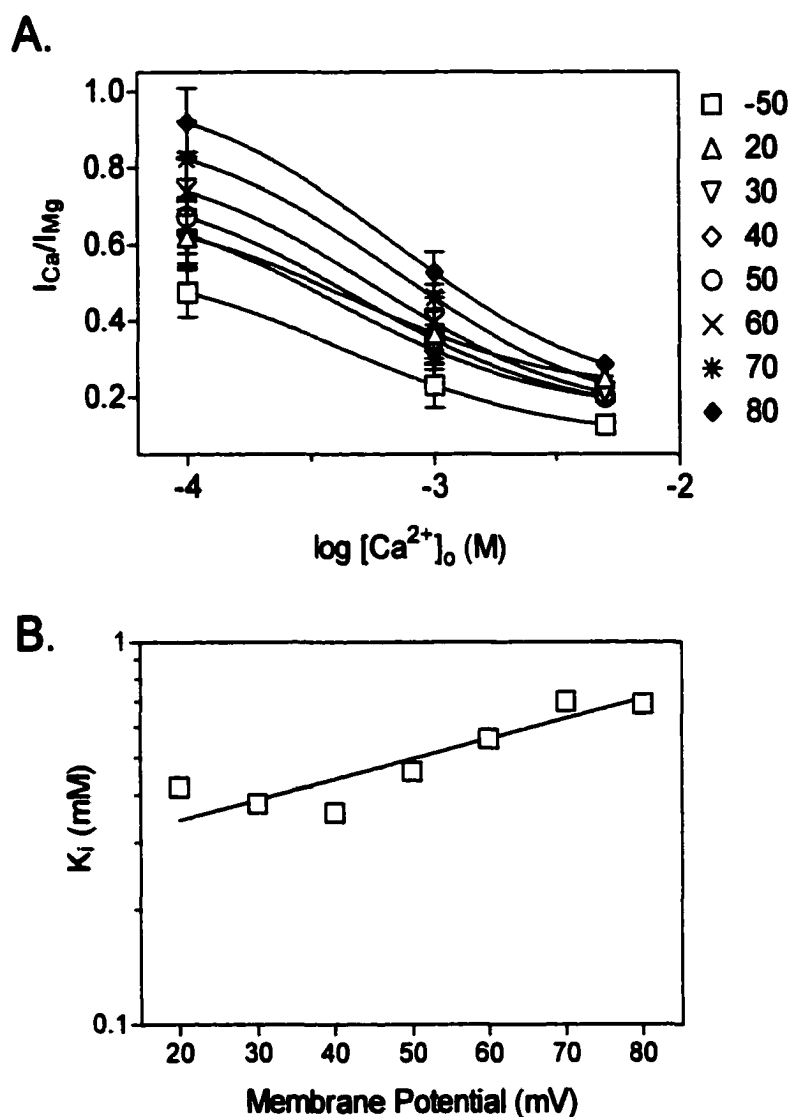
**Figure 3.4 Fraction of unblocked current for oocytes expressing HABIB in magnesium, calcium or barium saline.** **A.** Traces show tail currents evoked in response to 164ms steps from  $-120$  to  $+40$ mV in 10mV increments after an initial 164ms step to  $+40$ mV from a holding potential of  $-40$ mV in magnesium (top), calcium (middle) and barium saline (bottom). Arrows indicate the approximate locations of steady state current ( $I_{ss}$ ) and initial current values ( $I_{init}$ ) used to calculate the fraction of unblocked current at hyperpolarized potentials in panel C. Scale bars indicate  $3\mu\text{A}$  and 40ms ( $4.5\text{mM Mg}^{2+}$ ) and  $2\mu\text{A}$  and 40ms for  $4.5\text{mM Ca}^{2+}$  and  $4.5\text{mM Ba}^{2+}$ . **B.** Current traces evoked with 800ms steps from  $+80$  to  $-90$ mV from a holding potential of  $-40$ mV in HABIB-expressing oocytes after channel activation in magnesium saline (top) or after perfusion of the recording chamber with calcium (middle) or barium saline (bottom). Arrows indicate the approximate location of steady state ( $I_{ss}$ ; 4ms before the end of the voltage step) and initial current values ( $I_{init}$ ; approximately 2ms after the capacitance artifact) used to calculate the fraction of unblocked current between  $+80$  and  $+10$ mV in C. Scale bars indicate  $5\mu\text{A}$  and 100ms. **C.** The fraction of unblocked current ( $I_{UF}=(I_{ss}-I_{init})/I_{init}$ ) plotted as a function of membrane potential for oocytes expressing HABIB in magnesium saline ( $n=13$ ), calcium saline ( $n=7$ ) or barium saline ( $n=12$ ). The location of  $I_{ss}$  and  $I_{init}$  are indicated in panels A and B. Values of  $I_{UF}$  also are given in Table 3.3.



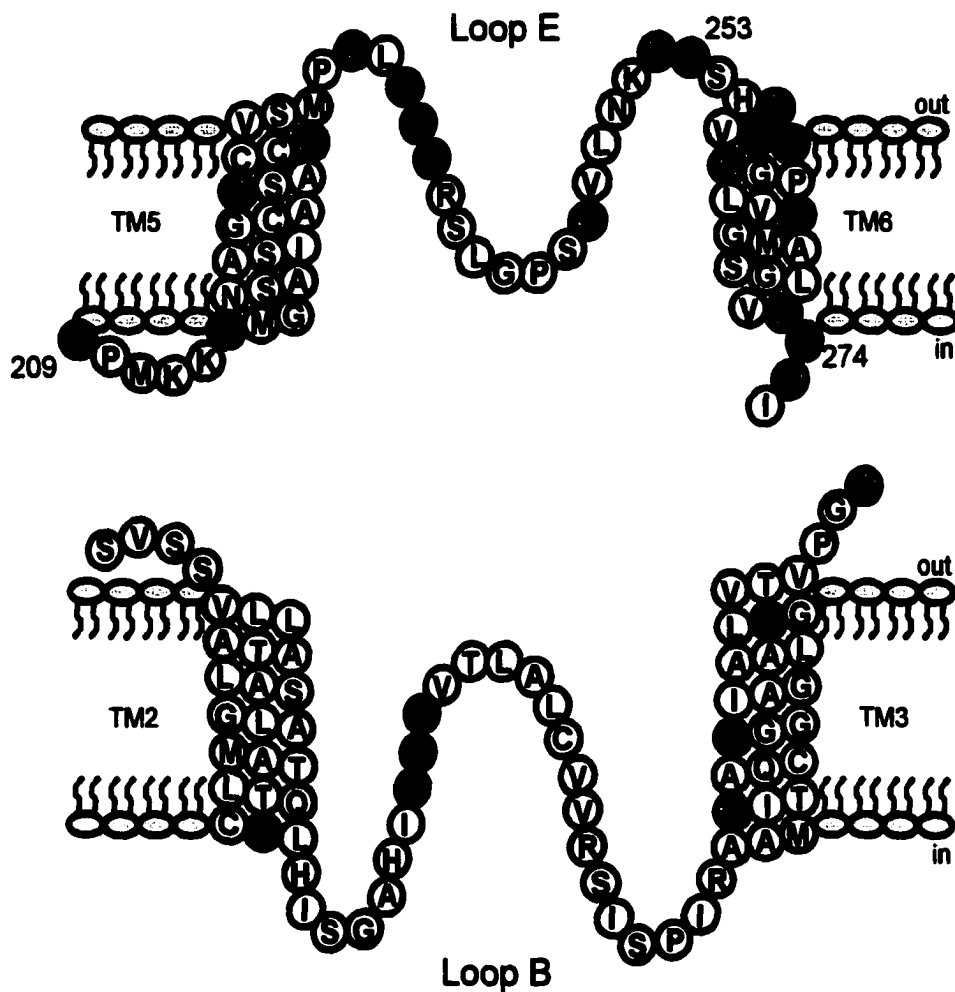
**Figure 3.5 Net rates of unblock show no apparent voltage dependence.** Fast (tau2; B) and slow (tau1; A) tau values for unblocking were obtained from double exponential fits of current traces such as those shown in Figure 3.4B. Data points show the mean $\pm$ SD for tau values in magnesium (squares, n=14), calcium (triangles, n=6) or barium saline (circles, n=13).



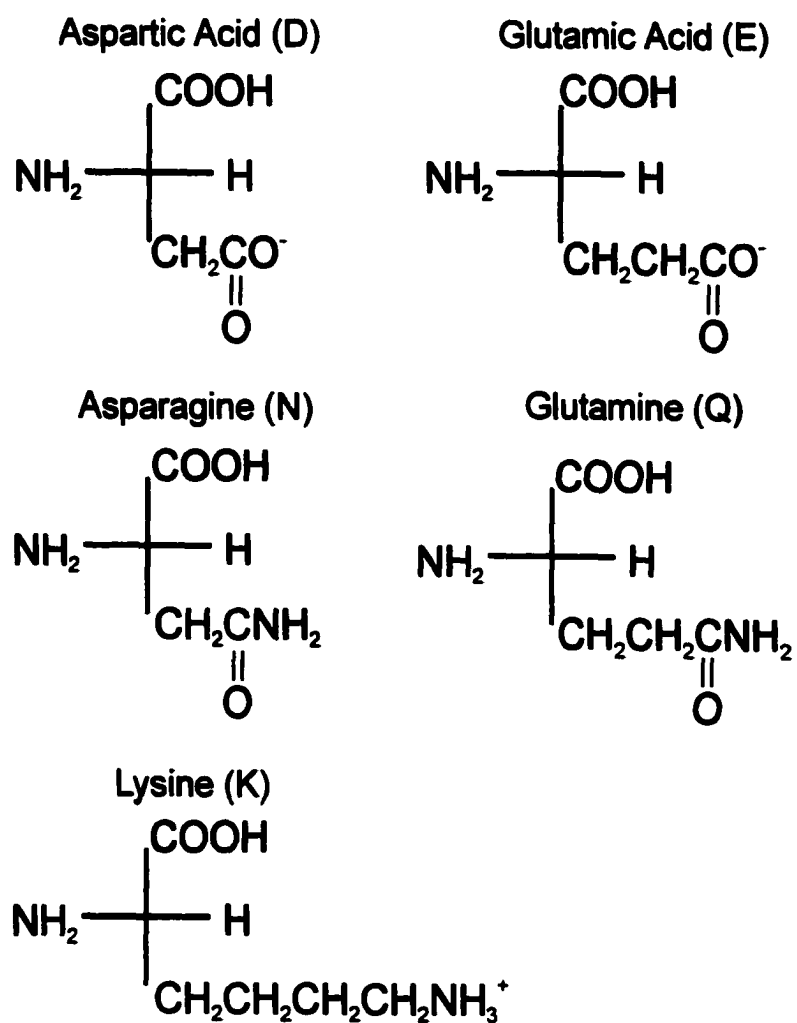
**Figure 3.6 Net rates of block show no apparent voltage dependence.** Fast (tau2; B) and slow (tau1; A) tau values for blocking were obtained from double exponential fits of tail current traces such as those shown in Figure 3.4A. Data points show the mean±SD for tau values in magnesium (squares, n=13), calcium (triangles, n=5) or barium saline (circles, n=10).



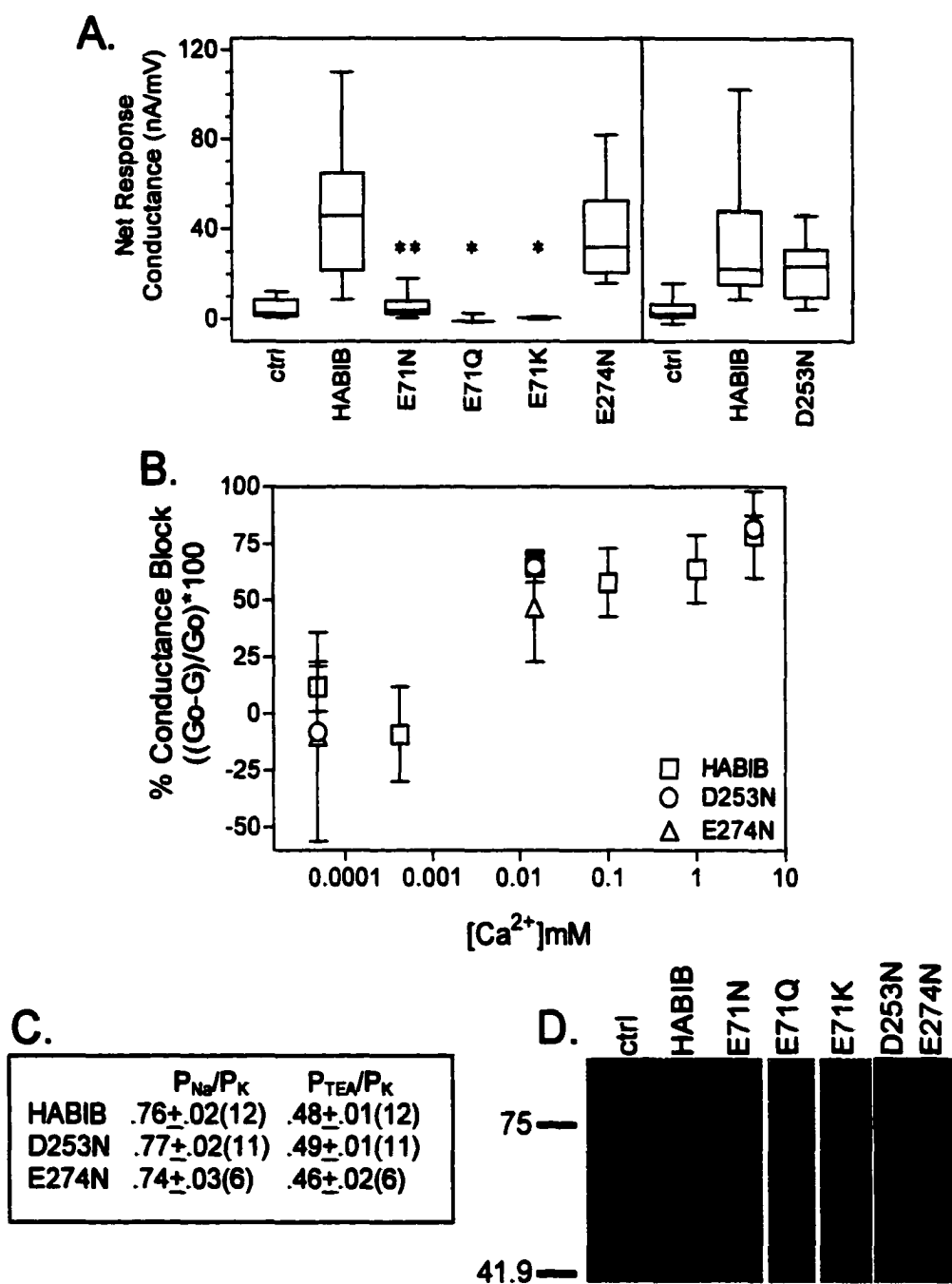
**Figure 3.7 Fractional Electrical Field Distance of block by calcium.** **A.** Currents from HABIB-expressing oocytes in calcium saline ( $I_{Ca}$ ) were normalized to currents in magnesium saline ( $I_{Mg}$ , as in Figure 3.3). The normalized currents at voltages ranging from +80 to +20 and -50mV were plotted as a function of free calcium concentration. The concentration of calcium that inhibited 50% of the current at each voltage was obtained from a fit of the data with sigmoidal dose response curve (Graph Pad Prism, version 3.0, San Diego, CA). **B.** The  $K_i$  values (obtained in A) were plotted as a function of membrane potential and fit with the equation  $K_{1/2} = K_{1/2}(0mV) \exp(z\delta FV/RT)$ , see text for details. The equation of the line through the data shown on the graph is  $y = 0.28115 \exp(0.0011261x)$ ,  $R = 0.92$ , yielding a calculation for the apparent fractional electrical field distance of  $\delta = 0.14$ .



**Figure 3.8 Schematic diagram of the amino acids in and surrounding Loops B and E of BIB** (sequence from Rao et al., 1990). Conserved amino acids among MIP family members are shown in green; negatively charged amino acids are shown in blue; positively charged amino acids are shown in yellow; and aromatic amino acids are shown in pink. Big Brain has only three negatively charged amino acids in putative pore lining regions (all in Loop E): D209N, D253 and E274.

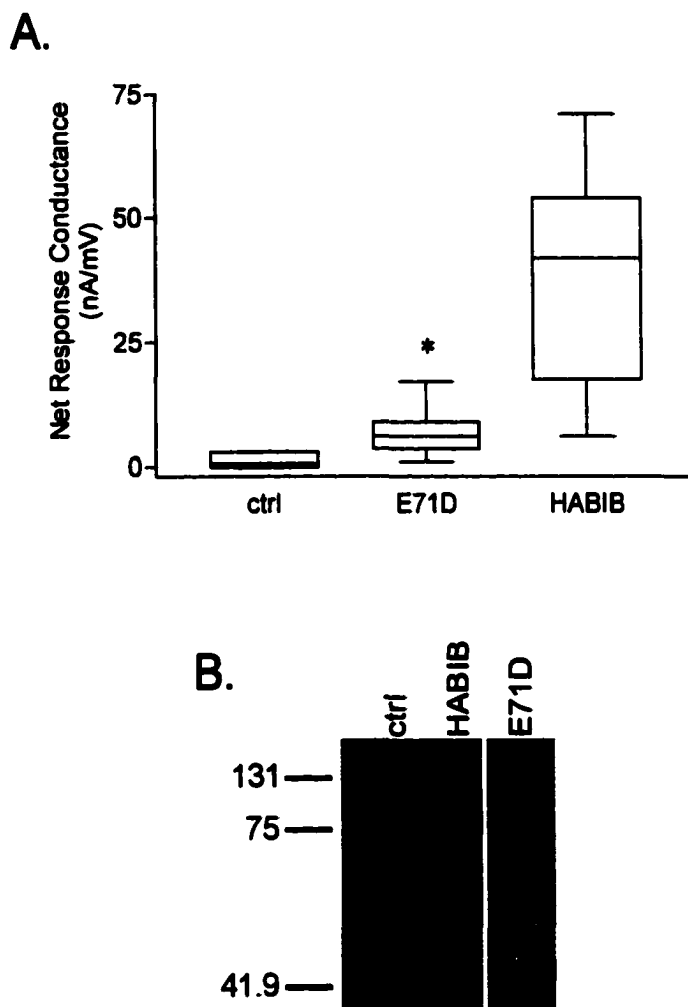


**Figure 3.9** *Amino acid structure of amino acids mutated in BIB to analyze divalent cation block.* Structures of the amino acid side chains of aspartic acid, glutamic acid, asparagine, glutamine and lysine are shown.

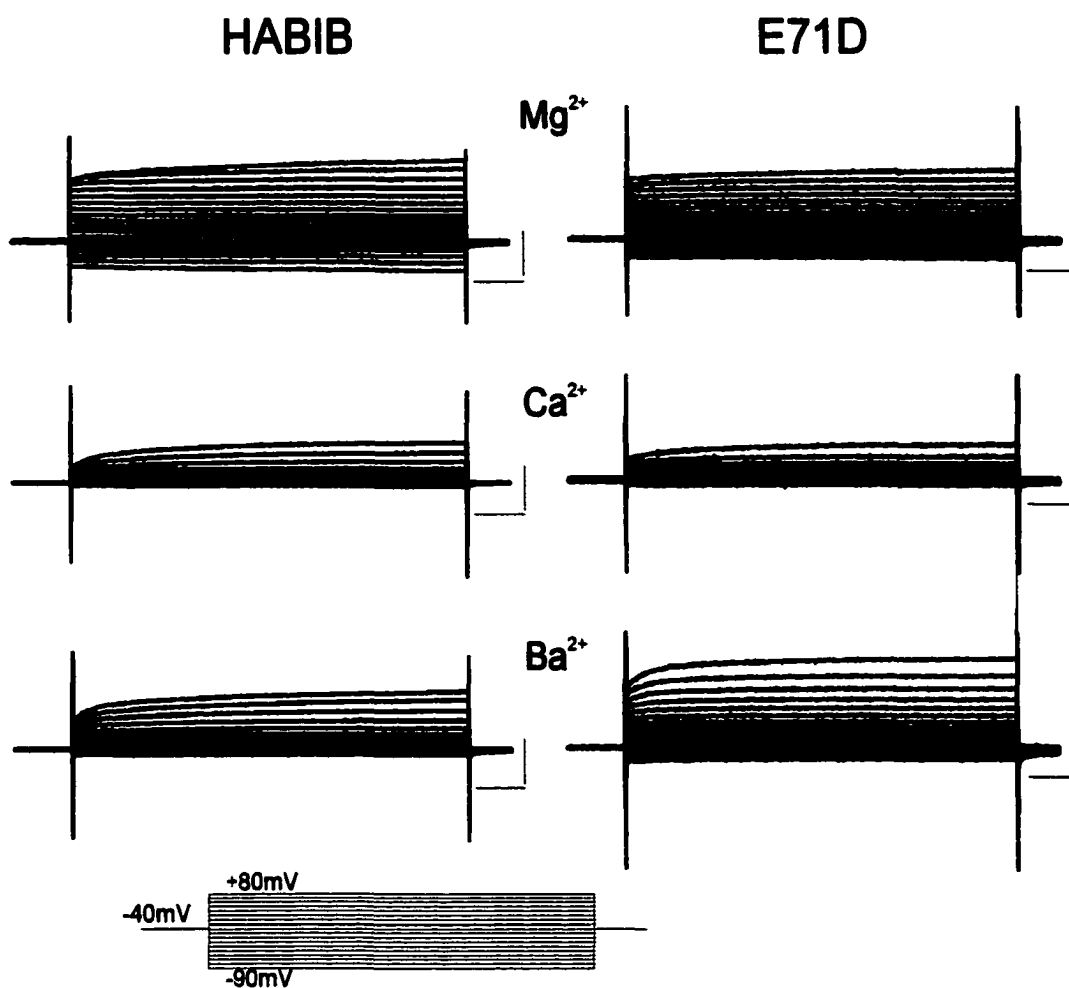


**Figure 3.10 Summary of the effect of the mutations D253N, E274N, E71N, E71Q and E71K.** See next page for details.

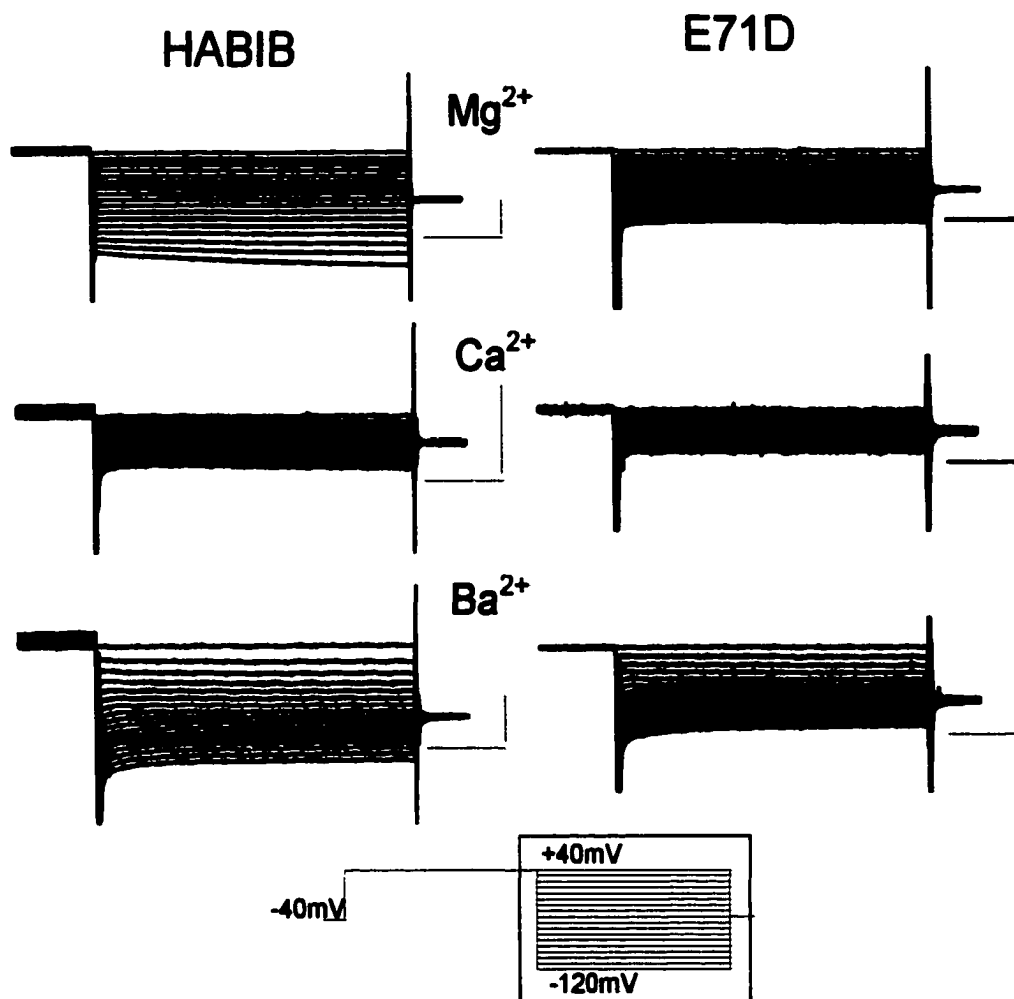
**Figure 3.10 Summary of the effect of the mutations D253N, E274N, E71N, E71Q and E71K. A.** Net conductance was obtained from linear fit of the current-voltage relationship from +40 to -70mV. Asterisks indicate that the net conductances of oocytes expressing E71N ( $6 \pm 5$  nA/mV,  $n=17$ ,  $p<0.01$ ), E71Q ( $0 \pm 2$  nA/mV,  $n=3$ ,  $p<0.05$ ) and E71K ( $0.4 \pm 0.3$  nA/mV,  $n=3$ ,  $p<0.05$ ) were significantly different as compared to wild-type HABIB ( $47 \pm 31$  nA/mV,  $n=13$ ) but not from control oocytes ( $4 \pm 4$  nA/mV,  $n=7$ ). Comparisons of control oocytes or those expressing mutant or wild type HABIB were performed within the same batches of oocytes (separated by vertical line). Oocytes expressing E274N ( $35 \pm 18$  nA/mV,  $n=19$ ) or D253N ( $21 \pm 13$  nA/mV,  $n=21$ ) had net conductance values indistinguishable from oocytes expressing wild type HABIB ( $47 \pm 30$  nA/mV,  $n=13$ , left and  $30 \pm 22$  nA/mV,  $n=19$ , right). **B.** Percent block for mutant D253N and E274N conductances was calculated as described in Figure 3.3. Mutation of D253 and E274 to asparagine (N) had no effect on the dose response of percent conductance block by calcium. **C.** Relative ionic permeability was calculated from reversal potentials after iso-osmotic substitution of KCl and TEACl for NaCl in the bath saline (see Methods). No differences in relative cationic permeability ( $P_{Na}/P_K$  and  $P_{TEA}/P_K$ ) were observed.  $n$  values are given in parentheses. **D.** Western blots of plasma membrane fractions of oocytes expressing E71N, E71Q, E71K D253N, and E274N. Blots were probed with rat anti-HA antibody (clone 3F10, Roche) to visualize wild-type and mutant channels containing the HA epitope. Wild-type, E71N, E71Q, D253N, and E274N channels resolved at approximately 80kD, the expected size of HABIB channels. No immunoreactive bands were seen from oocytes expressing E71K or control oocytes.



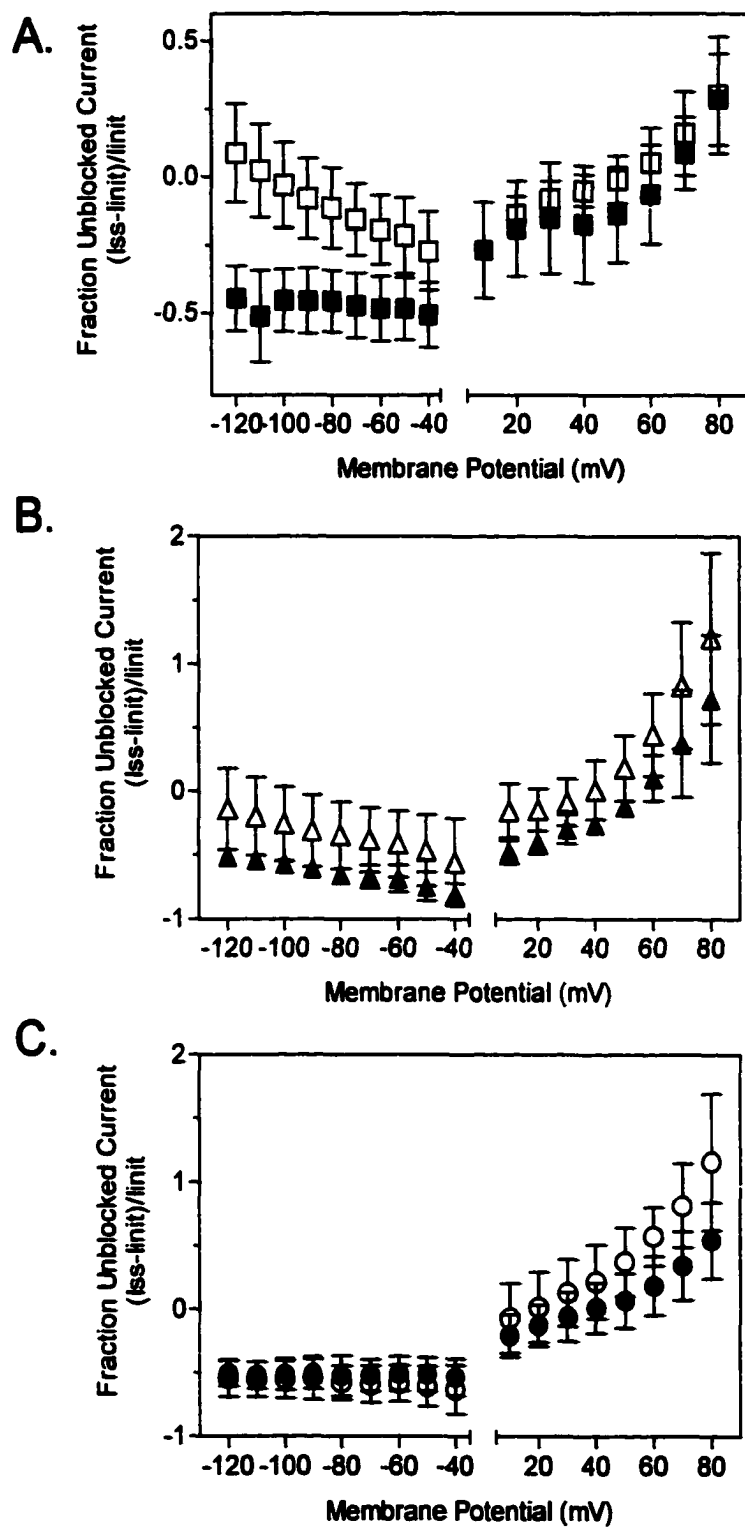
**Figure 3.11 Summary of the effect of E71D on properties of HABIB expressed in *Xenopus oocytes*.** **A.** Net conductance responses of oocytes expressing wild-type HABIB and E71D channels. Oocytes had significantly reduced conductance ( $6 \pm 4$  nA/mV,  $n=11$ ,  $p < 0.01$ ) compared to oocytes expressing HABIB ( $36 \pm 22$  nA/mV,  $n=12$ ) but significantly greater than that of control oocytes ( $1 \pm 1$  nA/mV,  $n=6$ ,  $p < 0.05$ ). Net conductance was calculated from linear fit of the current-voltage relationship between +40 and -70 mV. **B.** Western blot showing the plasma membrane expression of E71D. Total protein from plasma membrane fractions of control oocytes or those expressing E71D or wild-type HABIB channels was resolved by 10% SDS-PAGE and transferred to PVDF. The blot was probed with rat anti-HA antibody (clone 3F10, Roche) followed by goat anti-rat HRP conjugated secondary antibody. Immunoreactive bands were visualized by enhanced chemi-luminescence. Immunoreactive bands at approximately 80 kD, the expected size of HABIB and E71D channels were observed from proteins isolated from oocytes expressing E71D and HABIB but not from control oocytes.



**Figure 3.12** Current traces demonstrate that *mutation of E71 to aspartic acid induces  $Mg^{2+}$  block*. Current traces from oocytes expressing wild-type HABIB (left) or E71D channels (right) were evoked with 800ms steps from  $+80$  to  $-90mV$  in  $10mV$  increments from a holding potential of  $-40mV$  after channel activation in magnesium saline (top) and following perfusion of the recording chamber with calcium (middle) or barium saline (bottom). Scale bars for HABIB are  $5\mu A$  and  $100ms$ . Scale bars for E71D are  $1\mu A$  and  $100ms$ .

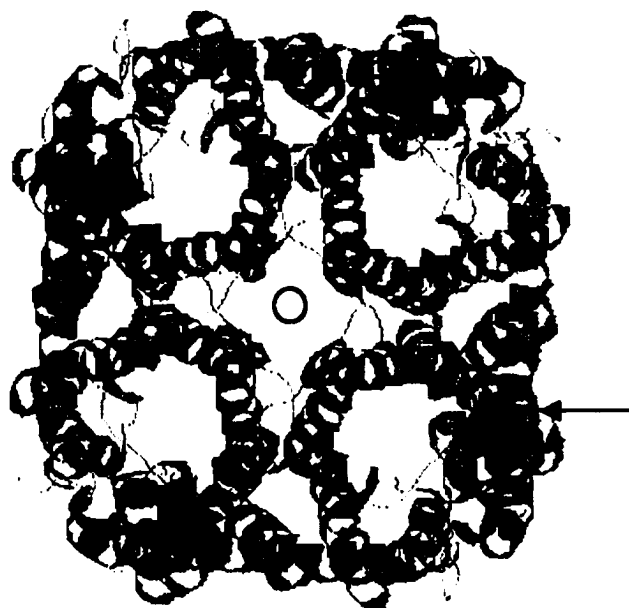


**Figure 3.13 Tail current traces demonstrate that mutation of E71 to aspartic acid induces  $Mg^{2+}$  block.** Current traces evoked with 164ms steps from  $-120$  to  $+40$ mV after an initial 164ms step to  $+40$ mV from a holding potential of  $-40$ mV are shown for oocytes expressing HABIB (left) or E71D-expressing oocytes (right) after channel activation in magnesium saline (top) or after perfusion of the recording chamber with calcium (middle) or barium saline (bottom). The box around the voltage protocol indicates the area of enlargement of the traces. Scale bars for HABIB traces indicate  $3\mu A$  and  $40$ ms ( $Mg^{2+}$ ) and  $2\mu A$  and  $40$ ms ( $Ca^{2+}$  and  $Ba^{2+}$ ). Scale bars for E71D traces indicate  $1\mu A$  and  $40$ ms ( $Mg^{2+}$ ),  $0.5\mu A$  and  $40$ ms ( $Ca^{2+}$ ), and  $1\mu A$  and  $40$ ms ( $Ba^{2+}$ ).



**Figure 3.14** *Fraction of unblocked current in oocytes expressing E71D or wild type HABIB in magnesium, calcium or barium saline. See next page for details.*

**Figure 3.14 Fraction of unblocked current in oocytes expressing E71D or wild type HABIB in magnesium, calcium or barium saline.** The fraction of unblocked current was calculated as described in Figure 3.3 and in the methods. Steady state and initial current values were obtained from current traces such as those shown in Figure 3.12 and Figure 3.13.  $I_{UF}$  values also are given in Table 3.4 for E71D and wild-type HABIB mediated conductances in magnesium, calcium and barium salines. **A.** Fraction of unblocked current in magnesium saline for oocytes expressing E71D (filled squares, n=10) and wild-type HABIB (open squares, n=13). **B.** Fraction of unblocked current in calcium saline for oocytes expressing E71D (filled triangles, n=3) and wild-type channels (open triangles, n=7). **C.** Fraction of unblocked current in barium saline for oocytes expressing E71D (filled circles, n=7) and wild-type HABIB channels (open circles, n=12).



**Figure 3.15** *Extracellular view of the GlpF tetramer showing the location of E14.* Sequence alignments of BIB and GlpF (see chapter 1) show that E14 of GlpF and E71 of BIB are in analogous positions. E14 is shown as a blue space-filled molecule in the image (arrow). A yellow circle indicates the four-fold axis of symmetry of the GlpF tetramer;  $\alpha$ -helices are shown as gray ribbons. The picture was generated with RASMOL from structural coordinates of GlpF (1FX8) deposited in RCSB protein databank.

$I_{Ca}/I_{Mg}$ 

mV	0.42 $\mu$ M	100 $\mu$ M	4.5mM
80	1.5 $\pm$ 0.2	0.9 $\pm$ 0.2	0.41 $\pm$ 0.04
70	1.45 $\pm$ 0.3	0.8 $\pm$ 0.2	0.34 $\pm$ 0.04
60	1.4 $\pm$ 0.2	0.7 $\pm$ 0.2	0.29 $\pm$ 0.03
50	1.3 $\pm$ 0.3	0.7 $\pm$ 0.2	0.23 $\pm$ 0.03
40	1.3 $\pm$ 0.2	0.6 $\pm$ 0.2	0.21 $\pm$ 0.04
30	1.3 $\pm$ 0.2	0.6 $\pm$ 0.1	0.2 $\pm$ 0.03
-40	0.9 $\pm$ 0.2	0.4 $\pm$ 0.1	0 $\pm$ 0.1
-50	0.9 $\pm$ 0.2	0.5 $\pm$ 0.1	0.11 $\pm$ 0.05
-60	0.9 $\pm$ 0.2	0.5 $\pm$ 0.1	0.14 $\pm$ 0.05
-70	0.9 $\pm$ 0.2	0.5 $\pm$ 0.1	0.13 $\pm$ 0.04

**Table 3.1 Dose and voltage-dependence of block by calcium on currents in oocytes expressing HABIB channels.** Values show the mean $\pm$ SD for currents after calcium saline perfusion ( $I_{Ca}$ ) normalized to currents in magnesium saline ( $I_{Mg}$ ) for different calcium concentrations: 0.42 $\mu$ M (n=3), 100 $\mu$ M (n=3) and 4.5mM (n=4).

$$I_{Ba}/I_{Mg}$$

mV	3 $\mu$ M	110 $\mu$ M	4.5mM
80	1.4 $\pm$ 0.3	1.1 $\pm$ .2	0.9 $\pm$ .5
70	1.3 $\pm$ .2	1.1 $\pm$ .2	0.9 $\pm$ .5
60	1.2 $\pm$ .2	1.0 $\pm$ .2	0.9 $\pm$ .5
50	1.2 $\pm$ .2	1.0 $\pm$ .2	0.8 $\pm$ .5
40	1.1 $\pm$ .2	1.0 $\pm$ .2	0.7 $\pm$ .5
30	1.0 $\pm$ .1	1.0 $\pm$ .2	0.7 $\pm$ .5
-40	0.7 $\pm$ .1	0.8 $\pm$ .2	0.3 $\pm$ .3
-50	0.72 $\pm$ .07	0.8 $\pm$ .2	0.3 $\pm$ .3
-60	0.8 $\pm$ .1	0.7 $\pm$ .1	0.3 $\pm$ .3
-70	0.8 $\pm$ .1	0.7 $\pm$ .1	0.3 $\pm$ .3

**Table 3.2 Dose and voltage dependence of block by barium on currents in oocytes expressing HABIB channels.** Values show the mean $\pm$ SD for currents after barium saline perfusion ( $I_{Ba}$ ) normalized to currents in magnesium saline ( $I_{Mg}$ ) for different barium concentrations: 3 $\mu$ M (n=4), 110 $\mu$ M (n=7) and 4.5mM (n=7).

mV	Mg <sup>2+</sup>	Ca <sup>2+</sup>	Ba <sup>2+</sup>
80	0.3±.2	1.2±.7	1.2±.5
70	0.2±.1	0.8±.5	0.9±.3
60		0.4±.3	0.6±.2
50	0±.1		0.4±.3
40	-0.1±.1	0±.2	0.2±.3
30	0±.3	-0.1±.2	
20	-0.1±.2	-0.1±.2	0±.3
-40	-0.3±.1	-0.5±.3	-0.6±.2
-50	-0.2±.1	-0.4±.3	-0.6±.2
-60	-0.2±.1	-0.3±.2	-0.6±.1
-70	-0.2±.1	-0.3±.2	-0.6±.1
-80	-0.1±.1	-0.3±.2	-0.6±.1
-90	-0.1±.1	-0.3±.3	-0.5±.1
-100	0±.2	-0.2±.3	-0.5±.1
-110	0±.2	-0.1±.3	-0.6±.1
-120	0.1±.2	-0.1±.3	-0.5±.1

**Table 3.3** *Fraction of unblocked current ( $I_{UF}$ ) for HABIB channels in the presence of 4.5mM magnesium, calcium or barium.* Values show mean±SD for IUF calculated for currents at different voltages in magnesium (n=13), calcium (n=7) and barium saline (n=12). See text for details.

mV	Mg <sup>2+</sup>		Ca <sup>2+</sup>		Ba <sup>2+</sup>	
	E71D	HABIB	E71D	HABIB	E71D	HABIB
80	.3±.2	.3±.2	.7±.5	1.2±.7	.5±.3	1.2±.5
70	.1±.1	.2±.1	.4±.4	.8±.5	.3±.3	.9±.3
60	-.1±.2	.05±.1	.1±.2	.4±.3	.2±.2	.6±.2
50	-.1±.2	0±.1	-.11±.04	.2±.3	.1±.2	.4±.3
40	-.2±.2	-.1±.1	-.26±.07	0±.2	0±0.2	.2±.3
30	-.2±.2	0±.3	-.3±.1	-.1±.2	-.05±.19	.1±.3
20	-.2±.2	-.1±.2	-.5±.1	-.1±.2	-.1±.1	0±.3
-40		-.3±.1	-.8±.08	-.5±.3	-.5±.1	-.6±.2
-50		-.2±.1	-.7±.1	-.4±.3	-.5±.1	-.6±.2
-60		-.2±.1	-.7±.1	-.3±.2	-.5±.1	-.6±.1
-70		-.2±.1	-.66±.09	-.3±.2	-.5±.1	-.6±.1
-80		-.1±.1	-.65±.07	-.3±.2	-.5±.2	-.6±.1
-90		-.1±.1	-.6±.1	-.3±.3	-.5±.1	-.5±.1
-100		0±.2	-.57±.03	-.2±.3	-.5±.1	-.5±.1
-110		0±.2	-.54±.03	-.1±.3	-.5±.1	-.6±.1
-120		.1±.2	-.51±.03	-.1±.3	-.5±.1	-.5±.1

**Table 3.4 Comparison of the fraction of unblocked current ( $I_{UF}$ ) in oocytes expressing wild-type and E71D HABIB channels in magnesium, calcium or barium saline. Values show mean±SD for  $I_{UF}$  values calculated in magnesium (n=10), calcium (n=3) or barium saline (n=7) for oocytes expressing E71D or wild type HABIB (shown also in Table 3.3). Shaded cells indicate the striking difference in  $I_{UF}$  between currents in E71D and wild type HABIB-expressing oocytes.**

## **CHAPTER 4: ROLE OF THE CARBOXY TAIL OF BIB**

### **4.1 INTRODUCTION**

In the previous chapters I have discussed the ion channel activity of Big Brain. Chapter 2 presented possible mechanisms of channel activation. Endogenous signaling pathways in oocytes, particularly through tyrosine kinases, activate BIB cationic channel activity. In this chapter, I explore the idea that the carboxy tail is the site of regulatory protein interactions necessary for activation.

The notably long carboxy tail of BIB makes it the largest member of the MIP family (the carboxy tail comprises amino acids 269-700). This region contains sites of potential functional regulation, such as: (i) phosphorylation consensus sites for serine/threonine kinases and tyrosine; (ii) SH3 binding domains; (iii) PDZ binding domains; and (iv) polyglutamine stretches (see Figure 4.1). Protein interactions involving these modular domains have a variety of effects that are not necessarily mutually exclusive. For example, the carboxy terminus of the inward rectifying potassium channel, Kir2.3 has a PKA phosphorylation site (underlined) and PDZ binding domain (gray) that overlap at the carboxy terminus: RRES (Cohen et al., 1996). Biochemical studies of Kir 2.3 indicate that phosphorylation by PKA inhibits the association of Kir 2.3 with the PDZ domain containing protein PSD-95 in HEK 293 cells (Cohen et al., 1996). PSD-95 localizes proteins into signaling complexes at the synaptic terminal. Therefore, phosphorylation of Kir2.3 by PKA is likely to have functional consequences by preventing the targeting of the channel to the synapse or by releasing the carboxy tail from protein interactions resulting in conformational changes that alter channel conductance. Although I will discuss each of these protein interaction domains

separately, they most likely exert their effects on BIB cationic channel activity through inter-related processes.

The carboxy tail of BIB contains eight sites of potential phosphorylation by serine/threonine kinases (Figure 4.1A). The amino acids that conform to consensus sequences for phosphorylation by cyclic GMP dependent protein kinase (XS\*RX; X indicates any amino is tolerated and \*indicates the site of phosphorylation), calmodulin kinase II (XRXXS\*X) and protein kinase C (XRXXS\*RX) are shown in Figure 4.1A (Kemp and Pearson, 1990). Phosphorylation affects the properties of ion channels in a subunit specific manner. Exposure of  $\alpha$  subunits of the calcium activated potassium channel expressed in HEK293 to the catalytic subunits of PKA, results in an increase in channel open probability. However, when  $\alpha$  and  $\beta$  subunits are co-expressed, PKA has opposite effects and causes a decrease in open probability (Dworetzky et al., 1996).

As shown in the previous chapter, BIB channels are tyrosine phosphorylated. 22 tyrosine residues are located on intracellular portions of the BIB channel; one in the amino terminus and 21 in the carboxy terminus (Rao et al., 1990). Of these, five appear to be potential sites of tyrosine phosphorylation based on comparison with optimal sequences for phosphorylation by tyrosine kinases (Songyang et al., 1995). The optimal substrate sequence for src is D/E-D/E-I/V/L-Y\*-G/E-E-F (where the asterisk indicates the phosphorylated tyrosine residue; and / indicates that any of the amino acids shown is tolerated). For another soluble kinase, Abl, the optimal sequence is X-V-I/V/L-Y\*-A-A-P (X indicates any amino acid is tolerated in this position). Figure 4.1B shows the sites of potential phosphorylation by src or Abl in the carboxy tail of BIB, residues conforming to the optimal sequence suggested by Songyang and colleagues (1995) are highlighted in bold. Three tyrosines (Y273, Y384 and Y478) are potential targets for src and two (Y367

and Y609) are potential targets for Abl. All but one tyrosine (Y273) is surrounded by three amino acids that fit the optimal substrate determined by Songyang and colleagues. Tyrosine phosphorylation of NMDA receptor subunits in the brain may contribute to long-term potentiation. Induction of long-term potentiation in rats results in increased tyrosine phosphorylation of NMDA NR2B subunits (Rostas et al., 1996; Rosenblum et al., 1996). Several studies suggest that the phosphorylation of NMDA receptors on tyrosine residues occurs through the actions of the tyrosine kinase src (Yu et al., 1997; Wang and Salter, 1994)

The interaction between tyrosine kinases and their substrates is mediated in part by SH3 binding domains, proline-rich sequences that mediate the targeted interaction between proteins. Figure 4.1C shows the location of four potential SH3 binding domains in the BIB carboxy tail. For both hKv1.5 and connexin 43, intact SH3 binding domains are critical for interaction of the channels with src (Holmes et al., 1996; Kanemitsu et al., 1997). Coexpression of v-src with hKv1.5 in HEK293 cells results in tyrosine phosphorylated channels and decreased currents (Holmes et al., 1996). SH3 binding domains are P-X-X-P (where X is any amino acid and P is proline; Koch et al., 1991; Rickles et al., 1994; Cohen et al., 1995).

The amino acid motif S/T-X-V/I represents a PDZ binding domain (X indicates any amino acid is tolerated; Cohen et al., 1996). These short domains interact with PDZ domain-containing proteins. PDZ domain protein interactions often organize proteins into signaling complexes (Craven and Bredt, 1998). For example, the Kv1.4 PDZ binding domain interacts with the PDZ containing protein, PSD-95 to localize Kv1.4 channels to the post-synaptic density of neurons (Nehring et al., 2000). PDZ binding domains are generally located at the carboxy terminus (Cohen et al., 1996) but can be

internal as in the TRP calcium channel of *Drosophila* (Shieh and Zhu, 1996; and other references here). Three internal PDZ domains (T-A-I and S-A-V) in the BIB carboxy tail are shown in Figure 4.1D.

A striking feature of the carboxy tail is the number of glutamine residues, which constitute 102 of 431 residues (24%) and include three regions of 10, 13 and 25 consecutive glutamines (Figure 4.1E). Polyglutamine regions are thought to act as polar zippers mediating protein-protein interactions (Perutz et al., 1994, Martindale et al., 1998). Abnormally long stretches of glutamine residues underlie certain progressive neurodegenerative diseases, such as Huntington's disease and Machado-Joseph disease (Paulson and Fischbeck, 1996). Interestingly, at least three other neurogenic gene products contain polyglutamine regions: Notch (described in detail in Chapter 1) has two domains of 13 and 17 glutamines, mastermind contains 13 stretches of 5-16 glutamines, and Suppressor of Hairless has three stretches of 6-14 glutamines. Polyglutamine regions might be a common mechanism of regulating neurogenesis.

In order to begin to elucidate the significance of these domains to BIB function, we generated two truncation mutations in the carboxy tail. The sites of truncation were determined by comparison of the alignment of BIB with human AQP1 ( $\Delta 317$ ) or rat AQP4 ( $\Delta 377$ ; Figure 4.2). The end of the carboxy terminus of AQP1 aligned with amino acid 316 of BIB. We introduced a stop codon at this site, deleting amino acids 317-700 of BIB ( $\Delta 317$ ). The carboxy terminus of AQP4 ended at a position comparable to amino acid 376 of BIB. We also introduced a stop codon at this site, deleting amino acids 377-700 ( $\Delta 377$ ). Full-length and truncated BIB constructs were expressed in *Xenopus* oocytes; the whole-cell conductance properties, effects of the tyrosine kinase inhibitor

Lavendustin A, and the tyrosine phosphorylation status of these channels were investigated with two-electrode voltage clamp and western blot analyses.

## 4.2 MATERIALS AND METHODS

(1) *Molecular techniques.* *bib* cDNA was generously donated by Dr. Lily Jan, UCSF (Rao et al., 1990). Truncation mutants were synthesized by polymerase chain reaction using the *bib* gene in a pSK-bluescript as the template. The general scheme is outlined in Figure 4.3. For each truncation mutant, the sense primer sequence (spanning the start codon, *italics*) was the same and contained an introduced *Bgl*III site to facilitate subcloning (underlined; mutated residues are in **bold**):

5'-AACAAATCGAGATCTGAGTCCGACATG-3' bp 277-303.

The antisense primer incorporated the introduced stop codon (**box**) and a *Bgl*III restriction site (underlined; mutated residues are in **bold**) for subsequent subcloning into the pXβG expression vector:

Δ317 5'-GGTGCAGATCTACTGCTG**TCA**CTTGTTGGGCTTCTC-3' bp 1266-1231

Δ377 5'-CAGAGAGATCTGCTGCTG**TCA**GTA**CTTCGAGGA**-3' bp 1448-1417

In order to visualize BIB channels by western blots, an epitope tag consisting of nine amino acids (YPYDVPDYA) from the influenza hemagglutinin protein (HA) was inserted in the amino terminus of both Δ317 and Δ377. This was done in the same manner as inserting the HA epitope into full length BIB, requiring two rounds of PCR. The sense primer for the first reaction contained the last seven codons of the HA epitope (underlined) followed by a region of overlap with the *bib* sequence:

5'-TACGACGTGCCGGACTACGCTGCCGACGAAAGTCTG-3' bp 304-318.

The antisense primer was the same as used for either  $\Delta 317$  or  $\Delta 377$  (above). The sense primer for the second PCR reaction contained the rest of the HA sequence (underlined), the start codon (*italics*), and a *Bgl*III restriction site (**bold**):

5'-TCGAGATCTGAGTCCGACATG TACCCGTACGACGTGCCGGAC-3'.

The antisense primers were the same as those used in the previous reactions (for either  $\Delta 317$  or  $\Delta 377$ ). The truncation mutant constructs were analyzed by diagnostic digests with restriction enzymes to verify the orientation and size of each insert (Figure 4.4A).

The entire coding sequences of all constructs were sequenced to confirm that no inadvertent mutations were introduced. RNA was synthesized as described in Chapter 2.

*(2) Oocyte preparation and injection.* Stage V-VI oocytes from adult female *Xenopus laevis* were obtained and defolliculated as described in Chapter 2. Prepared oocytes were injected with 50nl of sterile water (control oocytes) or 50nl of sterile water containing HAbib,  $\Delta 317$  or  $\Delta 377$  cRNA.

*(3) Electrophysiological recordings.* Two-electrode voltage clamp was used to investigate the macroscopic ion channel properties of HAbib  $\Delta 317$ ,  $\Delta 377$ , and HAbib wild-type as described in Chapter 2.

*(4) Osmotically-induced swelling assay.* Osmotically-induced swelling assays were performed as described in Chapter 2. Analysis of water permeability was performed as described in Rivers et al., 1997.

**(5) Cellular fractionation.** Oocyte plasma membrane fractions were obtained as described in Chapter 2.

**(6) Immunoprecipitation and Western Blotting.** Immunoprecipitation and western blotting were performed as described in Chapter 2.

Data values are presented as mean $\pm$ SD. Significance was tested by a Student's t-test, with significance indicated by  $p < 0.05$  unless otherwise indicated.

### **4.3 RESULTS**

Overall, BIB has approximately 30% overall amino acid sequence identity with the mammalian water channels AQP1 and AQP4. Loops B and E line the water pathway through aquaporins (Murata et al., 2001; Ren et al., 2000) and BIB has approximately 60% and 30% identity with AQP1 and AQP4 in these regions respectively. Despite this identity, results presented in Chapter 2 showed that BIB is not a water channel. In contrast to the high amount of identity between BIB and aquaporins in potential pore lining regions, the carboxy tail of BIB has 6-8 times as many amino acids as AQP1 and AQP4. As discussed in the introduction, the long carboxy tail of BIB contains many sites for protein interactions. One hypothesis for the lack of water permeability of oocytes expressing full-length BIB is that the carboxy tail domain inhibits water flux through BIB.

To test if truncation released inhibitory effects of the carboxy tail on water permeability we performed an osmotically induced swelling assay. Figure 4.5 shows the results of a representative experiment with oocytes expressing AQP1 or the BIB carboxy

tail truncation mutants  $\Delta 317$  and  $\Delta 377$ . When placed in hypotonic saline, the relative volume of AQP1-expressing oocytes increased by approximately 12.5% at five minutes and up to 20% at 10 minutes (Figure 4.5 A and B), yielding a calculated water permeability factor (Pf) value of  $26 \pm 13 \mu\text{m/s}$  ( $n=5$ ). As is seen with oocytes expressing full-length BIB (Chapter 2, Figure 2.1), the relative volume of oocytes expressing  $\Delta 317$  (Figure 4.5A) and  $\Delta 377$  (Figure 4.5B) did not increase and remained similar to that of control oocytes for up to 10 minutes of exposure to hypotonic saline. As expected, the calculated Pf values for  $\Delta 317$  ( $2 \pm 6 \mu\text{m/s}$ ,  $n=4$ ) and  $\Delta 377$  ( $7 \pm 4 \mu\text{m/s}$ ,  $n=4$ ) were not different than control oocytes ( $2 \pm 1 \mu\text{m/s}$ ,  $n=4$ ). Thus, truncation of the carboxy tail did not unmask a water pathway through BIB channels.

Since truncation removed sites known to be important for trafficking or retention at the plasma membrane we confirmed the correct localization of the truncated BIB channels with western blots of total proteins isolated from oocyte plasma membrane fractions. A representative experiment is shown in Figure 4.6. The expected size of full-length BIB channels is approximately 80kD. The expected size of  $\Delta 317$  and  $\Delta 377$  truncated channels are approximately 36 and 44 kD respectively. In Figure 4.6 bands representing full-length HABIB were visualized at approximately 80kD.  $\Delta 317$  channels were visualized at approximately 38kD (Figure 4.6, panel A) and  $\Delta 377$  channels were visualized at approximately 46kD (Figure 4.6, panel B). However,  $\Delta 377$  appeared as a doublet near 46kD and there was also a smear between 74 and 107kD. Similar banding patterns have been observed from oocytes expressing mutant AQP1 channels and have been attributed to altered patterns of glycosylation that result from defective protein folding patterns (Preston et al., 1993). Both truncated channels are isolated from plasma membrane fractions of oocytes and are localized to the plasma membrane of

oocytes. The lack of water permeability in oocytes expressing full-length or BIB channels is a fundamental property of BIB and not the result of lack of protein expression.

The ionic channel characteristics of  $\Delta 317$  and  $\Delta 377$  were investigated with two-electrode voltage clamp. Representative current-voltage relationships of control or oocytes expressing HABIB  $\Delta 317$ ,  $\Delta 377$ , or wild-type HABIB are shown in Figure 4.7A. Oocytes expressing  $\Delta 317$  and  $\Delta 377$  had decreased current amplitudes at all voltages after channel activation. Current traces, shown in 4.7B were evoked in response to steps from +60 to -90mV. The reversal potentials of  $\Delta 317$  ( $-18 \pm 8$ mV,  $n=22$ ) and  $\Delta 377$  ( $-22 \pm 9$ mV,  $n=16$ ) were not significantly different than full length HABIB ( $-19 \pm 8$ mV,  $n=24$ ).

Figure 4.8 summarizes the whole-cell conductance of control and oocytes expressing full-length HABIB,  $\Delta 317$ , and  $\Delta 377$ . Conductance was calculated from the slope of the linear fit of the current-voltage relationship (Figure 4.7A). Oocytes expressing either truncation mutant had reduced whole-cell conductance ( $\Delta 317$ ,  $6 \pm 5$ nA/mV,  $n=23$ ;  $\Delta 377$ ,  $3 \pm 1$ nA/mV,  $n=17$ ;) compared to full length HABIB ( $22 \pm 14$ nA/mV,  $n=30$ ) but significantly greater than that of control oocytes ( $2 \pm 2$ nA/mV,  $n=21$ ,  $p < 0.05$ ). Since full-length and truncated channels are expressed on the plasma membrane, the decreased conductance could be the result of removal of sites important for BIB regulation, changes in membrane retention, or conformational changes that decrease the single channel conductance.

Results presented in Chapter 2 showed that BIB was phosphorylated on tyrosine residues (Figure 2.7) and that the whole-cell conductance of oocytes expressing BIB was enhanced by pre-treatment with the tyrosine kinase inhibitor Lavendustin A. We

investigated the hypothesis that the carboxy tail is the site of regulatory interactions by tyrosine kinases with oocytes expressing  $\Delta 317$  since conductance in oocytes expressing  $\Delta 377$  was difficult to detect. Results of these experiments are shown in Figure 4.9. Immunoprecipitations of  $\Delta 317$  and HABIB were performed with either the rat anti-HA antibody or mouse anti-phosphotyrosine antibody (see Methods). After resolution by SDS-PAGE (10%) and western blot transfer to PVDF, bands for both full length HABIB and  $\Delta 317$  were detected in samples immunoprecipitated by the anti-HA antibody but only for full-length HABIB in samples immunoprecipitated by the anti-phosphotyrosine antibody. These results indicate that the HABIB channels truncated at amino acid 317 are not phosphorylated on tyrosine residues. Panel B summarizes the effect of one hour pre-incubation with 10 $\mu$ M Lavendustin A on oocytes expressing  $\Delta 317$ . Lavendustin A did not enhance the conductance of oocytes expressing  $\Delta 317$  ( $7 \pm 3$  nA/mV, n=8) compared to untreated  $\Delta 317$  expressing oocytes ( $6 \pm 2$  nA/mV, n=8). These results suggest that truncation of the carboxy tail at amino acid 317 removes regulation by oocyte tyrosine kinases and that a site or sites within amino acids 317-700 are targets of tyrosine phosphorylation.

#### 4.4 DISCUSSION

Oocytes expressing HABIB channels truncated at two different sites in the carboxy tail ( $\Delta 317$  and  $\Delta 377$ ) had decreased whole-cell conductance compared to oocytes expressing full-length HABIB. Despite the decreased conductance, channels were located on the plasma membrane as indicated by western blots showing that the decrease was not a result of lack of expression. Truncated channels were similar to full-length BIB channels with respect to ionic channel properties. Reversal potentials of

oocytes expressing  $\Delta 317$  and  $\Delta 377$  channels were  $-18 \pm 8$  mV and  $-22 \pm 9$  mV respectively and not significantly different than that of full-length HABIB ( $-19 \pm 8$  mV,  $n=24$ ) showing that the cation selectivity of truncated channels was similar to full-length HABIB. The current-voltage relationships were linear indicating no apparent change in voltage dependence, similar to full-length HABIB channels. Although truncated channels have carboxy termini roughly equivalent in length to those of AQP1 and AQP4, truncation did not uncover a hypothetical water pathway through BIB channels.

The decreased conductance of oocytes expressing  $\Delta 317$  and  $\Delta 377$  was hypothesized to be due to the deletion or destabilization of sites important for function. Although  $\Delta 377$  may be improperly processed, both truncated channels localize to the plasma membrane and formed ion channels with properties similar to those of full-length HABIB (*i.e.* linear current-voltage relationship and similar reversal potentials). The decreased whole-cell conductance may be the result of removing sites critical for protein interactions that regulate BIB cation channel activity, or may result from decreased single channel conductance or decreased open probability. Single channel studies are needed to examine this possibility. Although attempted here, patches containing  $\Delta 317$  and  $\Delta 377$  were not obtained despite injections of increased amounts of RNA.

The lack of tyrosine phosphorylation of  $\Delta 317$  and the lack of effect of Lavendustin A on these channels suggests that the carboxy tail is the site of tyrosine kinase modulation of HABIB in *Xenopus* oocytes (described in chapter 2). Since carboxy terminal deletion removed sensitivity of the channel to endogenous tyrosine kinases, the site of tyrosine phosphorylation in full-length BIB may be contained between amino acids 317-700. However, we cannot rule out the possibility that removing sites such as SH3 and PDZ binding domains and polyglutamine stretches removes protein interactions

involving carboxy tail regions that are critical for phosphorylation at sites other than the carboxy tail or that may prevent proper trafficking to and retention of truncated channels at specific sites on the plasma membrane. Site-directed mutagenesis of tyrosines 367, 384, 478, and 609 (four of the tyrosines in the carboxy tail that are within consensus sites for phosphorylation by src or Abl, see Introduction and Figure 4.1B) and expression in oocytes would address whether these four tyrosines are sites of phosphorylation and regulate channel activation. If, as described in Chapter 2, dephosphorylation is the mechanism of BIB channel activation, and if tyrosines 367, 384, 478 or 609 are sites of inhibitory phosphorylation, then one might speculate that mutation of these tyrosines to phenylalanine should result in constitutively active BIB cationic conductance. However, removing these sites by truncation of the carboxy tail did not induce constitutively active channels. A more complex relationship is likely, and may reflect the importance of the multiple protein interaction domains (SH3, PDZ and polyglutamine stretches) located in this region.

I propose that the carboxy tail is important for determining the ion conductance of BIB channels. The carboxy tail domains of many ion channels are sites of multiple modes of regulation. Calcium activated potassium channels ( $K_{Ca}$ ) are regulated by both membrane potential and intracellular calcium. Calcium ions bind to specific domains in the carboxy tail of  $K_{Ca}$  channels (Meera et al., 1997; Wei et al., 1994). Calcium binding alters the sensitivity to voltage in a subunit specific manner (Hille, 1992). The carboxy tail of Maxi-K  $K_{Ca}$  channels is also a site of phosphorylation, presumably by PKA (Nara et al., 1998). Currents in *Xenopus* oocytes expressing Maxi-K channels with S869 (located in the carboxy tail) mutated to alanine were no longer stimulated by forskolin or the  $\beta$ 2 agonist isoproterenol (Nara et al., 1998). The carboxy tail of the inward rectifying

potassium channels Kir2.1 and Kir2.3 contain PDZ binding domains at their carboxy termini (Cohen et al., 1996). In Kir2.3 this site overlaps with a PKA phosphorylation site. Phosphorylation by PKA inhibits the interaction of Kir2.3 with PSD-95 and may be a mechanism to regulate localization of Kir2.3 to specific sites in the nerve terminal or may regulate inhibitory effects of the carboxy tail on Kir2.3 conductance (Cohen et al., 1996). Multiple modes of regulation at the carboxy tail are also apparent for NMDA receptor NR1 subunits (Tingley et al., 1993). NR1 subunits heterologously expressed in HEK293 cells or isolated from primary cultures of rat cortical neurons are phosphorylated by PKC and the site of phosphorylation is in the carboxy tail (Tingley et al., 1993). However, the carboxy tail domain of NR1 contains two alternatively spliced exons and only one contains sites for phosphorylation by PKC (Tingley et al., 1993). These studies support the idea that BIB regulation at the carboxy tail is through multiple mechanisms.

The carboxy tail is also the site of regulatory interactions for channels in the MIP family. For example, phosphorylation of serine 256 in the carboxy tail of AQP2 by protein kinase A induces translocation of AQP2 to the apical membrane of collecting duct cells in the inner medulla in response to the anti-diuretic hormone vasopressin (Fushimi et al., 1997; Sasaki et al., 1998). The carboxy tail of AQP1 contains a number of conserved amino acids in positions identical to those in the binding regions of cyclic nucleotide-gated channels. The carboxy tail is likely to be the site of direct cGMP regulation of cationic ion channel activity in AQP1 (Anthony et al., 2000).

In this chapter, I discussed results from experiments with mutant BIB channels generated by truncation of the carboxy tail of BIB at two sites,  $\Delta 317$  and  $\Delta 377$ . These studies are interesting in that they add a further level of complexity to knowledge of the regulation of MIP family of channels and potentially narrow down the sites of tyrosine

**phosphorylation of BIB to tyrosines 367, 384, 478, and 609. Several ideas merit further investigation: (i) site-directed mutagenesis of tyrosines 367, 384, 478 and 609 to phenylalanine; (ii) identification of the tyrosine kinase and protein tyrosine phosphatases that act on BIB channels; (iii) elucidation of the effects of SH3, PDZ binding domains, and polyglutamine regions on cationic channel activity and trafficking to or retention of channels to specific molecular compartments.**

A.

269

SGLVYEYIFN **SR**NRNLRHNKGSIDNDSSSIHSEDELNYDMDMEKPNKYQOS  
 QGTYP**RGQS**NGNGGGQAAGNGQHQAANMGQMPGVVANAGQGNYC**ONLYTAP**  
 PLSSKYDQQQEPLYGGTRSLY **CRSPT**LTRSNL**RSOS**VYAKSNTAINRDIV  
 PRPGPLVPAQSLYPMRTQQQQQQQQQQQQQVASAPQSSHLQONQNVQNQMQQ  
**RSES**IYGMRGSMRGQQQPIQQQQQQQQQQQLQQQQPNMGVQQQQMQPPQMM  
 SDPQQQPQGFQPVYGTRTNPTPMDGNHKYDRRDPQQMYGVTGPR**RGOS**AQ  
 SDDSSYGSYHGSAVTPP**RHPS**VEPSPPPPQPNAHPQP**IRTSERK**VSAP  
 VVVSQPAACAVTYTTT**SQ**SAVTAQQQQQPMLMYAPP**PP**QQQQQQQQQQQQQQQQ  
 QQQQQQMMMQQQQQHYGMLPLRPN-700

B.

269

**SGLVYEYI**NSRNRNLRHNKGSIDNDSSSIHSEDELNYDMDMEKPNKYQOS  
 QGTYP**RGQS**NGNGGGQAAGNGQHQAANMGQMPGVVANAGQGNYC**ONLYTAP**  
 PLSSKYDQQQ**OEPLYGGT**SLYCRSPTLTRSNL**NRSQS**VYAKSNTAINRDIV  
 PRPGPLVPAQSLYPMRTQQQQQQQQQQQQQVASAPQSSHLQONQNVQNQMQQ  
**RSES**IYGMR**ES**SMRGQQQPIQQQQQQQQQQQLQQQQPNMGVQQQQMQPPQMM  
 SDPQQQPQGFQPVYGTRTNPTPMDGNHKYDRRDPQQMYGVTGPR**NRGQ**SAQ  
 SDDSSYGSYHGSAVTPP**ARHPS**VEPSPPPP**MLMYAPP**QPNAHPQP**PIRT**  
 QSERKVSAPVVVSQPAACAVTYTTT**SQ**SAVTAQQQQQQQQQQQQQQQQQQQQ  
 QQQQQQMMMQQQQQHYGMLPLRPN-700

C.

269

SGLVYEYIFNSRNRNLRHNKGSIDNDSSSIHSEDELNYDMDMEKPNKYQOS  
 QGTYP**RGQS**NGNGGGQAAGNGQHQAANMGQMPGVVANAGQGNYC**ONLYTAP**  
 PLSSKYDQQQEPLYGGTRSLYCRSPTLTRSNL**NRSQS**VYAKSNTAINRDIV  
 PRP**PLVE**AQSLYPMRTQQQQQQQQQQQQQVASAPQSSHLQONQNVQNQMQQ  
 RSESIYGMRGSMRGQQQPIQQQQQQQQQQQLQQQQPNMGVQQQQMQPPQMM  
 SDPQQQPQGFQPVYGTRTNPTPMDGNHKYDRRDPQQMYGVTGPR**NRGQ**SAQ  
 SDDSSYGSYHGSAVTPP**ARHPS**VEPS**PPPP**MLMYA**PP**QPNAHPQP**PIRT**  
 QSERKVSAPVVVSQPAACAVTYTTT**SQ**SAVTAQQQQQQQQQQQQQQQQQQQQ  
 QQQQQQMMMQQQQQHYGM**PLRE**N-700

## D.

269

SGLVY EY I FNSRNRNLRHNKGSIDNDSSSIHSEDELNYDMDMEKPNKYQQS  
 QGTYP RGQSNNGGGQAAGNGQHQAANMGQMPGVVANAGQGN YCONLYTAP  
 PLSSKYDQQQEPLYGGTRSLYCRSPTLTRS NLNRSQSVYAKSNTAINDIV  
 PRPGPLVPAQSLYPMRTQQQQQQQQQQQQQVASAPQSSHLQNONVQNMQQ  
 RSESIYGMRGSMRGQQQPIQQQQQQQQQQQLQQQQPNMGVQQQQMPPPPQMM  
 SDPQQQPQGFQPVYGTRTNPTPMDGNHKYDRRDPQQMYGVTGPRNRGQSAQ  
 SDDSSYGSYHCSAVT PPARHPSVEPSPPPPMLMYAPPPQPNAAHQPPIRT  
 QSERKVSAPVVVSQPAACAVTYTTSQCSAVTAQQQQQQQQQQQQQQQQQQQQ  
 QQQQQQMMMQQQQQHYGMLPLRPN-700

## E.

269

SGLVY EY I FNSRNRNLRHNKGSIDNDSSSIHSEDELNYDMDMEKPNKYQQS  
 QGTYP RGQSNNGGGQAAGNGQHQAANMGQMPGVVANAGQGN YCONLYTAP  
 PLSSKYDQQQEPLYGGTRSLYCRSPTLTRS NLNRSQSVYAKSNTAINRDIV  
 PRPGPLVPAQSLYPMRTQQQQQQQQQQQQQVASAPQSSHLQNONVQNMQQ  
 RSESIYGMRGSMRGQQQPIQQQQQQQQQQQLQQQQPNMGVQQQQMPPPPQMM  
 SDPQQQPQGFQPVYGTRTNPTPMDGNHKYDRRDPQQMYGVTGPRNRGQSAQ  
 SDDSSYGSYHGSAVT PPARHPSVEPSPPPPMLMYAPPPQPNAAHQPPIRT  
 QSERKVSAPVVVSQPAACAVTYTTSQCSAVTAQQQQQQQQQQQQQQQQQQQQ  
 QQQQQQMMMQQQQQHYGMLPLRPN-700

**Figure 4.1 Carboxy tail domain of BIB with sites of potential phosphorylation and protein interactions highlighted.** The carboxy tail of BIB (amino acids 269-700) is shown with consensus sequences for phosphorylation (A. serine/threonine kinases and B. tyrosine kinases), SH3 binding domains (C.), PDZ binding domains (D.) and polyglutamines (E.) highlighted in bold, black letters. For the consensus sequences given \* indicates the phosphorylated residue, X indicates any amino acid is tolerated, / indicates that any of the set of amino acids shown are tolerated. A. The carboxy tail of BIB contains eight sites of potential phosphorylation by serine/threonine kinases. The consensus sequences for phosphorylation are: XS\*RX (circled; cGMP dependent protein kinase); XRXS\*X (ovals; CAM kinase II); XRXS\*RX (boxed; protein kinase C; Kemp and Pearson, 1990; Burris et al, 1998). B. Three of the 21 tyrosines in the carboxy tail are potential substrates for the tyrosine kinase src (D/E-D/E-I/V/L-Y\*-G/E-E/F; ovals); two are potential substrates for Abl (X-V-I/V/L-Y\*-A-A-P; boxed). C. Four potential SH3 binding domains are boxed (minimal consensus P-X-X-P; Rickles et al, 1994). D. Three internal putative PDZ binding domains, S/T-X-V/I are enclosed in ovals (Saras and Heldin, 1996). E. 102 of the 431 amino acid residues (24%) are glutamine (Q) in the carboxy tail of BIB including three stretches of 10, 12 and 25 glutamines (Rao et al., 1990).

A.

```

hAQP1 218-GGALAVLIYDFILAPRSSDLTDRVKVWTSQVVEEYDL DADDINSRVEMKPK-268
bib    265-GGMASGLVYEYIFNSRNRNLRHNKGSIDNDSSSIHSEDELNYDMDMEKPNKYQSSQGTYP+
          ** * * * * * * * * *

```



B.

```

rAQP4 240-GAVLAGALYEVFCP-----DVELKRRLKEAFSKAAQQTKGSYME
bib    265-GGMASGLVYEYIFNSRNRNLRHNKGSIDNDSSSIHSEDELNYDMDMEKPNKYQSSQGTYP+
          * * *** * * * * * * * * * *

```

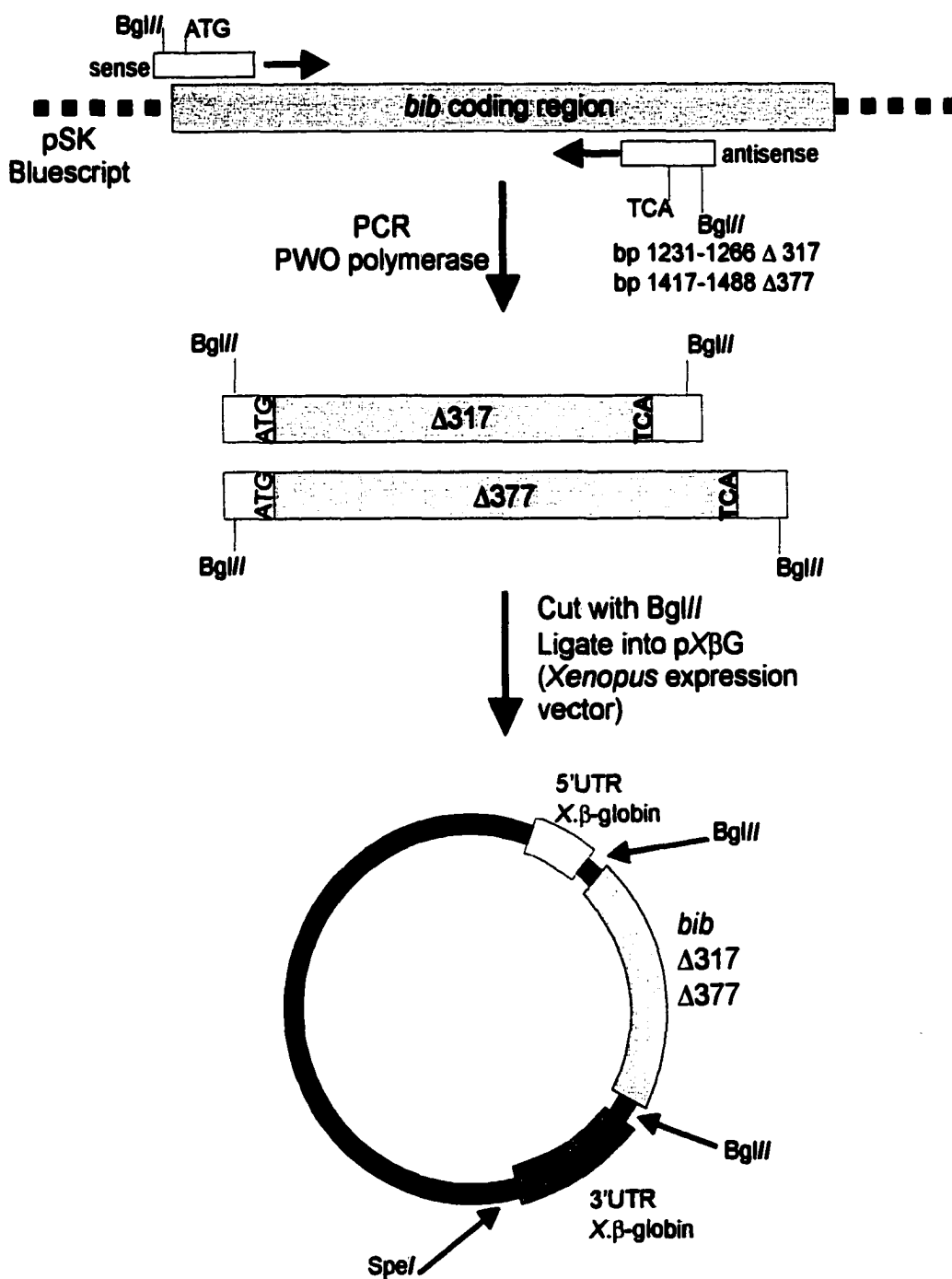
```

rAQP4      VEDN-----RSQVETEDLILKPGVVHVIDIDRGDEKKGKDSSGEVLSSV-323
bib        GQSNNGGGQAAGNGQHQAANMGQMPGVVANAGQ-GNYCQONLYTAPPLSSKYDQQQEPLY+
          * * * * * * * * * * * * *

```



**Figure 4.2 Alignment of carboxy tail domains of BIB with rat AQP4 and human AQP1.** Alignment of BIB with human AQP1 (A.) and rat AQP4 (B.) was performed with ClustalW ([www.clustalw.genome.ad.jp/](http://www.clustalw.genome.ad.jp/)). Amino acids 265-324 (A.) and 265-383 (B.) of BIB, accession number X53275; 218-268 of human AQP1, (M77829); 240-323 rat AQP4 (U14007) are shown. Underlined BIB sequence indicates the location of the end of transmembrane domain 6; asterisks below the alignment indicate identical amino acid residues between proteins; + indicates additional sequence not shown; - indicate gaps introduced for alignment. Alignment of BIB with hAQP1 and rAQP4 determined the positions used to truncate BIB yielding  $\Delta 317$  and  $\Delta 377$  mutant channels. White triangles indicate sites of BIB truncations.



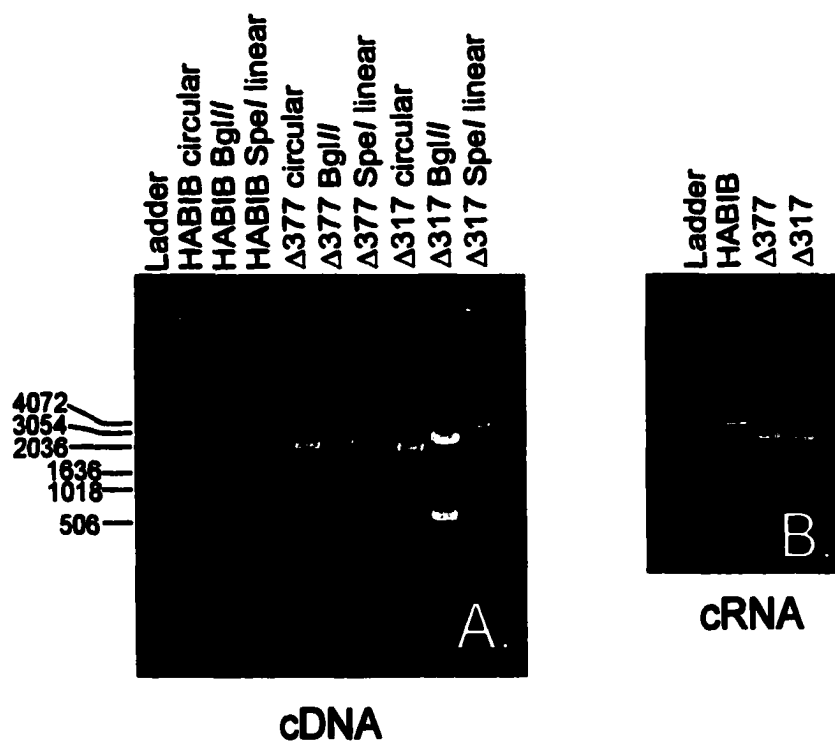
**Figure 4.3 Truncation strategy for *BIB*.**  
See next page for details.

**Figure 4.3 Truncation strategy for BIB.**  $\Delta 317$  and  $\Delta 377$  and truncation mutants were generated with polymerase chain reaction. For both mutants the sense primer incorporated an introduced *Bgl*III restriction site (underlined) upstream of the ATG start (*italics*) and unique antisense primers specific for the truncation site and incorporating the introduced stop codon (*italics*) as well as a novel *Bgl*III restriction site (underlined) for subcloning (primers are shown below; mutated bases are in bold). The resulting PCR products were digested with *Bgl*III restriction enzyme and ligated into the pXBG expression vector, which is a modified pSP64 vector containing the 5' and 3' untranslated regions (5'-UTR and 3'-UTR) of the *Xenopus*  $\beta$ -globin gene.

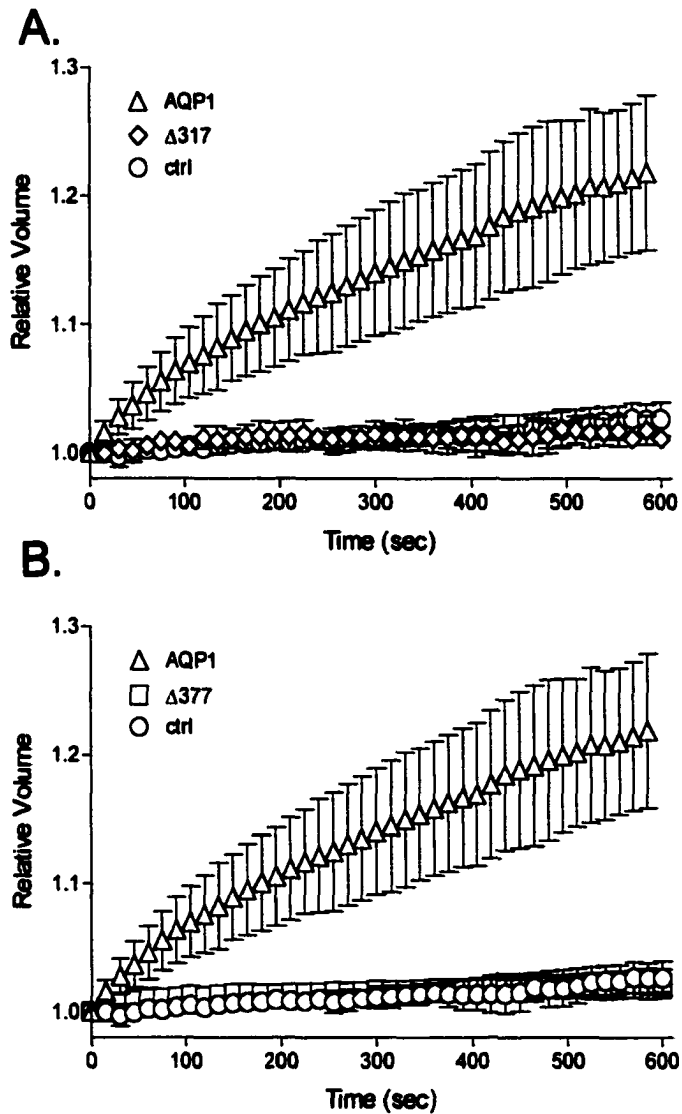
sense: 5'-AACAAATCGAGATCTGAGTCCGACATG-3' bp 277-303

$\Delta 317$  antisense: 5'-GGTGCAGATCTACTGCTGTCACCTTGTTGGGCTTCTC-3' bp 1266-1231

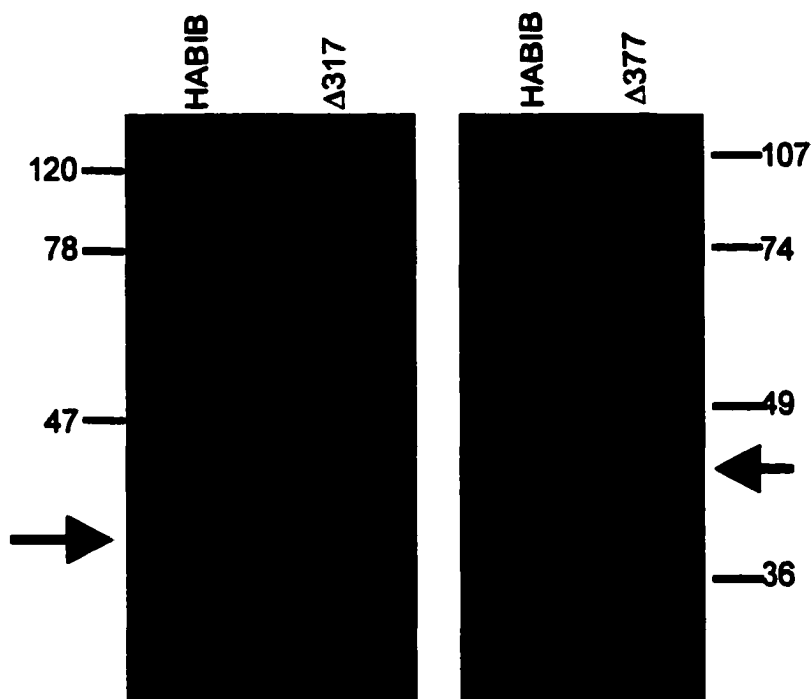
$\Delta 377$  antisense: 5'-CAG AGAGATCTGCTGCTGTCAGTACTTCGAGGA-3' bp 1448-1417



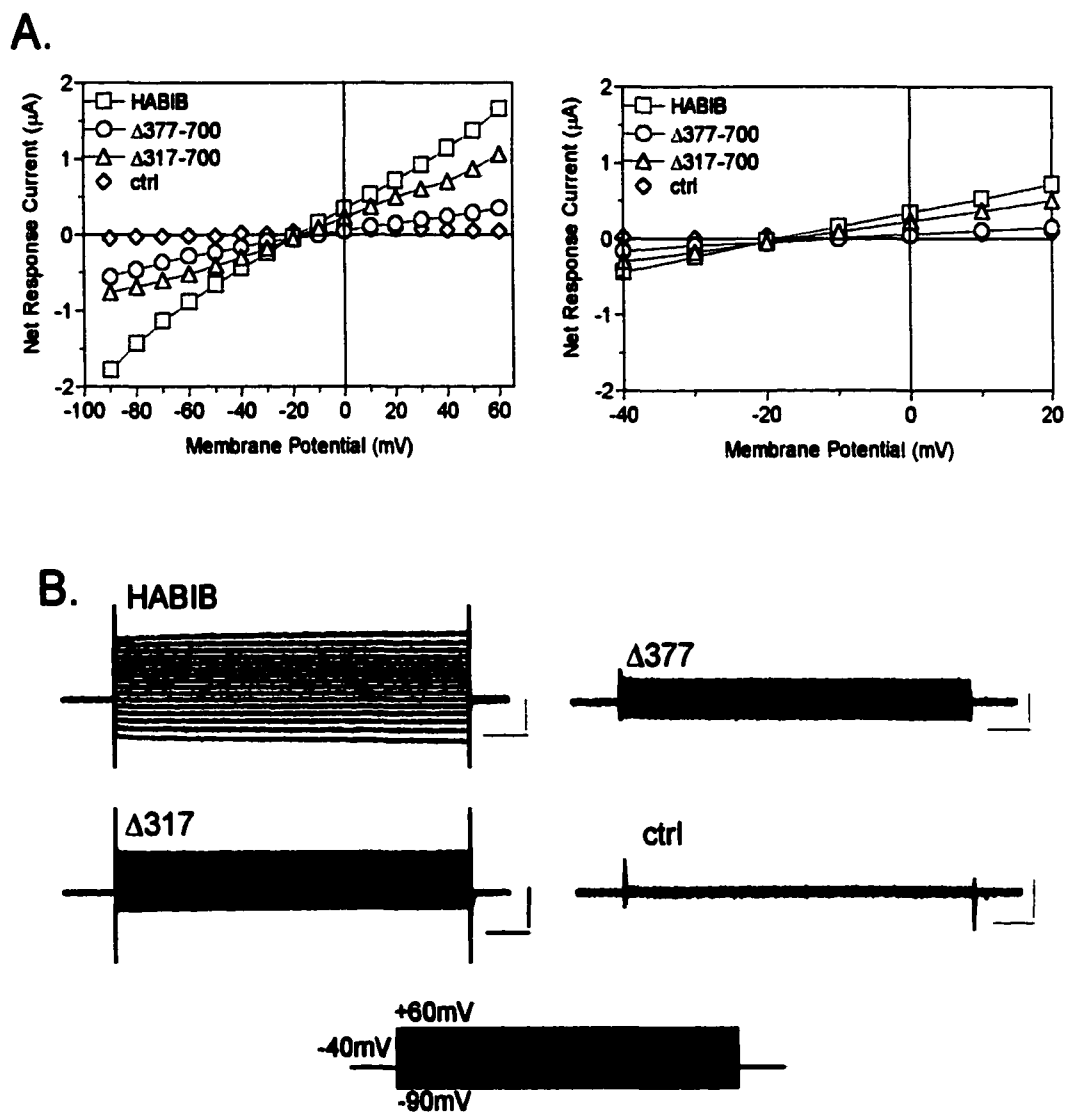
**Figure 4.4 Restriction digest analysis of full length and truncation mutants of BIB cDNA and illustration of cRNA products.** A. Aliquots of plasmids containing HABIB,  $\Delta 317$  and  $\Delta 377$  cDNA were analyzed by gel electrophoresis on a 1%(w/v) agarose gel and visualized with ethidium bromide staining. Circular plasmids were digested with *Bgl*II resulting in two fragments for each: the backbone pX $\beta$ G expression vector (2960bp) and either BIB (2128bp),  $\Delta 377$  (1393bp) or  $\Delta 317$  (1220bp). Digestion with *Spe*I linearized the plasmids yielding a band at 5088bp for BIB, 4353bp for  $\Delta 377$  and 4180  $\Delta 317$ . B. cRNA was synthesized in vitro from *Spe*I-linearized plasmid DNA and analyzed on a 1%(w/v) agarose gel with 6.7% formaldehyde and visualized with ethidium bromide staining. RNA ladder sizes correspond to (bases): 9490, 4400, 2370, 1350 and 240.



**Figure 4.5 Truncation of the carboxy tail domain does not confer water permeability to BIB.** Water permeability was tested with an oocyte swelling assay in which oocytes (expressing either AQP1,  $\Delta 317$ ,  $\Delta 377$  or ctrl) were placed into 50% hypotonic saline at time 0. Two-dimensional images of the oocyte were captured at fifteen-second intervals. The two-dimensional area of the oocyte was converted to relative volume ( $V/V_0$ ;  $V_0$ , the volume at time zero;  $V/V_0=(A/A_0)^{3/2}$ ) and used to calculate the osmotic water permeability ( $P_f$ ) as described in Rivers et al, (1997).

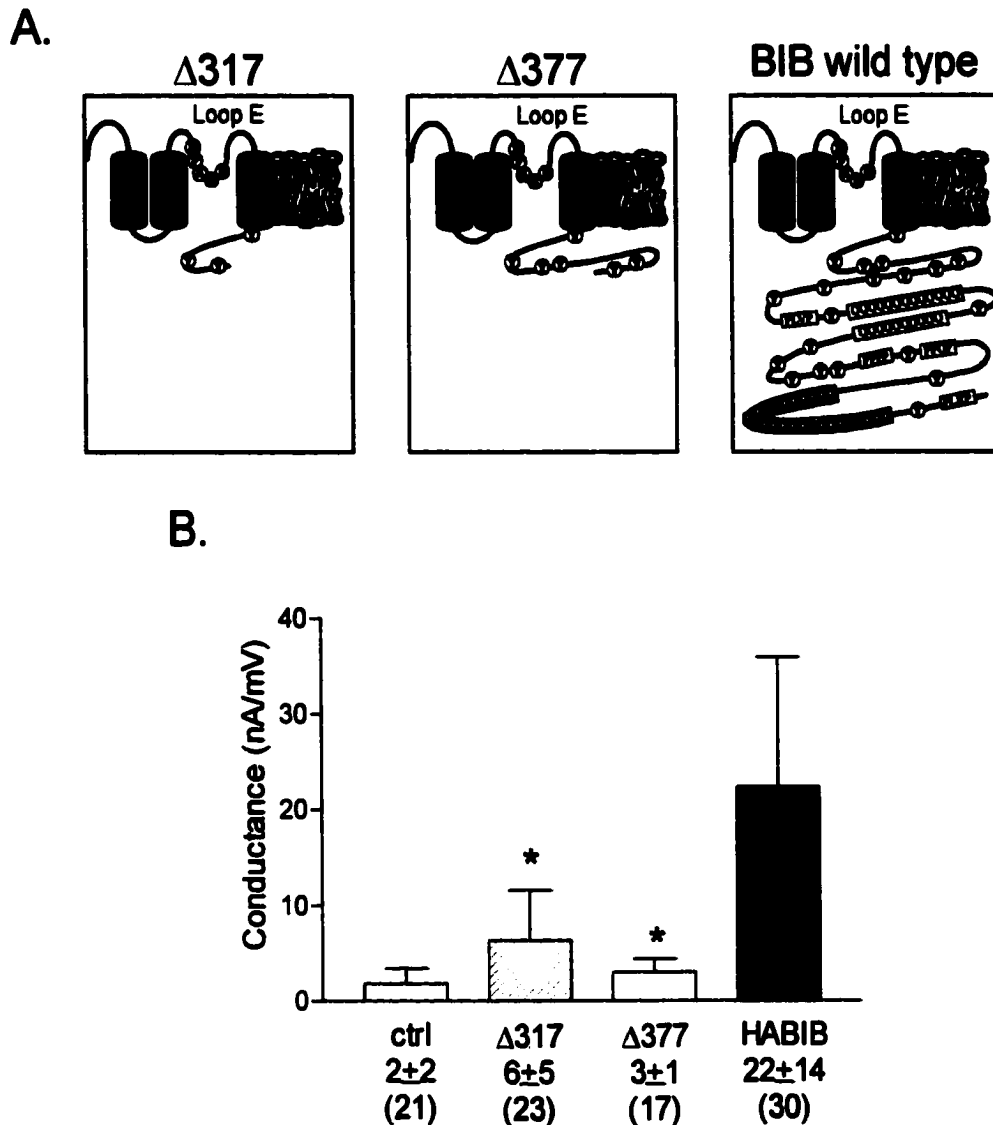


**Figure 4.6**  $\Delta 317$  and  $\Delta 377$  are expressed on the plasma membrane of *Xenopus* oocytes. Plasma membrane fractions of *Xenopus* oocytes expressing  $\Delta 317$ ,  $\Delta 377$  or HABIB were isolated by differential centrifugation, resolved by 8% SDS-PAGE and transferred to nitrocellulose. The blot was probed by immunoblotting with rat anti-HA antibodies (clone 3F10, Roche) followed by goat anti-rat IgG HRP-conjugate secondary. Bands were visualized by enhanced chemi-luminescence. Sizes of molecular weight markers are indicated. HABIB channels resolve at approximately 80kD. **A.**  $\Delta 317$  channels resolve at approximately 38kD (arrow). **B.**  $\Delta 377$  channels resolve at approximately 46kD (arrow). The upper bands at approximately 48kD and the smear between 80-100kD may be the result of abnormal processing of  $\Delta 377$  as has been seen for AQP1 mutants (Jung et al., 1994).

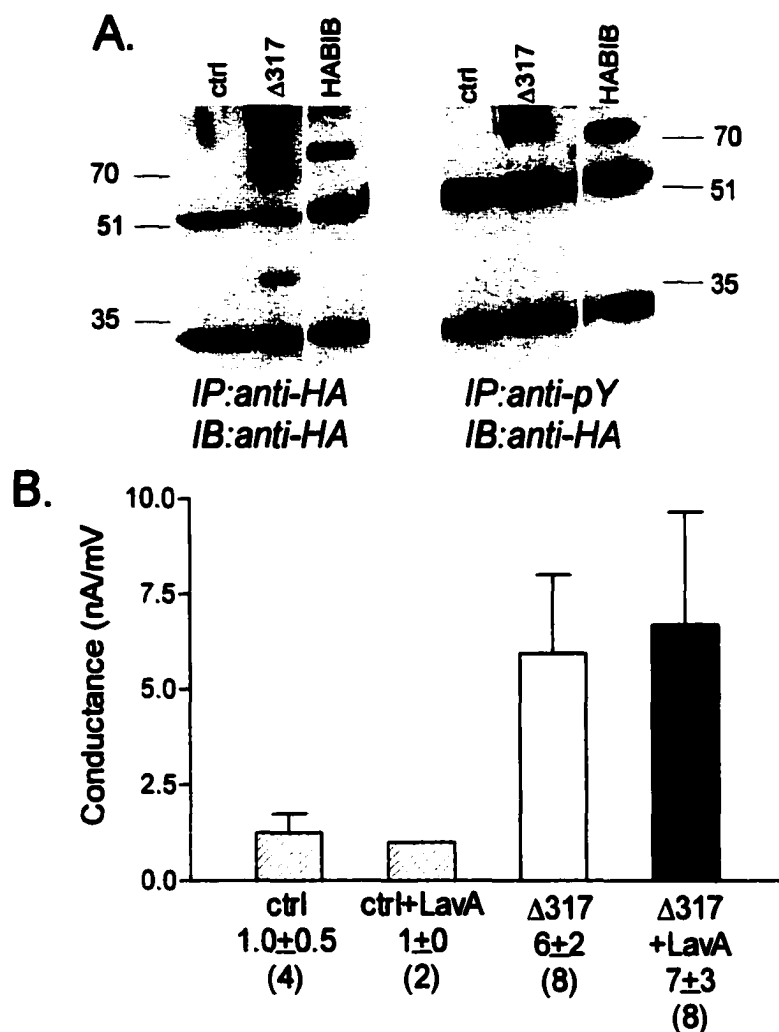


**Figure 4.7**  $\Delta 317$  and  $\Delta 377$  have a linear current-voltage relationship.

**A.** Current-voltage relationships for representative HABIB,  $\Delta 317$ ,  $\Delta 377$  and control oocytes. Full-length and truncated channels have linear current-voltage relationships (left panel). Right panel shows an enlargement of the x-axis to reveal similar reversal potentials of truncated and full-length BIB channels. Reversal potentials for  $\Delta 317$  ( $-18 \pm 8$  mV,  $n=22$ ),  $\Delta 377$  ( $-22 \pm 9$  mV,  $n=16$ ) and HABIB ( $-19 \pm 8$  mV,  $n=24$ ) were not significantly different. **B.** Current traces were evoked by stepping from +60 to  $-90$  mV in 10 mV increments from a holding potential of  $-40$  mV for oocytes expressing HABIB,  $\Delta 317$ ,  $\Delta 377$ , or control oocytes. Scale bars are  $1 \mu\text{A}$  and 100 ms.



**Figure 4.8**  $\Delta 317$  and  $\Delta 377$  have reduced whole-cell conductance compared to full length BIB. **A.** Diagram of the carboxy terminal half of full-length and truncated BIB channels with tyrosines, SH3 binding domains and polyglutamine regions indicated for  $\Delta 317$  (left),  $\Delta 377$  (middle) and full-length BIB (right). **B.** Summary of the conductance values of control and oocytes expressing  $\Delta 317$ ,  $\Delta 377$  and full-length BIB. Bar height indicates mean, error bars indicate standard deviation, values (mean $\pm$ SD) and number of samples (parentheses) are shown below the graph. Conductance was calculated from a linear fit of the current-voltage relationship obtained from traces as in Figure 4.7. \* indicates significance compared to ctrl and HABIB ( $p < 0.05$ , t-test).



**Figure 4.9 Truncation of the carboxy tail removes detectable tyrosine phosphorylation of BIB.** **A.** Western blot of proteins immunoprecipitated from oocyte plasma membrane fractions with a rat anti-HA antibody (clone 3F10, Roche, left) or a mouse anti-phosphotyrosine antibody (PY11120, Transduction Labs, right). The blot was probed with the rat anti-HA antibody and goat anti-rat IgG HRP-conjugated secondary antibody (both panels). HA-tagged BIB constructs (HABIB and  $\Delta$ 317) were visualized by enhanced chemi-luminescence (Pierce). Shown in each panel are proteins from control,  $\Delta$ 317 and wild type HABIB-expressing oocytes. Wild type HABIB but not  $\Delta$ 317 is phosphorylated on tyrosine residues. **B.** Summary of the lack of effect of pre-treatment with 10 $\mu$ M Lavendustin A on oocytes expressing  $\Delta$ 317. Bar height indicates mean conductance, error bars indicate standard deviation, values and number of samples (parentheses) are indicated below the graph. In contrast to the significant effect on wild type channels (see Figure 2.6) no differences were observed between Lavendustin A treated and untreated  $\Delta$ 317-expressing oocytes.

## **SUMMARY AND CONCLUSIONS**

Proper BIB function during neurogenesis is fundamentally important; lack-of-function mutations in BIB override intact Notch receptor signaling and cause a neurogenic phenotype. Despite the importance of BIB for proper neural development its function has remained unknown. This dissertation describes experiments designed to test the hypothesis that BIB is an ion channel. Results using two-electrode voltage clamp, demonstrated that BIB is a non-selective monovalent cation channel regulated by endogenous signaling pathways involving tyrosine kinases in oocytes. Cell-attached patch clamp experiments revealed channels with a large single channel conductance in BIB-expressing oocytes ( $300 \pm 30$  pS). Our novel finding of a cationic channel through BIB fits logically with experiments by Goodman and Spitzer designed to examine the development of electrical excitability of neurons in the grasshopper embryo (Goodman and Spitzer, 1979). The resting membrane potential of differentiating neuroblasts was  $-60$  to  $-80$  mV while non-neuronal cells had more depolarized membrane potentials,  $-40$  to  $-60$  mV (Goodman and Spitzer, 1979). Based on the results presented in this dissertation, one might speculate that the depolarized membrane potential of non-neural cells could be the result of BIB acting to inhibit neural fate. Additionally, the novel regulation of BIB by a mechanism involving tyrosine kinase pathways appears to fit logically with the role of BIB in neurogenesis, a process that is governed by growth factors and other environmental cues (Pimentel et al., 1996; Kimble and Simpson, 1997; Skeath, 1998; Udolph et al., 1998; Chen et al., 1999). Several new questions emerge from the finding that BIB is a cationic channel regulated by tyrosine kinase signaling: (i) what changes in phosphorylation status occur with BIB channel activation; (ii) how does membrane depolarization, mediated by BIB, affect cell fate decision-making; (iii) is BIB

regulated by tyrosine kinases during *Drosophila* development; (iii) what is the involvement of BIB in Notch receptor signaling and in growth factor signaling during development; and (iv) is BIB channel activity regulated through additional pathways *in vivo*?

Cationic permeability through BIB is blocked by extracellular calcium and barium. Calcium and barium probably inhibit currents in BIB-expressing oocytes by mechanisms other than simple occlusion of the pore since the ionic radii of calcium and barium (0.99Å and 1.35Å respectively) are similar to those of the permeant ions, sodium (0.95Å), and potassium (1.33Å) but less than that of tetraethylammonium (~5Å). Current amplitudes from oocytes expressing any one of several mutations at E71 were dramatically reduced compared to wild type HABIB channels. A conservative substitution of E71 to aspartic acid resulted in currents that were blocked by  $Mg^{2+}$ . These results are the first to demonstrate experimentally that E71, a highly conserved residue in MIP channels, is critical for determining channel properties. Further experiments should address the effect of mutating E71 on single channel properties as well as any changes in trafficking or retention of mutant channels on the plasma membrane since E71 is conserved in over 90% of MIP channels and appears to be critical for proper channel function. As described in the introduction to Chapter 3, divalent cation blockade is a common mechanism to regulate the properties of ion channels. This feature of BIB channels could be an additional mechanism of regulation of BIB function *in vivo*, however additional studies to determine the effect of calcium block on single channel properties as well as the effect of intracellular calcium are required to better understand the physiological effects of calcium on BIB.

For me, the most intriguing structural feature of BIB has been the carboxy tail domain. Chapter 4 described results demonstrating that the carboxy tail of BIB is critical for channel activation; channels truncated at amino acids 317 or 377 exhibited decreased whole-cell conductance. Furthermore, truncation at amino acid 317 removes tyrosine phosphorylation of BIB. However, one might have expected that if tyrosine phosphorylation were the primary regulatory mechanism then truncation would result in constitutively active BIB channels. The opposite results obtained with these studies suggest that BIB regulation is a complex process that may involve sites such as those present for serine/threonine phosphorylation, PDZ binding domains and polyglutamine stretches. In this regard, future studies should focus on (i) molecular dissection of the importance of SH3 and PDZ binding domains and polyglutamine stretches for BIB cationic channel activity; (ii) characterizing the site of tyrosine phosphorylation; and (iii) investigating protein-protein interactions between BIB and other neurogenic genes. Further studies into the functional domains of the BIB protein should provide more clues to the unique involvement of *bib* in neurogenesis, and further evidence of the diversity of function in the MIP family of channels.

## REFERENCES

- Adams, M. D., Dubnick, M., Kerlavage, A. R., Moreno, R., Kelley, J. M., Utterback, T. R., Nagle, J. W., Fields, C., and Venter, J. C. (1992) Sequence identification of 2,375 human brain genes. *Nature* 355: 632-634.
- Anthony, T. L., Brooks, H. L., Boassa, D, Leonov, S., Yanochko, G. M., Regan, J. W., and Yool, A. J. (2000) Cloned human Aquaporin-1 is a cyclic-GMP-gated ion channel. *Molecular Pharmacology* 57: 576-588.
- Arenander AT, de Vellis J (1994) Development of the nervous system. In: *Basic Neurochemistry: Molecular, Cellular, and Medical Aspects* (Siegel GJ ed), pp 573-606. New York: Raven Press, Ltd.
- Artavanis-Tsakonas, S. & Simpson, P. (1999b) Choosing a cell fate: a view from the *Notch* locus. *Trends in Genetics* 7: 403-408.
- Artavanis-Tsakonas, S., Matsuno, K., and Fortini, M. E. (1995) Notch signaling. *Science* 268: 225-232.
- Artavanis-Tsakonas, S., Rand, M. D., and Lake, R. J. (1999) Notch signaling: cell fate control and signal integration in development. *Science* 284: 770-776.
- Bailey, A. M. & Posakony, J. W. (1995) Suppressor of Hairless directly activates transcription of *Enhancer of split* complex genes in response to Notch receptor activity. *Genes & Development* : 2609-2622.
- Baker, M. E. & Saier, M. H. Jr. (1990) A common ancestor for bovine lens fiber major intrinsic protein, soybean nodulin-26 protein, and *E. coli* glycerol facilitator. *Cell* 60: 185-186.
- Bier, E. (1997) Anti-neural-inhibition: a conserved mechanism for neural induction. *Cell* 89: 681-684.
- Blaumueller, C. M., Qi, H., Zagouras, P., and Artavanis-Tsakonas, S. (1997) Intracellular cleavage of Notch leads to heterodimeric receptor on the plasma membrane. *Cell* 90: 281-291.
- Borgnia, M. J. & Agre, P. (2001) Reconstitution and functional comparison of purified GlpF and AQPZ, the glycerol and water channels from *Escherichia coli*. *Proceedings of the National Academy of Sciences* 98: 2888-2893.
- Bossing, T., Udolph, G., Doe, C. Q., and Technau, G. M. (1996) The embryonic central nervous system lineages of *Drosophila melanogaster*. I. Neuroblast lineages derived from the ventral half of the neuroectoderm. *Developmental Biology* 179: 41-64.

- Brand M, Campos-Ortega JA (1988) Two groups of interrelated genes regulate early neurogenesis in *Drosophila melanogaster*. *Roux's Archives of Developmental Biology* 197:457-470.
- Brooks, H. L., Regan, J. W., and Yool, A. J. (2000) Inhibition of Aquaporin-1 water permeability by tetraethylammonium: Involvement of the Loop E pore region. *Molecular Pharmacology* 57: 1021-1026.
- Burris, P. A., Zhang, Y., Rusconi, J. C., and Corbin, V. (1998) The pore-forming and cytoplasmic domains of the neurogenic gene product, Big Brain; are conserved between *Drosophila virilis* and *Drosophila melanogaster*. *Gene* 206: 69-76.
- Campos-Ortega, J. A. & Jan, Y. N. (1991) Genetic and molecular bases of neurogenesis in *Drosophila melanogaster*. *Annual Review of Neuroscience* 14: 399-420.
- Chan, Y.-M. & Jan, Y. N. (1999) Conservation of neurogenic genes and mechanisms. *Current Opinion in Neurobiology* 9: 582-588.
- Chandy, G., Zampighi, G. A., Kreman, M., and Hall, J. E. (1997) Comparison of the water transporting properties of MIP and AQP1. *The Journal of Membrane Biology* 159: 29-39.
- Chen, C., Jack, J., and Garofalo, R. S. (1999) The *Drosophila* insulin receptor is required for normal growth. *Endocrinology* 137: 846-856.
- Chitnis, A. B. (1999) Control of neurogenesis - lessons from frogs, fish and flies. *Current Opinion in Neurobiology* 9: 18-25.
- Chung, S., Reinhart, P. H., Martin, B. L., Brautigan, D. L., and Levitan, I. B. (1991) Protein kinase activity closely associated with a reconstituted calcium-activated potassium channel. *Science* 253: 560-562.
- Cohen NA, Brenman JE, Snyder SH, Brecht DS (1996) Binding of the inward rectifier K<sup>+</sup> channel Kir 2.3 to PSD-95 is regulated by protein kinase A phosphorylation. *Neuron* 17:759-767.
- Cohen, G. B., Ren, R., and Baltimore, D. (1995) Modular binding domains in signal transduction proteins. *Cell* 80: 237-248.
- Craven, S. E. & Brecht, D. S. (1998) PDZ proteins organize synaptic signaling pathways. *Cell* 93: 495-498.
- Dascal, N. (1987) The use of *Xenopus* oocytes for the study of ion channels. *Critical Reviews in Biochemistry* 22: 317-387.
- de Groot, B. L., Heymann, J. B., Engel, A., Mitsuoka, K., Fujiyoshi, Y., and Grubmüller, H. (2000) The fold of human aquaporin 1. *Journal of Molecular Biology* 300: 987-994.

- de la Concha, A., Dietrich, U., Weigel, D., and Campos-Ortega, J. A. (1988) Functional interactions of neurogenic genes of *Drosophila melanogaster*. *Genetics* 118: 499-508.
- Delidakis, C. & Artavanis-Tsakonas, S. (1992) The Enhancer of split [*E(spI)*] locus of *Drosophila* encodes seven independent helix-loop-helix proteins. *Proceedings of the National Academy of Sciences, USA* 89: 8731-8735.
- Diederich, R. J., Matsuno, K., Hing, H., and Artavanis-Tsakonas, S. (1994) Cytosolic interaction between *deltex* and Notch ankyrin repeats implicates *deltex* in the Notch signaling pathway. *Development* 120: 473-481.
- Doe CQ (1992) The generation of neuronal diversity in the *Drosophila* embryonic central nervous system. In: *Determinants of Neuronal Identity* (Shankland M, Macagno ER eds), pp 119-154. Academic Press, Inc.
- Doe, C. Q. & Goodman, C. S. (1985a) Early events in insect neurogenesis. II. The role of cell interactions and cell lineage in the determination of neuronal precursor cells. *Developmental Biology* 111: 206-219.
- Doe, C. Q. & Goodman, C. S. (1985b) Early events in insect neurogenesis. I. Development and segmental differences in the pattern of neuronal precursor cells. *Developmental Biology* 111: 193-205.
- Doe, C. Q. & Skeath, J. B. (1996) Neurogenesis in the insect central nervous system. *Current Opinion in Neurobiology* 6: 18-24.
- Doherty, D., Jan, L. Y., and Jan, Y. N. (1997) The *Drosophila* neurogenic gene *big brain*, which encodes a membrane-associated protein, acts cell autonomously and can act synergistically with Notch and Delta. *Development* 124: 3881-3893.
- Doyle, D. A., Cabral, J. M., Pfuetzner, R. A., Kuo, A., Gulbis, J. M., Cohen, S. L., Chait, B. T., and MacKinnon, R. (1998) The structure of the potassium channel: molecular basis of K<sup>+</sup> conduction and selectivity. *Science* 280: 69-77.
- Dworetzky, S. I., Boissard, C. G., Lum-Ragan, J. T., McKay, M. C., Post-Munson, D. J., Trojnacki, J. T., Chang, C. P., and Gribkoff, V. K. (1996) Phenotypic alteration of a human BK (*hslö*) channel by *hslöβ* subunit coexpression: Changes in blocker sensitivity, activation/relaxation and inactivation kinetics, and protein kinase A modulation. *The Journal of Neuroscience* 16: 4543-4550.
- Ehring, G. R., Lagos, N., Zampighi, G. A., and Hall, J. E. (1991) Phosphorylation modulates the voltage dependence of channels reconstituted from the Major Intrinsic Protein of lens fiber membranes. *Journal of Membrane Biology* 126: 75-88.
- Ehring, G. R., Zampighi, G. A., Horwitz, J., Bok, D., and Hall, J. E. (1990) Properties of channels reconstituted from the major intrinsic protein of lens fiber membranes. *Journal of General Physiology* 96: 631-664.

- Fehon, R. G., Kooh, P. J., Rebay, I., Regan, C. L., Xu, T., Muskavitch, M. A. T., and Artavanis-Tsakonas, S. (1990) Molecular interactions between the protein products of the neurogenic loci *Notch* and *Delta*, two EGF-homologous genes in *Drosophila*. *Cell* 61: 523-534.
- Fortini, M. E. & Artavanis-Tsakonas, S. (1994) The Suppressor of Hairless protein participates in Notch receptor signaling. *Cell* 79: 273-282.
- Fu, D., Libson, A., Miercke, L. J. W., Weitzman, C., Nollert, P., Krucinski, J., and Stroud, R. M. (2000) Structure of a glycerol-conducting channel and the basis for its selectivity. *Science* 290: 481-486.
- Fushimi, K., Sasaki, S., and Marumo, F. (1997) Phosphorylation of serine 256 is required for cAMP-dependent regulatory exocytosis of the aquaporin-2 water channel. *The Journal of Biological Chemistry* 272: 14800-14804.
- Geering, K., Theulaz, I., Verrey, F., Häuptle, T, and Rossier, B. C. (1989) A role for the  $\beta$ -subunit in the expression of functional  $\text{Na}^+$ - $\text{K}^+$ ATPase in *Xenopus* oocytes. *American Journal of Physiology* 257: C851-C858.
- Girsch, S. J. & Peracchia, C. (1985) Lens cell-to-cell channel protein: I. Self assembly into liposomes and permeability regulation by calmodulin. *The Journal of Membrane Biology* 83: 217-225.
- Glahn, D., Mark, S. D., Behr, R. K, and Nuccitelli, R. (1999) Tyrosine kinase inhibitors block sperm-induced egg activation in *Xenopus laevis*. *Developmental Biology* 205: 171-180.
- Goodman, C. S. & Spitzer, N. C. (1979) Embryonic development of identified neurones: differentiation from neuroblast to neurone. *Nature* 280: 208-214.
- Goodman, C. S. & Spitzer, N. C. (1981) The development of electrical properties of identified neurones in grasshopper embryos. *Journal of Physiology* 313: 385-403.
- Goriely, A., Dumont, N., Dambly-Chaudière, C, and Ghysen, A. (1991) The determination of sense organs in *Drosophila*: effect of the neurogenic mutations in the embryo. *Development* 113: 1395-1404.
- Gorin, M. B., Yancey, S. B., Cline, J., Revel, J.-P., and Horwitz, J. (1984) The major intrinsic protein (MIP) of the bovine lens fiber membrane: characterization and structure based on cDNA cloning. *Cell* 39: 49-59.
- Gotoh, Y., Masuyama, N., Dell, K., Shirakabe, K., and Nishida, E. (1995) Initiation of *Xenopus* oocyte maturation by activation of the mitogen-activated protein kinase cascade. *The Journal of Biological Chemistry* 270: 25898-25904.

- Greenspan RJ (1992) Initial determination of the neurectoderm in *Drosophila*. In: *Determinants of Neuronal Identity* (Shankland M, Macagno ER eds), pp 155-188. Academic Press, Inc.
- Greenwald, I. (1998) LIN-12/Notch signaling: lessons from worms and flies. *Genes & Development* 12: 1751-1762.
- Gridley, T. (1997) Notch signaling in vertebrate development and disease. *Molecular and Cellular Neuroscience* 9: 103-108.
- Han, Z. & Patil, R. V. (2000) Protein kinase A-dependent phosphorylation of Aquaporin-1. *Biochemical and Biophysical Research Communications* 273: 328-332.
- Han, Z., Wax, M. B., and Patil, R. V. (1998) Regulation of Aquaporin-4 water channels by phorbol ester-dependent protein phosphorylation. *The Journal of Biological Chemistry* 273: 6001-6004.
- Han, Z., Wax, M. B., and Patil, R. V. (1998a) Potential role of aquaporins and atrial natriuretic peptides in the aqueous humor dynamics. *Experimental Eye Research* 67: 251-253.
- Han, Z., Wax, M. B., and Patil, R. V. (1998b) Regulation of Aquaporin-4 water channels by phorbol ester-dependent protein phosphorylation. *The Journal of Biological Chemistry* 273: 6001-6004.
- Hartenstein V, Campos-Ortega JA (1984) Early neurogenesis in wild-type *Drosophila melanogaster*. *Roux's Archives of Developmental Biology* 193:308-325.
- Heymann, J. B. & Engel, A. (2000) Structural clues in the sequences of the aquaporins. *Journal of Molecular Biology* 295: 139-1053.
- Hidaka, H., Inagaki, M., Kawamoto, S., and Sasaki, Y. (1984) Isoquinolinesulfonamides, novel and potent inhibitors of cyclic nucleotide dependent protein kinase and protein kinase C. *Biochemistry* 23: 5036-5041.
- Hille B (1992) *Ionic channels of excitable membranes*. Sunderland, MA: Sinauer Associates, Inc.
- Holmes, T. C., Fadool, D. A., Ren, R., and Levitan, I. B. (1996) Association of src tyrosine kinase with a human potassium channel mediated by SH3 domain. *Science* 274: 2089-2091.
- Horster, M. (2000) Embryonic epithelial membrane transporters. *American Journal of Physiology* 279: F982-F996.
- Ingham, P. W. (1988) The molecular genetics of embryonic pattern formation in *Drosophila*. *Nature* 335: 25-34.

- Ishibashi, K., Kuwahara, M., Kageyama, Y., Tohsaka, A., Marumo, F., and Sasaki, S. (1997) Cloning and functional expression of a second new aquaporin abundantly expressed in testis. *Biochemical and Biophysical Research Communications* 237: 714718-718.
- Jan, Y. N. & Jan, L. Y. (1994) Neuronal cell fate specification in *Drosophila*. *Current Opinion in Neurobiology* 4: 8-13.
- Jap, B. K. & Li, H. (1995) Structure of the osmo-regulated H<sub>2</sub>O-channel, AQP-CHIP, in projection at 3.5 Å resolution. *Journal of Molecular Biology* 251: 413-420.
- Jessell TM, Schacher S (1991) Control of cell identity. In: *Principles of Neural Science* (Kandel ER, Schwartz JH, Jessell TM eds), pp 887-907. Norwalk, CT: Appleton & Lange.
- Joutel, A., Corpechot, C., Ducros, A., Vahedi, K., Chabriat, H., Mouton, P., Alamowitch, S., Domenga, V., Cecillion, M., Marechal, E., Maciazek, J., Vayssiere, C., Cruaud, C., Cabanis, E. A., Ruchoux, M. M., Weissenbach, J., Bach, J. F., Bousser, M. G., and Tournier-Lasserre, E. (1996) Notch3 mutations in CADASIL, a hereditary adult-onset condition causing stroke and dementia. *Nature* 383: 707-710.
- Jung, J. S., Preston, G. M., Smith, B. L., Guggino, W. B., and Agre, P. (1994) Molecular structure of the water channel through Aquaporin CHIP. *The Journal of Biological Chemistry* 269: 14648-14654.
- Kanemitsu, M. Y., Loo, L. W. M., Simon, S., Lau, A. F., and Eckhart, W. (1997) Tyrosine phosphorylation of Connexin 43 by v-src is mediated by SH2 and SH3 domain interactions. *The Journal of Biological Chemistry* 272: 22824-22831.
- Kemp, B. E. & Pearson, R. B. (1990) Protein kinase recognition sequence motifs. *Trends in Biochemical Science* 15: 342-346.
- Kim, M-J., Lee, Y-S., and Han, J-K. (2000) Modulation of lysophosphatidic acid-induced Cl<sup>-</sup> currents by protein kinases A and C in the *Xenopus* oocyte. *Biochemical Pharmacology* 59: 241-247.
- Kimble, J. & Simpson, P. (1997) The LIN-12/Notch signaling pathway and its regulation. *Annual Review of Cellular and Developmental Biology* 13: 333-361.
- King LS, Nielsen S, Agre P (1997) Aquaporins in complex tissues. I. Developmental patterns in respiratory and glandular tissues of rat. *American Journal of Physiology* 273:C1541-C1548
- King, L. S. & Agre, P. (1996) Pathophysiology of the aquaporin water channels. *Annual Review of Physiology* 58: 619-648.

- Klussmann, E., Maric, K., Wiesner, B., Beyermann, M., and Rosenthal, W. (1999) Protein Kinase A anchoring proteins are required for vasopressin-mediated translocation of aquaporin-2 into cell membranes of renal principal cells. *The Journal of Biological Chemistry* 274: 4934-4938.
- Koch, C. A., Anderson, D., Moran, M. F., Ellis, C., and Pawson, T. (1991) SH2 and SH3 domains: Elements that control interactions of cytoplasmic signaling proteins. *Science* 252: 668-674.
- Koyano-Nakagawa, N., Wettstein, D., and Kintner, C. (1999) Activation of *Xenopus* genes required for lateral inhibition and neuronal differentiation during primary neurogenesis. *Molecular and Cellular Neuroscience* 14: 327-339.
- Kubota, H. Y., Yoshimoto, Y., Yoneda, M., and Hiramoto, Y. (1987) Free calcium wave upon activation in *Xenopus* eggs. *Developmental Biology* 119: 129-136.
- Kuwahara, M., Fushimi, K., Terada, Y., Bai, L., Marumo, F., and Sasaki, S. (1995) cAMP-dependent phosphorylation stimulates water permeability of aquaporin-collecting duct water channel protein expressed in *Xenopus* oocytes. *The Journal of Biological Chemistry* 270: 10384-10387.
- Kuwahara, M., Shinbo, I., Sato, K., Terada, Y., Marumo, F., and Sasaki, S. (1999) Transmembrane helix 5 is critical for the high water permeability of aquaporin. *Biochemistry* 38: 16340-16346.
- Lagrée, V., Froger, A., Deschamps, S., Pellerin, I., Delamarche, C., Bonnac, G., Gouranton, J., Thomas, D., and Hubert, J.-F. (1998) Oligomerization state of water channels and glycerol facilitators: Involvement of Loop E. *The Journal of Biological Chemistry* 273: 33949-33953.
- Lai, E. C., Bodner, R., Kavalier, J., Freschi, G., and Posakony, J. W. (2000) Antagonism of Notch signaling activity by members of a novel protein family encoded by the *Bearded* and *Enhancer of split* gene complexes. *Development* 127: 291-306.
- Lanahan, A., Williams, J. B., Sanders, L. K., and Nathans, D. (1992) Growth factor-induced delayed early response genes. *Molecular and Cellular Biology* 12: 3919-3929.
- Lawrence, D. S. & Niu, J. (1998) Protein kinase inhibitors: the tyrosine-specific protein kinases. *Pharmacological Therapeutics* 77: 81-114.
- Lehmann R, Jimenez F, Dietrich U (1983) On the phenotype and development of mutants of early neurogenesis in *Drosophila melanogaster*. *Roux's Archives of Developmental Biology* 192:62-74.
- Levitan, I. B. (1994) Modulation of ion channels by protein phosphorylation and dephosphorylation. *Annual Review of Physiology* 56: 193-212.

- Manley, D. M., McComb, M. E., Perreault, H., Donald, L. J., Duckworth, H. W., and O'Neil, J. D. (2000) Secondary structure and oligomerization of the *E. coli* glycerol facilitator. *Biochemistry* 39: 12303-12311.
- Martindale, D., Hackam, A., Wieczorek, A., Ellerby, L., Wellington, C., McCutcheon, K., Singaraja, R., Kazemi-Esfarjani, P., Devon, R., Kim, S. U., Bredesen, D. E., Tufaro, F., and Hayden, M. R. (1998) Length of huntingtin and its polyglutamine tract influences localization and frequency of intracellular aggregates. *Nature Genetics* 18: 150-154.
- Matsuno, K., Diederich, R. J., Go, M. J., Blaumueller, C. M., and Artavanis-Tsakonas, S. (1995) Deltex acts as a positive regulator of Notch signaling through interactions with the Notch ankyrin repeats. *Development* 121: 2633-2644.
- Maurel, C., Kado, R. T., Guern, J., and Chrispeels, M. J. (1995) Phosphorylation regulates the water channel activity of the seed-specific aquaporin  $\alpha$ -TIP. *EMBO Journal* 14: 3028-3035.
- Maurel, C., Reizer, J., Schroeder, J. I., Chrispeels, M. J., and Saier, M. H. Jr. (1994) Functional characterization of the *Escherichia coli* glycerol facilitator, GlpF, in *Xenopus* oocytes. *The Journal of Biological Chemistry* 269: 11869-11872.
- Meera, P., Wallner, M., Song, M., and Toro, L. (1997) Large conductance voltage- and calcium-dependent  $K^+$  channel, a distinct member of voltage-dependent ion channels with seven N-terminal transmembrane segments (S0-S6), an extracellular N terminus, and an intracellular (S9-S10) C terminus. *Proceedings of the National Academy of Sciences* 94: 14066-14071.
- Merves, M., Bobbitt, B., Parker, K., Kishore, B. K., and Choo, D. (2000) Developmental expression of Aquaporin-2 in the mouse inner ear. *Laryngoscope* 110: 1925-1930.
- Mishina, M., Takai, T., Imoto, K., Noda, M., Takahashi, T., Numa, S., Methfessel, C., and Sakmann, B. (1986) Molecular distinction between fetal and adult forms of muscle acetylcholine receptor. *Nature* 321: 406-411.
- Molokanova, E., Savchenko, A., and Kramer, R. H. (2000) Interactions of cyclic nucleotide-gated channel subunits and protein tyrosine kinase probed with genistein. *Journal of General Physiology* 115: 685-696.
- Molokanova, E., Trivedi, B., Savchenko, A., and Kramer, R. H. (1997) Modulation of rod photoreceptor cyclic nucleotide-gated channels by tyrosine phosphorylation. *The Journal of Neuroscience* 17: 9068-9076.
- Moody, W. J. (1995) Critical periods of early development created by the coordinate modulation of ion channel properties. *Perspectives on Developmental Neurobiology* 2: 309-315.

- Moody, W. J. (1998a) Control of spontaneous activity during development. *Journal of Neurobiology* 37: 97-19.
- Moody, W. J. (1998b) The development of voltage-gated ion channels and its relation to activity-dependent developmental events. *Current Topics in Developmental Biology* 39: 159-185.
- Murata, K., Mitsuoka, K., Hirai, T., Walz, T., Agre, P., Heymann, J. B., Engel, A., and Fujiyoshi, Y. (2000) Structural determinants of water permeation through aquaporin-1. *Nature* 407: 599-605.
- Nagelhus, E. A., Veruki, M. L., Torp, R., Haug, F.-M., Laake, J. H., Nielsen, S., Agre, P., and Ottersen, O. P. (1998) Aquaporin-4 water channel protein in the rat retina and optic nerve: Polarized expression in Müller cells and fibrous astrocytes. *The Journal of Neuroscience* 18: 2506-2519.
- Nara, M., Dhulipala, P. D. K., Wang, Y. X., and Kotlikoff, M. I. (1998) Reconstitution of  $\alpha$ -adrenergic modulation of large conductance calcium-activated potassium (Maxi-K) channels in *Xenopus* oocytes. *The Journal of Biological Chemistry* 273: 14920-14924.
- Nehring, R. B., Wischmeyer, E., Döring, F., Rüdiger, W. V., Sheng, M., and Karschin, A. (2000) Neuronal inwardly rectifying K<sup>+</sup> channels differentially couple to PDZ proteins of the PSD-95/SAP90 family. *The Journal of Neuroscience* 20: 156-162.
- Németh-Cahalan, K. L. & Hall, J. E. (2000) pH and calcium regulate the water permeability of aquaporin 0. *The Journal of Biological Chemistry* 275: 6777-6782.
- Nico, B., Frigeri, A., Nicchia, G. P., Quondamatteo, F., Herken, R., Errede, M., Ribatti, D., Svelto, M., and Roncali, L. (2001) Role of aquaporin-4 water channel in the development and integrity of the blood brain barrier. *Journal of Cell Science* 114: 1297-1307.
- Nielsen, S., Nagelhus, E. A., Amiry-Moghaddam, M., Bourque, C., Agre, P., and Ottersen, O. P. (1997) Specialized membrane domains for water transport in glial cells: High-resolution immunogold cytochemistry of Aquaporin-4 in rat brain. *The Journal of Neuroscience* 17: 171-180.
- Nikaido, H. & Rosenberg, E. Y. (1985) Functional reconstitution of lens gap junction proteins into proteoliposomes. *The Journal of Membrane Biology* 85: 87-92.
- O'Dell, T. J., Kandel, E. R., and Grant, S. G. N. (1991) Long-term potentiation in the hippocampus is blocked by tyrosine kinase inhibitors. *Nature* 353: 558-560.
- O'Dowd, D. K., Ribera, A. B., and Spitzer, N. C. (1988) Development of voltage-dependent calcium, sodium, and potassium currents in *Xenopus* spinal neurons. *The Journal of Neuroscience* 8: 792-805.

- Pan, D. & Rubin, G. M. (1997) Kuzbanian controls proteolytic processing of Notch and mediates lateral inhibition during *Drosophila* and vertebrate neurogenesis. *Cell* 90: 271-280.
- Park, C.-S. & MacKinnon, R. (1995) Divalent cation selectivity in a cyclic nucleotide-gated ion channel. *Biochemistry* 34: 13328-13333.
- Park, J. H. & Saier, M. H. (1996) Phylogenetic characterization of the MIP family of transmembrane channel proteins. *The Journal of Membrane Biology* 153: 171-180.
- Patil, R. V., Han, Z., and Wax, M. B. (1997) Regulation of water channel activity of Aquaporin-1 by arginine vasopressin and atrial natriuretic peptide. *Biochemical and Biophysical Research Communications* 238: 392-396.
- Paulson, H. L. & Fischbeck, K. H. (1996) Trinucleotide repeats in neurogenetic disorders. *Annual Review of Neuroscience* 19: 79-107.
- Perutz, M. F., Johnson, T., Suzuki, M., and Finch, J. T. (1994) Glutamine repeats as polar zippers: Their possible role in inherited neurodegenerative diseases. *Proceedings of the National Academy of Sciences, USA* 91: 5355-5358.
- Pimentel, B., de la Rosa, E. J., and De Pablo, F. (1996) Insulin acts as an embryonic growth factor for *Drosophila* neural cells. *Biochemical and Biophysical Research Communications* 226: 855-861.
- Preston, G. M. & Agre, P. (1991) Isolation of the cDNA for erythrocyte integral membrane protein of 28 kilodaltons: Member of an ancient channel family. *Proceedings of the National Academy of Sciences USA* 88: 11110-11114.
- Preston, G. M., Carroll, T. P., Guggino, W. B., and Agre, P. (1992) Appearance of water channels in *Xenopus* oocytes expressing red cell CHIP28 protein. *Science* 256: 385-387.
- Preston, G. M., Jung, J. S., Guggino, W. B., and Agre, P. (1993) The mercury-sensitive residue at cysteine 189 in the CHIP28 water channel. *The Journal of Biological Chemistry* 268: 17-20.
- Preston, G. M., Jung, J. S., Guggino, W. B., and Agre, P. (1994) Membrane topology of Aquaporin CHIP: analysis of functional epitope-scanning mutants by vectorial proteolysis. *The Journal of Biological Chemistry* 269: 1668-1673.
- Rao, Y., Bodmer, R., Jan, L. Y., and Jan, Y. N. (1992) The big brain gene of *Drosophila* functions to control the number of neuronal precursors in the peripheral nervous system. *Development* 116: 31-40.
- Rao, Y., Jan, L. Y., and Jan, Y. N. (1990) Similarity of the product of the *Drosophila* neurogenic gene big brain to transmembrane channel proteins. *Nature* 345: 163-167.

- Ratcliffe, C. F., Qu, Y., McCormick, K. A., Tibbs, V. C., Dixon, J. E., Scheuer, T., and Catterall, W. A. (2000) A sodium channel signalling complex: modulation by associated receptor protein tyrosine phosphatase □. *Nature Neuroscience* 3: 437-444.
- Reaume, A. G., Conlon, R. A., Zimigbi, R., Yamaguchi, T. P., and Rossant, J. (1992) Expression analysis of a Notch homologue in the mouse embryo. *Developmental Biology* 154: 377-387.
- Reizer, J., Reizer, A., and Saier, M. H. (1993) The MIP family of integral membrane channel proteins: Sequence comparisons, evolutionary relationships, reconstructed pathway of evolution, and proposed functional differentiation of the two repeated halves of the proteins. *Critical Reviews in Biochemistry and Molecular Biology* 28: 235-257.
- Ren, G., Reddy, V. S., Cheng, A., Melnyk, P., and Mitra, A. K. (2000) Visualization of a water-selective pore by electron crystallography in vitreous ice. *Proceedings of the National Academy of Sciences* 98: 1398-1403.
- Rickles, R. J., Botfield, M. C., Weng, Z., Taylor, J. A., Green, O. M., Brugge, J. S., and Zoller, M. J. (1994) Identification of Src, Fyn, Lyn, PI3K, and Abl SH3 domain ligands using phage display libraries. *The EMBO Journal* 13: 5598-5604.
- Rigaud, J.-L., Chami, M., Lambert, O., Levy, D., and Ranck, J.-L. (2000) Use of detergents in two-dimensional crystallization of membrane proteins. *Biochimica et Biophysica Acta* 1508: 112-128.
- Rivers, R. L., Dean, R. M., Chandy, G., Hall, J. E., Roberts, D. M., and Zeidel, M. L. (1997) Functional analysis of nodulin 26, an aquaporin in soybean root nodule symbiosomes. *The Journal of Biological Chemistry* 272: 16256-16261.
- Rosenblum, K., Dudai, Y., and Richter-Levin, G. (1996) Long-term potentiation increases tyrosine phosphorylation of the N-methyl-D-aspartate receptor subunit 2B in rat dentate gyrus *in vivo*. *Proceedings of the National Academy of Sciences* 93: 10457-10460.
- Rostas, J. A. P., Brent, V. A., Voss, K., Errington, M. L., Bliss, T. V. P., and Gurd, J. W. (1996) Enhanced tyrosine phosphorylation of the 2B subunit of the N-methyl-D-aspartate receptor in long-term potentiation. *Proceedings of the National Academy of Sciences* 93: 10452-10456.
- Ruel, L., Bourouis, M., Heitzler, P., Pantesco, V., and Simpson, P. (1993) *Drosophila shaggy* kinase and rat glycogen synthase kinase-3 have conserved activities and act downstream of *Notch*. *Nature* 362: 557-560.
- Sasaki, S., Ishibashi, K., and Marumo, F. (1998) Aquaporin-2 and -3: Representatives of two subgroups of the aquaporin family colocalized in the kidney collecting duct. *Annual Review of Physiology* 60: 199-220.

- Sato, K., Iwao, Y., Fujimura, T., Tamaki, I., Ogawa, K., Iwasaki, T., Tokmakov, A. A., Hatano, O., and Fukami, Y. (1999) Evidence for the involvement of a src-related tyrosine kinase in *Xenopus* egg activation. *Developmental Biology* 209: 308-320.
- Sato, K., Iwasaki, T., Tamaki, I., Aoto, M., Tokmakov, A. A., and Fukami, Y. (1998) Involvement of protein-tyrosine phosphorylation and dephosphorylation in sperm-induced *Xenopus* egg activation. *FEBS Letters* 424: 113-118.
- Scavo, L., Shuldiner, A. R., Serrano, J., Dashner, R., Roth, J., and De Pablo, F. (1991) Genes encoding receptors for insulin and insulin-like growth factor I are expressed in *Xenopus* oocytes and embryos. *Proceedings of the National Academy of Sciences* 88: 6214-6218.
- Schmid, A., Chiba, A., and Doe, C. Q. (1999) Clonal analysis of *Drosophila* embryonic neuroblasts: neural cell types, axon projections and muscle targets. *Development* 126: 4653-4689.
- Schmidt, H., Rickert, C., Bossing, T., Vef, O., Urban, J., and Technau, G. M. (1997) The embryonic central nervous system lineages of *Drosophila melanogaster*: II. Neuroblast lineages derived from the dorsal part of the neuroectoderm. *Developmental Biology* 189: 186-204.
- Shieh, B. H. & Zhu, M. Y. (1996) Regulation of the TRP Ca<sup>2+</sup> channel by INAD in *Drosophila* photoreceptors. *Neuron* 16: 991-998.
- Shiels, A. & Bassnett, S. (1996) Mutations in the founder of the *MIP* gene family underlie cataract development in the mouse. *Nature Genetics* 12: 212-215.
- Skeath, J. B. (1998) The *Drosophila* EGF receptor controls the formation and specification of neuroblasts along the dorso-ventral axis of the *Drosophila* embryo. *Development* 125: 3301-3312.
- Skeath, J. B., Panganiban, G., Selegue, J., and Carroll, S. B. (1992) Gene regulation in two dimensions: the proneural *achaete* and *scute* genes are controlled by combinations of axis-patterning genes through a common intergenic control region. *Genes & Development* 6: 2606-2619.
- Smith, B. L. & Agre, P. (1991) Erythrocyte M<sub>r</sub> 28,000 transmembrane protein exists as a multisubunit oligomer similar to channel proteins. *The Journal of Biological Chemistry* 266: 6407-6415.
- Smith, B. L., Lu, M., Lee, M. D., Jung, J. S., Agre, P., Verduk, M. A. J., Merckx, G., Russ, J. P. L., and Deen, P. M. T. (1996) The human AQP4 gene: Definition of the locus encoding two water channel polypeptides in brain. *Proceedings of the National Academy of Sciences* 93: 10908-10912.

- Songyang, Z., Carraway, K. L. III, Eck, M. J., Harrison, S. C., Feldman, R. A., Mohammadi, M., Schlessinger, J., Hubbard, S. R., Smith, D. P., Eng, C., Lorenzo, M. J., Ponder, B. A. J., Mayer, B. J., and Cantley, L. C. (1995) Catalytic specificity of protein-tyrosine kinases is critical for selective signalling. *Nature* 373: 536-539.
- Spitzer, N. C. & Ribera, A. B. (1998) Development of electrical excitability in embryonic neurons: mechanisms and roles. *Journal of Neurobiology* 37: 190-197.
- Stamer, W. D., Snyder, R. W., and Regan, J. W. (1996) Characterization of the transmembrane orientation of aquaporin-1 using antibodies to recombinant fusion proteins. *Biochemistry* 35: 16313-16318.
- Tingley, W. G., Roche, K. W., Thompson, A. K., and Huganir, R. L. (1993) Regulation of NMDA receptor phosphorylation by alternative splicing of the C-terminal domain. *Nature* 364: 70-73.
- Tsakaguchi, H., Shayakul, C., Berger, U. V., Mackenzie, B., Devidas, S., Guggino, W. B., van Hoek, A. N., and Hediger, M. A. (1998) Molecular characterization of a broad selectivity neutral solute channel. *The Journal of Biological Chemistry* 273: 24737-24743.
- Udolph, G., Urban, J., Rüsing, G., Lürer, K., and Technau, G. M. (1998) Differential effects of EGF receptor signalling on neuroblast lineages along the dorsoventral axis of the *Drosophila* CNS. *Development* 125: 3291-3000.
- Unger, V. M. (2000) Fraternal twins: AQP1 and GlpF. *Nature Structural Biology* 7: 1082-1084.
- Volk, K. A., Husted, R. F., Snyder, P. M, and Stokes, J. B. (2000) Kinase regulation of hENaC mediated through a region in the COOH-terminal portion of the  $\alpha$ -subunit. *American Journal of Physiology* 278: C1047-C1054.
- Walz, T. & Grigorieff, N. (1998) Electron crystallography of two-dimensional crystals of membrane proteins. *Journal of Structural Biology* 121: 142-161.
- Walz, T., Smith, B. L., Agre, P., and Engel, A. (1994a) The three-dimensional structure of human erythrocyte aquaporin CHIP. *EMBO Journal* 13: 2985-2993.
- Walz, T., Smith, B. L., Zeidel, M. L., Engel, A., and Agre, P. (1994b) Biologically active two-dimensional crystals of Aquaporin CHIP. *The Journal of Biological Chemistry* 269: 1583-1586.
- Walz, T., Tittmann, P., Fuchs, K. H., Smith, B. L., Agre, P., Gross, H., and Engel, A. (1996) Surface topographies at subnanometer-resolution reveal asymmetry and sidedness of aquaporin-1. *Journal of Molecular Biology* 264: 907-918.
- Wang, Y-T & Salter, M. W. (1994) Regulation of NMDA receptors by tyrosine kinases and phosphatases. *Nature* 369: 235.

- Wangh, L. J. (1989) Injection of *Xenopus* eggs before activation, achieved by control of extracellular factors, improves plasmid DNA replication after activation. *Journal of Cell Science* 93: 1-8.
- Weaver, C. D., Shomer, N. H., Louis, C. F., and Roberts, D. M. (1994) Nodulin 26, a nodule-specific symbiosome membrane protein from soybean, is an ion channel. *The Journal of Biological Chemistry* 269: 17858-17862.
- Wei, A., Solaro, C., Lingle, C., and Salkoff, L. (1994) Calcium sensitivity of BK-type  $K_{Ca}$  channels determined by a separable domain. *Neuron* 13: 671-681.
- Wen, H., Nagelhus, E. A., Amiry-Moghaddam, M., Agre, P., Ottersen, O. P., and Nielsen, S. (1999) Ontogeny of water transport in rat brain: postnatal expression of the aquaporin-4 water channel. *European Journal of Neuroscience* 11: 935-945.
- Williams, K., Pahk, A. J., Kashiwagi, K., Masuko, T., Nguyen, N. D., and Igarashi, K. (1998) The selectivity filter of the N-methyl-D-aspartate receptor: A tryptophan residue controls block and permeation of  $Mg^{2+}$ . *Molecular Pharmacology* 53: 933-941.
- Wolf, D. P. (1974) The cortical response in *Xenopus laevis* Ova. *Developmental Biology* 40: 102-115.
- Woodhull, A.M. (1973) Ionic blockage of sodium channels in nerve. *Journal of General Physiology* 61(6): 687-708.
- Yang, B. & Verkman, A. S. (1997) Water and glycerol permeabilities of Aquaporins 1-5 and MIP determined quantitatively by expression of epitope-tagged constructs in *Xenopus* oocytes. *The Journal of Biological Chemistry* 272: 16140-16146.
- Yasui, M., Hazama, A., Kwon, T.-H., Nielsen, S, Guggino, W. B., and Agre, P. (1999a) Rapid gating and anion permeability of an intracellular aquaporin. *Nature* 402: 184-187.
- Yasui, M., Kwon, T.-H., Knepper, M. A., Nielsen, S, and Agre, P. (1999b) Aquaporin-6: an intracellular vesicle water channel protein in renal epithelia. *Proceedings of the National Academy of Sciences* 96: 5808-5813.
- Yool AJ, Stamer WD (2001) Novel roles for aquaporins as gated ion channels. In: *Molecular Insights into Ion Channel Biology in Health and Disease* (Maue R ed), Elsevier Science.
- Yool, A. J., Stamer, W. D., and Regan, J. W. (1996) Forskolin stimulation of water and cation permeability in Aquaporin 1 water channels. *Science* 273: 1216-1218.
- Yu, X.-M., Askalan, R., Keil, G. J. II, and Satter, M. W. (1997) NMDA channel regulation by channel-associated protein tyrosine kinase src. *Science* 275: 674-678.

**Zagouras, P., Stifani, S., Blaumueller, C. M., Carcangiu, M. L., and Artavanis-Tsakonas, S. (1995) Alterations in Notch signaling in neoplastic lesions of the human cervix. Proceedings of the National Academy of Sciences USA 92: 6414-6418.**

**Zelenin, S., Gunnarson, E., Alikina, T., Bondar, A., and Aperia, A. (2000) Identification of a new form of AQP4 mRNA that is developmentally expressed in mouse brain. Pediatric Research 48: 335-339.**